Tesi di Dottorato di MARCO SACCONE
Matricola 768876

POLITECNICO DI MILANO

**DIPARTIMENTO
DI
CHIMICA,
MATERIALI
E
INGEGNERIA CHIMICA
"Giulio Natta"**

ENGINEERING EFFICIENT MATERIALS FOR OPTOELECTRONICS APPLICATIONS THROUGH HALOGEN BONDING

**Dottorato di Ricerca in
Chimica Industriale e
Ingegneria Chimica (CII)**

XXVI ciclo

2011 - 2013

Coordinatore: prof. Tiziano Faravelli

Tutore: prof. Giuseppe Resnati

Relatore: prof. Pierangelo Metrangolo

To *Anna*, *Pietro* and *Andrea*

Acknowledgements.

I wish to thank my advisor, Prof. Pierangelo Metrangolo and my tutor Prof. Giuseppe Resnati for giving me the opportunity to work in a professional and stimulating environment and to discover the world of halogen bonding and crystal engineering.

I'm gratefully indebt to Dr. Arri Priimagi that helped me through my PhD, not only in the understanding of the fascinating optical properties of azobenzenes, but also in being a great scientist.

I wish also to thank Dr. Giancarlo Terraneo and Dr. Tullio Pilati for many valuable comments about my research activity and for solving and refining the crystals structures present in this thesis.

Thanks are due to Prof. Matti Kaivola of Aalto University that accepted me in his research group at the Department of Applied Physics and provided for me a beautiful accommodation.

I would thank all the staff of Aalto University that assisted me during my research period in Finland, especially Dr. Jaana Vaapavuori, with which I enjoyed the long discussions about Italian politics.

I would also thank all the Finland guys: M.Sc. Arianna Bertolani, M.Sc. Lara Gazzera, M.Sc. Veronica Bono, M.Sc. Claudio Corti and Dr. Roberto Milani. I had a great time with you and I will never forget you.

Thanks to all my colleagues of the NFMLab with which I enjoyed many stimulating scientific discussions.

Thanks to all my friends, especially those in Milano, who contributed in making these years less difficult.

Thanks to my family, to whom this thesis is dedicated, for having encouraged me in pursuing the PhD and for their help through the years.

A very special thanks to my girlfriend Fanny, that always encouraged me and (being herself a PhD student) that perfectly understood my troubles and frustrations.

List of Publications.

Papers accepted for publication.

Photoalignment and Surface-Relief-Grating Formation are Efficiently Combined in Low-Molecular-Weight Halogen-Bonded Complexes.
Priimagi Arri; Saccone Marco; Cavallo Gabriella; Shishido Atsushi; Pilati Tullio; Metrangolo Pierangelo; Resnati Giuseppe *Adv. Mater*. **2012**, *24*, OP 345.
(Top 15% paper in the opinion of the referees)

Halogen bond directionality translates tecton geometry into self-assembled architecture geometry.
Saccone Marco; Cavallo Gabriella; Metrangolo Pierangelo; Pace Andrea; Pibiri Ivana; Pilati Tullio; Resnati Giuseppe; Terraneo Giancarlo *CrystEngComm*, **2013**, *15*, 3102.
(Hot article in the opinion of the referees and highlighted in the *CrystEngComm* blog)

Azobenzene-based difunctional halogen-bond donor: towards the engineering of photoresponsive co-crystals.
Saccone Marco; Terraneo Giancarlo; Pilati Tullio; Cavallo Gabriella; Priimagi Arri; Metrangolo Pierangelo; Resnati Giuseppe *Acta Cryst. B* **2014**, *70*.

Papers to be submitted.

Self-assembly of superfluorinated ionic liquid crystals through halogen bonding.
Saccone Marco; Priimagi Arri; Cavallo Gabriella; Terraneo Giancarlo; Pilati Tullio; Monfredini Alessandro; Metrangolo Pierangelo; Resnati Giuseppe; Bruce Duncan W.
Ready for publication, intention to submit to *Advanced Materials.*

Supramolecuar hierarchy among halogen and hydrogen bonding donors in driving the performances of photoactive polymers.
Saccone Marco; Dichiarante Valentina; Vapaavuori Jana; Forni Alessandra; Kaivola Matti; Metrangolo Pierangelo; Pilati Tullio; Resnati Giuseppe; Priimagi Arri
Ready for publication, intention to submit to *Journal of the American Chemical Society.*

Halogen bonding in dye-doped liquid crystals.
Priimagi Arri; Saccone Marco; Shishido Atsushi; Metrangolo Pierangelo; Resnati Giuseppe
Ready for publication, intention to submit to *ACS Photonics.*

Conferences.

X Congresso Nazionale di Chimica Supramolecolare, Perugia (Italy) 25 September **2011**.
Title of the oral presentation: *Halogen bonding driven self-assembly of highly efficient photoresponsive supramolecules.*

XXXIV Convegno della Divisione di Chimica Organica, Pavia (Italy) 10 September **2012**.
Title of the oral presentation: *A low-molecular weight halogen bonded complex showing highly efficient photoalignment and Surface Relief Greating formation*.

SAYCS 2012, Riccione (Italy) 1 October **2012**.
Title of the oral presentation: *Halogen-bonded liquid crystals combining efficient photoalignment and Surface Relief Greating formation*.

European Conference on Liquid Crystals 2013, Rhodes (Greece) 22 September **2013**.
Title of the oral presentation: *Engineering photoresponsive liquid crystals through halogen bonding*.

Other contributions.

Giancarlo Terraneo, Michele Baldrighi, Serena Biella, Pierangelo Metrangolo, Tullio Pilati, Giuseppe Resnati, Marco Saccone, *Halogen Bonding: A new strategy for pharmaceutical cocrystals*, XXIV Congresso della Società Chimica Italiana, Lecce 11 September **2011**.

Gabriella Cavallo, Pierangelo Metrangolo, Tullio Pilati, Giuseppe Resnati, Marco Saccone, Giancarlo Terraneo, *Fluorinated ionic liquid crystals assembled by halogen bonding*, 3rd International Symposium on Organofluorine Compounds in Biomedical and Agricultural Sciences, Valencia 20 May **2012**.

Gabriella Cavallo, Pierangelo Metrangolo, Roberto Milani, Arri Priimagi, Tullio Pilati, Giuseppe Resnati, Marco Saccone, Giancarlo Terraneo, *Halogen bonding: A new tool for the self-assembly of photoresponsive materials*, V International Conference on Molecular Materials MolMat2012, Barcelona 3 July **2012**.

Giuseppe Resnati, Pierangelo Metrangolo, Jane S. Murray, Peter Politzer, Gabriella Cavallo, Tullio Pilati, Marco Saccone, Giancarlo Terraneo, *Fluorine atom as a positive site viz halogen bonding donors*, 20th International Symposium on Fluorine Chemistry, Kyoto 22 July **2012**.

Index.

Index of figures.

Upon irradiation with circularly polarized light (488 nm, 30 s, 100 mW/cm^2), the crystal structure is destroyed and the film becomes opaque when imaged between crossed polarizers. (d) Normalized I3d core-level XPS spectra of the starting compound **1** (black and gray curves), **3** (blue curve), and **3** after irradiation with circularly polarized light (red curve). The red-shift in the binding energy in **3** as compared to **1** is an indication of halogen-bond formation between **1** and **2**. (e) Light irradiation induces significant changes to the absorption spectrum of **3**, and reduces optical scattering of a 633 nm He–Ne probe beam (inset).

27 (a) Selected polarized absorption spectra of a spin-coated thin film of **3** after irradiation with linearly polarized light (488 nm, 100 mW/cm^2). Black curve: initial spectrum (same for both polarizations). The red and blue curves correspond to the polarized absorption spectra in the directions parallel ($A_{||} < A_0$) and perpendicular ($A_{\perp} > A_0$) to the polarization plane, taken after 30 s and 120 s of irradiation time, respectively. (b) The time evolution of the order parameter of molecular alignment at different irradiation intensities. **57**

28 Atomic-force microscope views of the spin-coated thin film of **3** (a) before, and (b) after the SRG inscription (5 min, 300 mW/cm^2). (c) The surface-modulation depth of the grating shown in (b); (d) The time evolution of the first-order diffraction efficiency of a He–Ne probe beam upon SRG formation using different irradiation intensities. **58**

29 Molecular electrostatic potential of CF_4 (All electron MP2 aug-cc-pCV5Z wavefunction) mapped on the 0.001 au contour of the electron density. The computed C-F bond length is 1.316 Å compared to 1.392 Å of CH_3F. **64**

30 Schematic representation of structures showing how the angle between the two XBs formed by a bidentate XB donor is strictly similar to the angle between its two C-halogen covalent bonds. Ball and stick representation (Mercury 3.0) of selected structures are also given. **65**

31 General representation of an Azine-Azole-Azine heteroaromatic triad. **66**

32 General structure of bis(pyridyl)-1,2,4-oxadiazoles. **67**

33 Building blocks used for the synthesis of XB-based co-crystals **4** and **5**. **68**

34 Ball and stick representation (Mercury 3.0) of X-bonded infinite chains in **4** (top) and **5** (bottom). Hydrogen atoms have been omitted. **69**

35 A view of the unit cell of the complex **5** along the b axis, showing the segregation of the perfluoroalkyl chains and the stacking of the heterocyclic cores. **70**

36 Chemical structures of the starting tectons and corresponding halogen-bonded adducts. **72**

37 Ellipsoid representation (50% probability) of supramolecular layer of **HoFAZO** **74**

Index of tables.

Abstract.

The concepts of supramolecular chemistry are used throughout this work for the design and synthesis of efficient molecules and supramolecules for optoelectronics applications.

This work differs from the excellent work of Priimagi and Vaapavuori (see ref. 10 and 30 in the Introduction) because all the structures present here are formed by a self-assembly process induced by *halogen bonding*.

Halogen bonding (XB) is a high directional, strong and tunable non-covalent interaction that shares many features with the much better known hydrogen bonding. In particular the halogen bonding directionality is the main driving force of the interesting properties of the materials reported here.

This thesis is composed of five chapters.

In the introduction the features of supramolecular chemistry, photoactive materials, and halogen bonding are highlighted.

In the second and the third chapter, were investigated photoactive polymers and liquid crystals, respectively. In the case of the polymers it is demonstrated that halogen bonding is more reliable than hydrogen bonding in promoting the photoreponsive behavior. In the case of the liquid crystals it is demonstrated that halogen bonding is strong and directional enough to promote efficient photoalignment and Surface Relief Grating formation in the same complex. These phenomena usually occur in very different molecular environments.

In the fourth chapter, highly fluorinated azobenzene and heterocyclic supramolecules were studied. The investigation of the structure-function relationships in these structures will lead in the next future to very interesting supramolecular liquid crystals (in the case of the eterocycles) or photomoble crystals (in the case of the azobenzenes).

The fifth chapter is the experimental part.

1 Introduction.

1.1 Supramolecular science: a new tool for the design of complex materials.

In 1897 Paul Gaugain completed his masterpiece: "*D'où Venons Nous? Que Sommes Nous? Où Allons Nous?*" and this work certainly posed the greatest existential questions of mankind (**Fig. 1**).

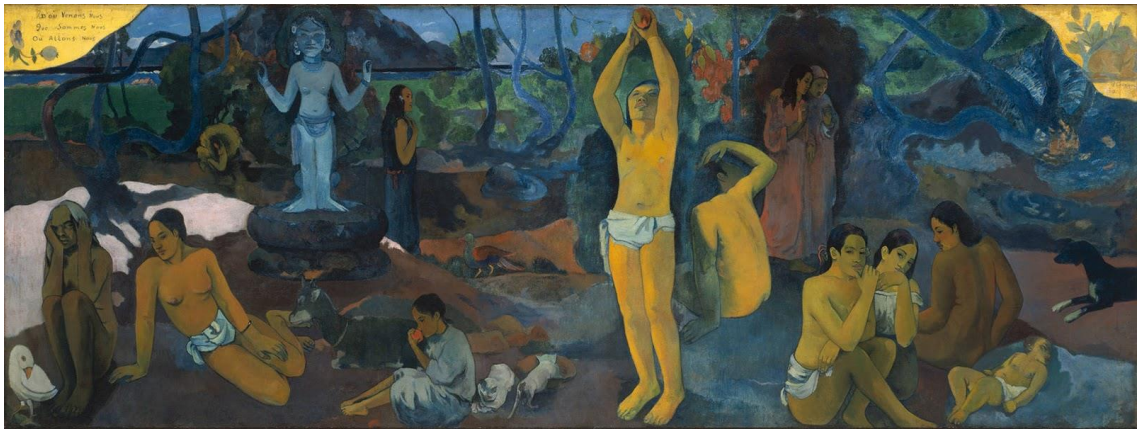

Fig. 1: *D'où Venons Nous? Que Sommes Nous? Où Allons Nous?* The painting is in the museum of fine arts in Boston, Massachusetts, USA.

Here Gaugain was mainly concerned with the philosophical aspects of these questions[1] but nowadays, science could provide useful hints about possible answers. While the ultimate physical theory is still missing, -with the two main candidate, strings[2] and loop quantum gravity[3], occupying two mutually exclusive positions- the Big Bang Theory[4] (not the American sitcom!) is certainly a good starting point. After about half a million of years –obviously after the Big Bang- universe had cooled down to 6000 K, allowing for the formation of the first atoms and molecules that constitute about the 4% of the whole energy. Chemistry born in those years, and it is primarily due to chemistry, and later to biology, that the first atoms organized into molecules and then into living and thinking entities (**Fig. 2**). In this perspective, covalent chemistry played the main role at the beginning, because of the assembly of the first molecules, but it cannot explain the high complexity of the constituents of living organisms, and we have to switch to a new concept, namely supramolecular chemistry[5], that developed highly complex structures from chemical components that interacts by means of non-covalent interactions.

Supramolecular chemistry studies the storage, transfer and processing of information at the molecular level through recognition events mediated by specific interactions, such as hydrogen bonding[6], ion cordination[7] or halogen bonding[8]. In this sense, molecular recognition and self-organization are the main themes of supramolecular science[5].

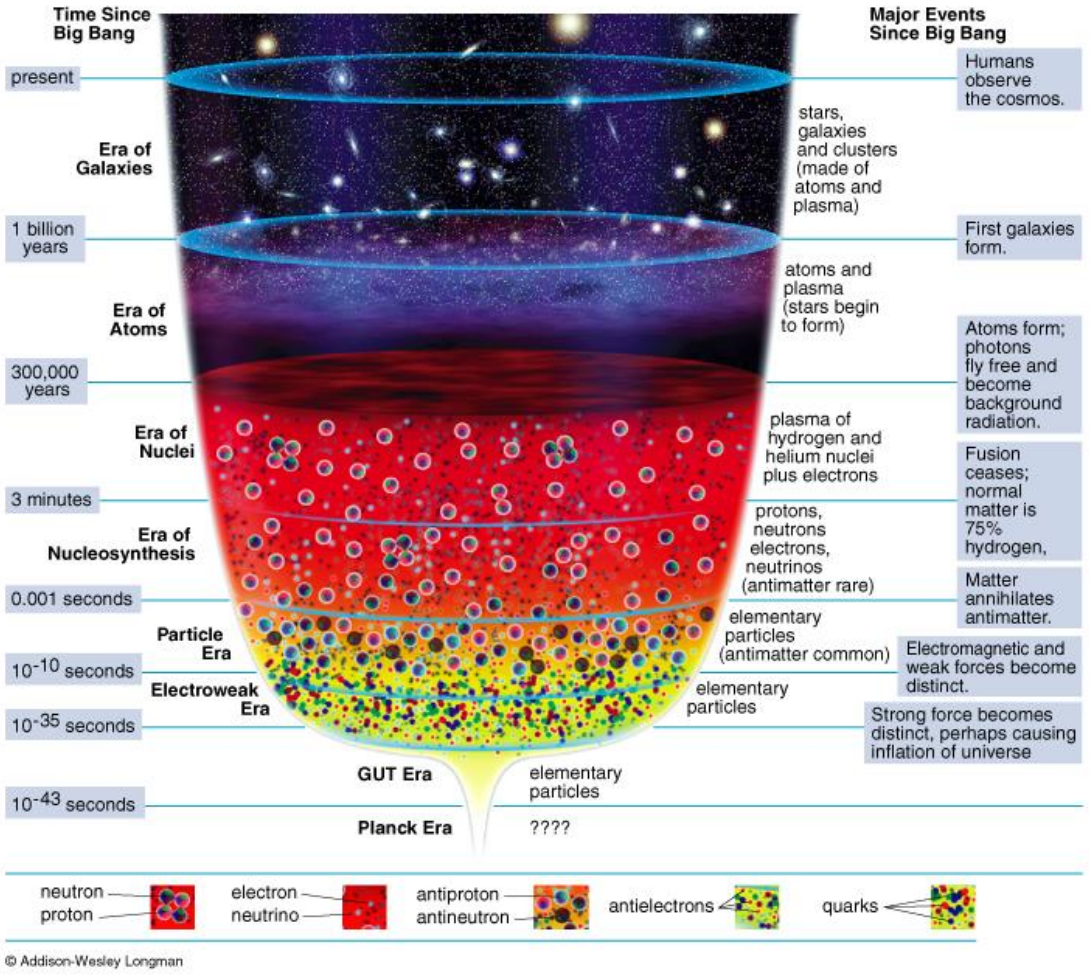

Fig. 2: The evolution of the universe, from the Plank Era to the Era of mankind.

All the work performed in this thesis is concerned about the construction of efficient supramolecules for materials applications. Given the fact that the properties of a material depend both on the constituents and on the interaction among them, it is expected that supramolecular chemistry could be a perfect tool to finely tune the intermolecular forces among the components, thus controlling their self-assembly towards the desired structure. The examples featured here includes supramolecular polymers and liquid crystals: recently polymers have been used to obtain highly efficient photoresponsive materials[9] through the direct incorporation of photoswitchable

modules into the final supramolecular structure[10], while liquid crystals with high conductivity and electro-optical activity have also been reported[11]. The intriguing features of these materials demonstrate the reliability of supramolecular chemistry to progressively assembly more and more complex systems by self-assembly and, together with supramolecular physics, it merges to supramolecular science that could give an answer to another fundamental question of mankind: “How does and did matter become complex?”[12]. Let’s hope to have an answer in the next future!

1.2 Photocontrolable supramolecules: towards a light driven materials world.

The problem of a sustainable energy harnessing is one of the most significant issues that the mankind has to address in the 21st century[13]. While it is certainly true that nuclear and especially fossil fuels will play a major role in the first half of the century[13], a greener change of paradigm is necessary. This could be addressed by solar energy[14]. Solar fuel serves to a broad range of applications, from artificial photosynthesis[15], to photovoltaic and photoelectrochemical cells[16], to the production of mechanical work[17]. While the problem of the energy harnessing is far from being solved, the photoisomerizable azobenzene supramolecules presented in this thesis are designed to accomplish the goal of a clean mechanical work production since they enable purely photo-controlled actuation, and thus use light as fuel to produce motion[9]. The effectiveness of azobenzene-based motors[18] and artificial muscles[19] lies in the process of photoisomerization that is clean, reversible and highly tunable by subtle variations of the chemical structure. It is also sensitive to the polarization direction of the incident radiation. These qualities are highly significant because they give rise to important differences between our materials and conventional photoresponsive media such as photoresists and photocurable polymers, which are typically isotropic and not able to carry any directional information[20]. The detailed connection between the molecular-level properties and the observed photoinduced motions occurring in azobenzene systems is still far from being completely understood, even if known to be driven by photoisomerization. As anticipated in the previous paragraph, in this work the features of supramolecular chemistry merges with those of azobenzene materials to produce highly efficient photoresponsive supramolecules having a structure that can be changed by tuning the non-covalent forces between the starting modules. This enables the control and the understanding of the structure-function relationship that govern the photoinduced movements in azobenzene-containing materials, that is very important to further develop the concept of clean and efficient energy-to-motion conversion by photocontrolable structures.

1.3 An overview on the azobenzene system.

Azobenzenes are molecules containing two aromatic rings held together by a nitrogen-nitrogen double bond. Due to the N=N link, they exist in two stereoisomeric forms, *trans* and *cis* (**Fig. 3**).

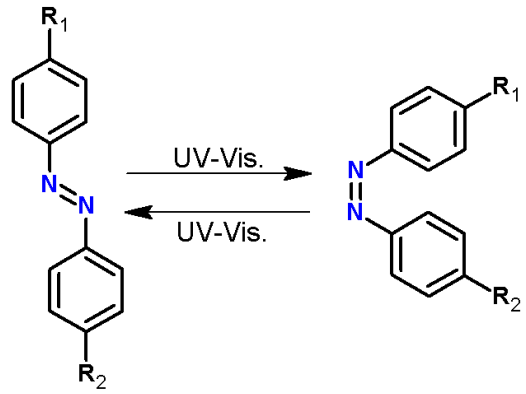

Fig. 3: Photoisomerization of a generic *trans* azobenzene to *cis* azobenzene and *viceversa*.

The *trans* form is thermodynamically more stable than the *cis* form, mainly due to the close proximity of the rings in the latter that leads to steric repulsion: this lead the *trans* isomer to be predominant at room temperature. The latter can be switched to the *cis* form by absorption of UV-visible radiation and the overall process depends on both the transition involved ($\pi \rightarrow \pi^*$ for the *trans* azobenzene) and on the wawelenght of the absorbed photon. Indeed, the maximum in the absorption spectra of azobenzene molecules can be easily tuned by changing the functional groups attached to the ring scaffold. This leaded Rau[21] to divide the azobenzenes into three classes, depending on the absorption spectra: (1) azobenzene type materials, that are chemically and electronically similar to the azobenzene molecule, (2) aminoazobenzenes, that have a weak *push-pull* character, and (3) pseudostilbenes that have strong electron donor and acceptor functional groups attached on the rings and thus have a pronounced *push-pull* character (**Fig. 4**). Azobenzene type molecules have a strong $\pi \rightarrow \pi^*$ band in the UV and a very weak $n \rightarrow \pi^*$ band at 440 nm (visible), while in pseudostilbenes the strong $\pi \rightarrow \pi^*$ band is red shifted and overlaps with the $n \rightarrow \pi^*$ one[22]. The *cis* isomer can isomerize to the *trans* form also by thermal relaxation. This process is slower than the photodriven isomerization and is in the order of days or hours for azobenzene type molecules, minutes for aminoazobenzene type molecules and seconds for pseudostilbenes. The stability of the *cis* form greatly influences the potential applications of an azobenzene derivative, and from an optic point of view the pseudostilbenes are the most interesting, because of the highly anisotropic electronic

distribution that leads to non-linear optic response[23]. Moreover, due to the overlap of the *trans* and *cis* spectra, irradiation at the maximum of absorption drives both the trans-cis and the cis-trans isomerization, thus resulting in an improvement of many optic effects[9].

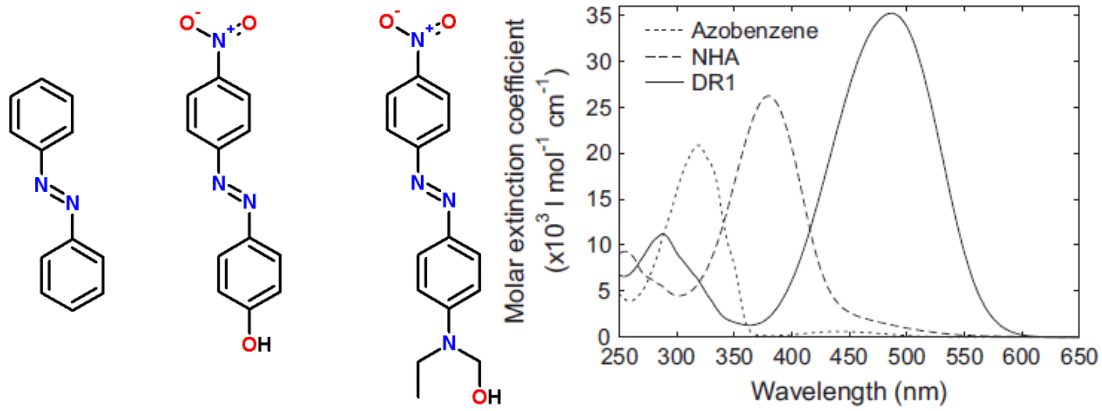

Fig. 4: On the left, examples of azobenzene molecules of azobenzene-type [azobenzene,first left], aminoazobenzene-type [4-nitro-4'-hydroxyazobenzene (NHA), center], and pseudostilbene-type [Disperse Red 1 (DR1), right]. On the right, absorption spectra of azobenzene, NHA and DR1 in $2*10^{-5}$ mol/l THF solution.

Up to now I discussed the photophysical features of azobenzenes that are relevant for useful applications, however, the most striking feature of azobenzenes is the possibility to produce photoinduced motions upon irradiation with UV-Vis. light. Two kinds of motions deserve a special discussion because of their relevance in this thesis: photoalignment[9], and surface relief grating (SRG) formation[24].

Photoalignment of azobenzenes is an effect that occurs at the *molecular level* as reported in **Fig. 5**. It could be interpreted with the tendency of azobenzenes in changing their orientation if irradiated. With linearly polarized light, the photoisomerization is only activated when the chromophore's $\pi \rightarrow \pi^*$ transition dipole moment axis has a component parallel to the light polarization[9]. The direction perpendicular to the light polarization is excluded from optical activation and will become enriched in chromophores. The concentration of the chromophores aligned perpendicular to the light polarization steadily increases under illumination with polarized light, until a saturation level is attained. The degree of alignment can be probed by measuring the polarized absorption spectra of the film. As illustrated in **Fig. 5**, the orientation of the chromophores can be disrupted by irradiation with unpolarized or circularly polarized light. The photoalignment phenomenon was first observed in solution in 1957[25] and applied in optics for the first time in 1984[26]; than starting from

90's the field started to be much more developed with hundreds of publications each year[27]. Photoalignment of liquid crystals[28] is an important topic of this thesis and will be discussed later.

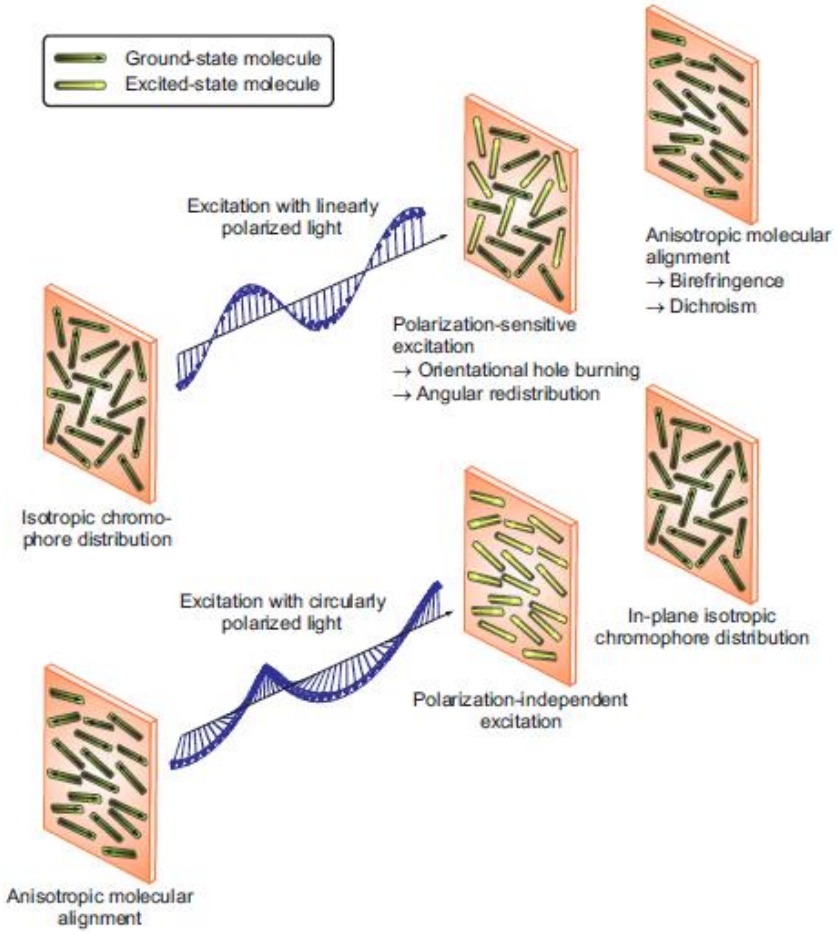

Fig. 5: Top: Schematic illustration of the photoinduced in-plane alignment of azobenzenes upon excitation with polarized light. Bottom: The initial isotropic state can be restored by irradiating the sample with unpolarized or circularly polarized light. (Reproduced from ref. 10 with permission)

The second type of motion, namely SRG formation, is more recent but has triggered a great amount of both fundamental and applied research since the discovery in 1995[29]. SRG formation occurs mainly in amorphous azopolymers: if a thin film is irradiated with an optical interference pattern, the material starts to migrate and move away from high-intensity areas to form a replica of the incident irradiation in the form of a surface-relief grating (**Fig. 6**). The complex process of SRG formation is not yet completely understood but it is thought to be driven by continuous *trans-cis-trans* cycling of the azobenzene molecules; this is the reason why pseudostilbenes -that isomerize with blue or green light- are the azobenzenes of choice to induce SRG. It is very important

that azobenzene groups are strongly bound to the polymer matrix because the SRG formation is very weak if the azobenzene derivative is simply mixed with a conventional polymer.

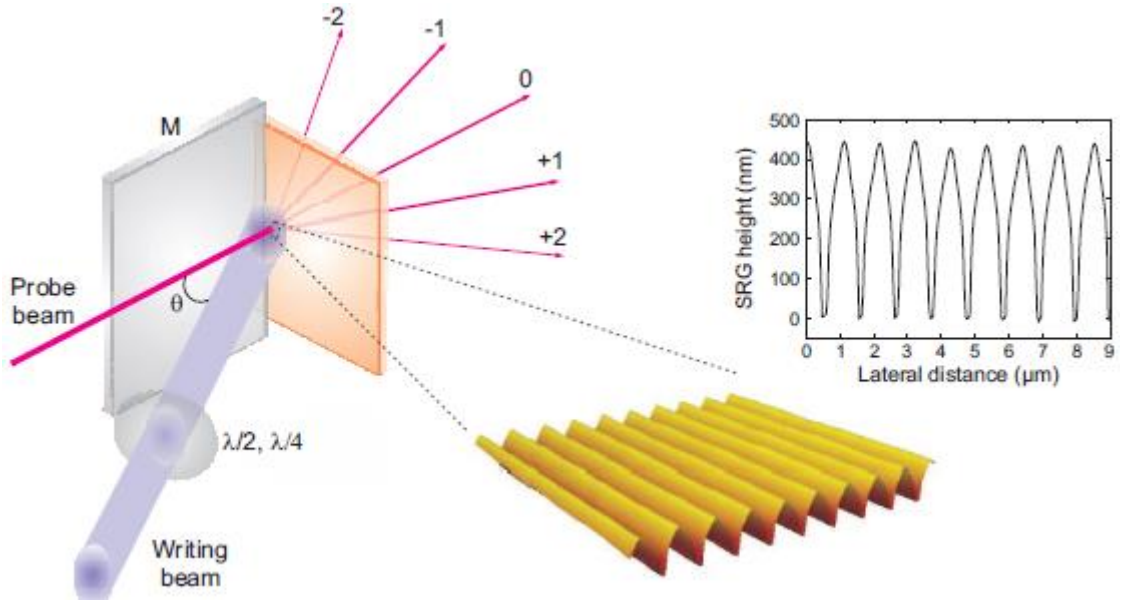

Fig. 6: Experimental setup for the inscription of surface-relief gratings. λ/2 and λ/4 denote wave plates that are used to control the polarization of the irradiation beam, and M refers to a mirror that reflects half of the incident beam onto the sample to form the interference pattern. (Reproduced from ref. 10 with permission)

This goal could be accomplished by covalent link, giving a polymer like the poly(Disperse Red 1 acrylate), or by non-covalent functionalization[10,30]; in this thesis, I adopted the former approach. Quite recently, it has been realized that patterned azopolymer films can be also used as molds and etching masks for an efficient and cost-effective microstructuring and nanostructuring of other materials[24]. This has significantly broadened the application potential of azopolymer SRGs, since they can now be used as a starting point for creation of periodic or self-assembled quasiperiodic[24] structures. Though much less common than in polymeric materials, the SRG phenomenon can also be observed on pure azobenzenes[31] or non-polymeric supramolecular structures[32], the latter being one of the main topics of this thesis.

1.4 Halogen bonding: history and theory.

In the first paragraph, halogen bonding (XB) was mentioned as one of the specific non-covalent interaction used in supramolecular science: It could be defined as an attractive interaction between an electrophilic region associated with a halogen atom in a molecular entity and a nucleophilic region in another, or the same, molecular entity[33]. Although the halogen bonding has a venerable history, only in the last 15 years the term "halogen bond" has been found frequently in the literature and the field is quickly expanding. The first described example of halogen bonding is the complex $H_3N\cdots I_2$ in 1863[34] followed by the benzene-iodine adduct in 1949[35]. In the 1950's and 1960's Hassel[36] and Mulliken[37] investigated extensively the dihalogen-Lewis base complexes, both theoretically and by single crystal X-ray diffraction, while in 1976 Dumas[38] was the man who coined the term "halogen bond" referring to the interaction between carbon and silicon halides with aliphatic and aromatic ethers. The first quantum chemical explanation of the origin of the halogen bonding is due to Politzer[39]; it could be understood in terms of molecular electrostatic potential $V(\mathbf{r})$ that is created by the nuclei and electrons of the molecule, and whose sign in a region depends upon whether the effect of the nuclei or that of the electrons is dominating there[40]. Electrostatic potential is computed on an isodensity surface of the molecule and it is usually negative near the lone pair of electronegative atoms, so one should expect to find a negative $V(\mathbf{r})$ in halogen atoms, making difficult to explain an interaction in which halogens interact with nucleophilic sites. In **Fig. 7** I reported the electrostatic potentials of the whole series of trifluomethanes CF_3X: X= F, Cl, Br, I. In CF_4 the halogen surface is negative, while a positive area appears with the other halogens; this region is located on the extension of the C-X bond; it enlarges and become more positive in the F→I series, while it decreases if the fluorine atoms in the CF_3 moiety are replaced with hydrogens (disappears in CH_3Cl). For this region the name σ-hole has been proposed[40]. The presence of σ-holes and their magnitude could be explained by a simple orbital model: when the halogen -iodine for example- interacts with carbon as in CF_3I it has the configuration $5s^2\ 5p_x^2\ 5p_y^2\ 5p_z^1$ and the $5p_z$ electron will be localized in the bond region, while the electron density of the outer lobe of the orbital will be depleted, forming the σ-hole. The positive potential of this region increases if one increase the polarizability of the halogen (iodine is the most polarizable) or the electron attracting power of the group attached to the halogen.

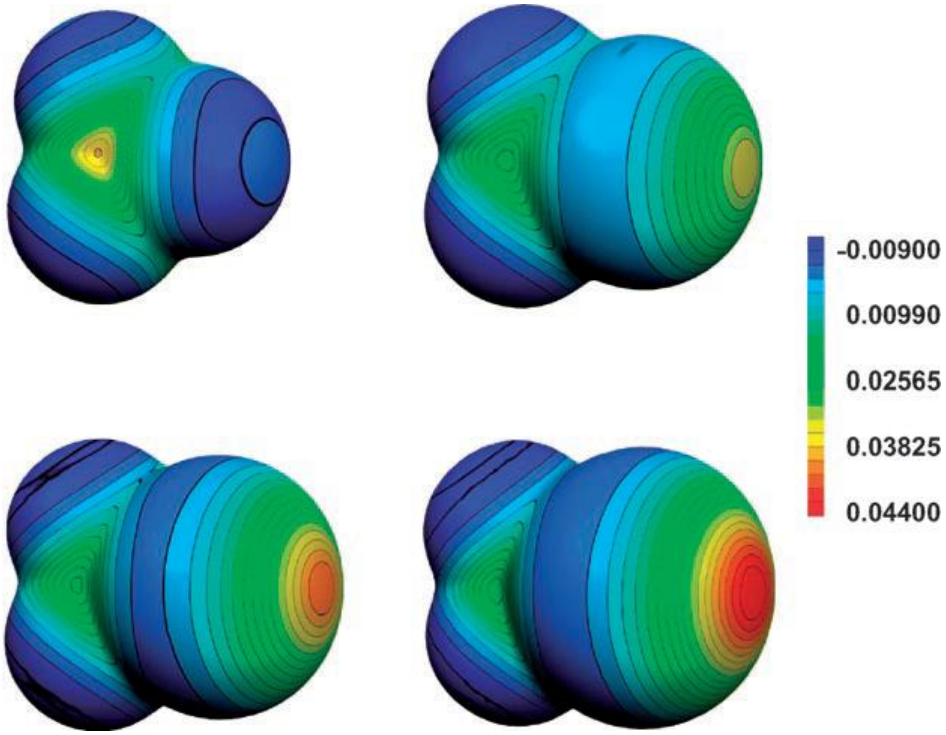

Fig. 7: Molecular electrostatic potential (Hartrees) mapped on the 0.001 au contour of the electron density: CF_4 (top left), CF_3Cl (top right), CF_3Br (bottom left), CF_3I (bottom right). Reproduced with permission from ref. 8

This means that the electron density distribution could be highly anisotropic, depending on the molecular environment, with the halogen having two different radii[41], a shorter one along the C-X bond and a longer one perpendicular to it: the first is due to the σ-hole, the second is due to the occupied $5p_x$ and $5p_y$ orbitals that create a negative $V(\mathbf{r})$ in the lateral side of the halogen (**Fig. 8**). The polarized halogen atom could thus interact with both nucleophiles, *via* σ-hole in a linear fashion, or with electrophiles *via* their negative lateral side in a "T-shaped" fashion, and this accounts for the high *directionality* of halogen bonding. Directionality is highly important for halogen bonding, because it allows for a direct comparison with other interactions, such as hydrogen bonding (HB) that is another non-covalent force which could be explained with electrostatic arguments, similarly to XB. Giving the fact that hydrogen has only one electron, one could expect that it's involvement in a covalent bond would leave a σ-hole on the extension of the covalent bond to H, in a similar fashion of halogen bonding[42] but it is more hemispherical and less narrowly focused than that of halogen atoms, making the HB less directional than XB[43]. The possibility to systematically change the halogen atom in a moiety allows one to finely tune the *strength* of halogen bond. It is

difficult to precisely quantify the strength of non-covalent interactions and theoretical calculations are the method of choice[44].

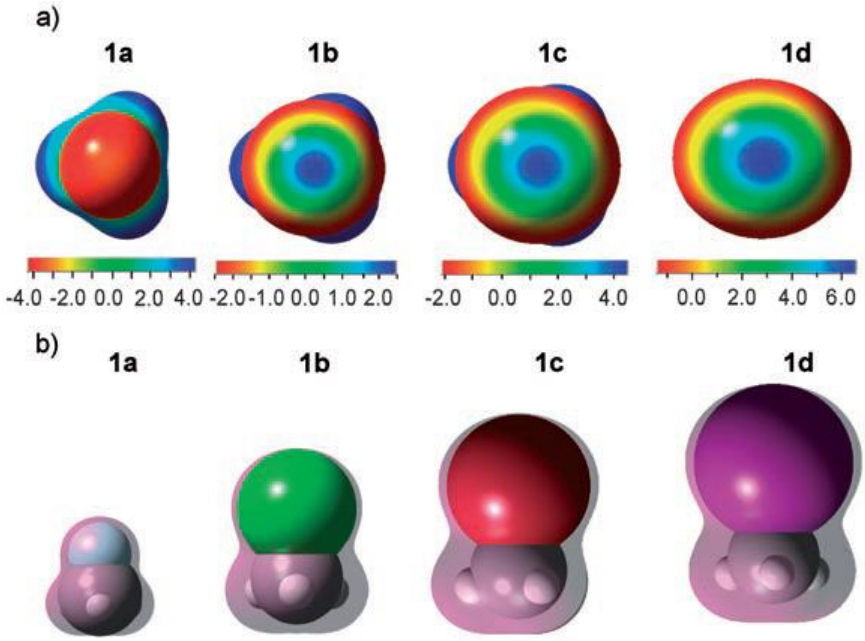

Fig. 8: a) Electrostatic potential surface -red more negative, blue more positive- for the series CH_3X. b) Electron density for the series CH_3X. The anisotropy in the electronic charge distribution is represented by the umbra around the spherical halogen. Reproduced with permission from ref. 21.

Halogen bonding is also more complicate to describe by theoretical methods than hydrogen bonding, because of two main reasons: first of all, the non-negligible contribution of the dispersion forces in the former requires high level *ab initio* methods[45]; moreover in heavy atoms such as iodine and even bromine, the features of *special relativity*[46] -relativistic effects[47,48]- are very important and an appropriate treatment is mandatory[49]. Despite these difficulties it has been shown that halogen bonds have a comparable or slightly weaker strength than hydrogen bonds[50] and this feature, combined with the directionality, makes the halogen bonding very attractive to assembly a plethora of new supramolecular architectures[8].

1.5 Halogen bonding: from crystal engineering to photoresponsive materials.

Crystal engineering studies molecular recognition and intermolecular interactions that drive the crystal packing in solids, with the purpose of obtaining new materials with desired topology and functions[51]. Given the directionality and strength of the halogen bonding, it is thus not surprising that it was first exploited in crystal engineering and later in materials science[52]. I want to discuss here two examples highly relevant for this work: the prevalence of halogen bonds over hydrogen bonds in co-crystals formation and in driving the performance of photoresponsive materials. It has been shown that 1,4-diiodotetrafluorobenzene forms one dimensional infinite chains in the 1:1 co-crystal with 1,2-bis(4-pyridyl)-ethane and that the formation of such a structure is driven by the N···I halogen bonding. A similar co-crystal has been obtained from the former derivative with hydroquinone -a hydrogen bonding donor- in the same conditions (**Fig. 9**).

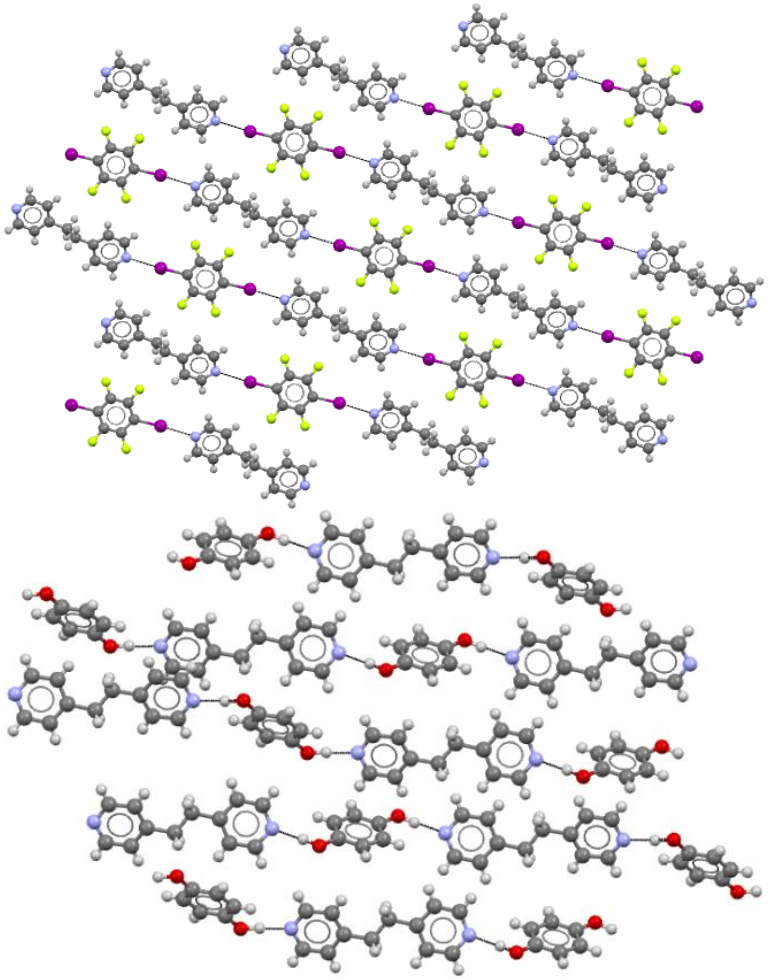

Fig. 9: The crystal packing of the halogen bonded co-crystals (Top) and the hydrogen bonded one (bottom).

While there has been some debate about the effective contribution of halogen bonding in driving the crystals packing of organic solids when aromatic tectons are involved[53], an experiment has been performed to demonstrate the effectiveness of XB compared to HB. The three components were co-crystallized together and only the halogen bonded co-crystal could be recovered[54] (**Fig. 10**).

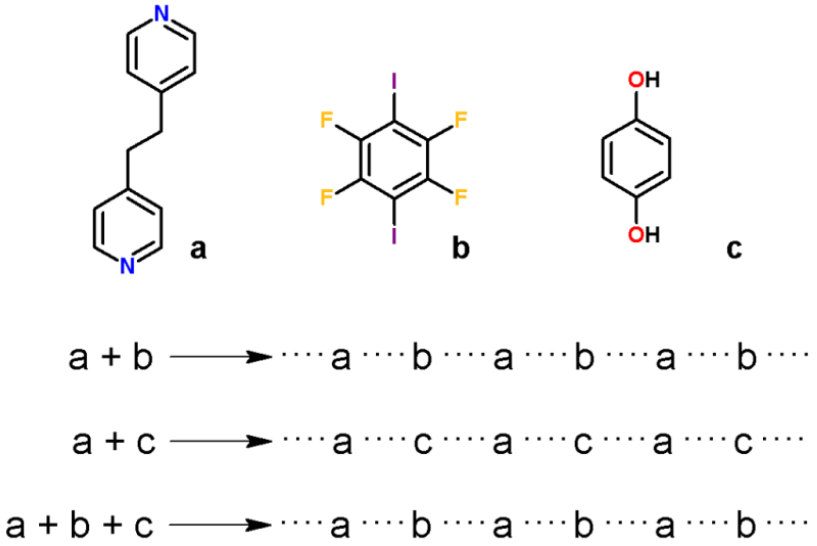

Fig. 10: The materials used in the co-crystallization experiments[54]. From a mixture of the three components, the hydroquinone remained in solution, while the pure a + b co-crystal was recovered.

Very recently, halogen bonding has been used also in materials science. Photoresponsive hydrogen bonded supramolecular polymers were extensively investigated by Priimagi[10] and Vaapavuori[36]. Very interesting results from a comparison between supramolecular polymers having hydrogen and halogen bonding donor azobenzene molecules come in 2012 by an Italian-finnish collaboration[55]. In **Fig. 11** are reported the materials used in that paper.

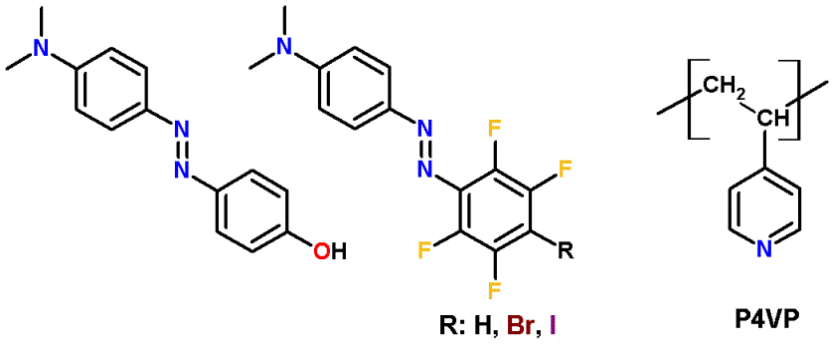

Fig. 11: The chemical structure of the azobenzenes used in ref. 55 and the structure of the poly(4-vinylpyridine).

Given the fact that it has basic sites that could interact with both hydrogen and halogen bonding donors, the poly(4-vinylpyridine) was used as polymer matrix. New pseudostilbene-class molecules were designed and synthetized, having a fluorinated ring with a halogen atom in *para* position (para in respect to the azo group). The molecule with the H atom *para* to azo was also prepared as a control molecule. It was found that the SRG formation efficiency develops in the order **I**> **Br**>> **H** and also the surface modulation depth was superior in the iodine containing azobenzene. The non-fluorinated azophenol was used to compare an hydrogen bonded azobenzene with the new halogen bonded systems, and quite surprisingly, the halogen bonded azobenzene with the iodine atom was superior to the azophenol, despite it is much strongly bound to the polymer matrix[56].

1.6 Conclusions.

In these few introductive paragraphs I highlighted the main features of this thesis. I started with supramolecular chemistry, because the concepts of self-assembly and molecular recognition were used for the design of all the materials prepared here. Then I reported the main features of photocontrollable materials because they are the main subject of this work, and could represent a great opportunity for a self-sustainable world. The majority of photocontrollable materials (all of those that are used here) are based on azobenzenes and this is the reason why I dedicated a paragraph to them. Last, but not least, halogen bonding is a recently rediscovered intermolecular force that proved to be particularly useful to assemble many functional supramolecular structures[57] and is the force that drives the self-assembly of all the supramolecular structures reported here.

References and notes:

(1) Gayford M. *The Yellow House: Van Gogh, Gauguin, and Nine Turbulent Weeks in Arles* Fig Tree, Penguin **2006**, 99.

(2) Chalmers M. *Phys. World* **2007**, *Sept*, 35.

(3) Rovelli C. *Int. J. Mod. Phys. D* **2003**, *12*, 1509.

(4) Linewear C. H.; Davis T. M. *Sci. Am.* **2005**, *292*, 36.

(5) Lehn J.-M. *Supramolecular Chemistry: Concepts And Perspectives* VCH, Weinheim, **1995**. ; Steed J. W.; Atwood J. L. *Supramolecular Chemistry (Second Edition)* John Wiley & Sons Ltd, Cheichester, **2009**. ; Lehn J.-M. *Science* **2002**, *295*, 2400.

(6) Prins L. J.; Reinhoudt D. N.; Timmerman P. *Angew. Chem. Int. Ed*. **2001**, *40*, 2383.

(7) Cotton F. A.; Lin C.; Murillo C. A. *Acc. Chem. Res*. **2001**, *34*, 759. ; Northrop B. H.; Zheng Y-R.; Chi K-W.; Stang P. J. *Acc. Chem. Res*. **2009**, *42*, 1554.

(8) Metrangolo P.; Meyer F., Pilati T.; Resnati G.; Terraneo G. *Angew. Chem. Int. Ed*. **2008**, *47*, 6114.

(9) Natansohn A.; Rochon P. *Chem. Rev*. **2002**, *102*, 4139.

(10) Priimagi A. *Polymer-Azobenzene Complexes: From Supramolecular Concepts to Efficient Photoresponsive Polymers* Helsinki University of Technology, Espoo, **2009**.

(11) Kato T.; Mizoshita N.; Kishimoto K. *Angew. Chem. Int. Ed*. **2006**, *45*, 38.

(12) Lehn J.-M. *Angew. Chem. Int. Ed*. **2013**, *52*, 2836.

(13) Armaroli N.; Balzani V. *Energy for a Sustainable World* Wiley-VCH, Wheinheim, **2011**.

(14) Balzani V.; Credi A.; Venturi M. *ChemSusChem* **2008**, *1*, 26.

(15) Gust D.; Moore T. A.; Moore A. L. *Acc. Chem. Res*. **2009**, *42*, 1890.

(16) O'Regan B.; Grätzel M. *Nature* **1991**, *353*, 737.

(17) Ikeda T.; Ube T. *Mater. Today* **2011**, *14*, 480.

(18) Haberhauer G.; Kallweit C. *Angew. Chem. Int. Ed*. **2010**, *49*, 2418.

(19) Nabetani Y.; Takamura H.; Hayasaka Y.; Shimada T.; Takagi S.; Tachibana H.; Masui, Z. D.; Inoue H. *J. Am. Chem. Soc*. **2011**, *133*, 17130.

(20) Seki T. *Light-Directed Smart Responses in Azobenzene-Containing Liquid-Crystalline Polymer Thin Films*, in *Functional Polymer Films*, edited by Knoll V. and Advincula R. Wiley-VCH, Wheinheim, **2011**.

(21) Rau H. *Photochemistry and Photophysics*, CRC Press, Boca Raton, **1990**.

(22) Dhammika Bandara H. M.; Burdette S. C. *Chem. Soc. Rev*. **2012**, *41*, 1809.

(23) Burland D. M.; Miller R. D.; Walsh C. A. *Chem. Rev*. **1994**, *94*, 31.

(24) Priimagi A.; Shevchenko A. *J. Polym. Sci. Part B. Polym. Phys*. **2013**, DOI: 10.1002/polb.23390.

(25) Teitel A. *Naturwissenschaften* **1952**, *44*, 376.

(26) Todorov S. T.; Nikolova L.; Tomova N. *Appl. Opt*. **1984**, *23*, 4309.

(27) From Web of Knowledge^{SM} (Accessed December 2013).

(28) Yaroshchuk O.; Reznikov Y. *J. Mater. Chem*. **2012**, *22*, 286.
(29) Rochon P.; Batalla E.; Natansohn, A. *Appl. Phys. Lett*. **1995**, *66*, 136.
(30) Vaapavuori J. *Design of efficient photoresponsive azobenzene materials through supramolecular functionalization* Aalto University, Espoo, **2013**.
(31) Nakano H.; Tanino T.; Shirota Y. *Appl. Phys. Lett*. **2005**, *87*, 061910.
(32) Priimagi A.; Saccone M.; Cavallo G.; Shishido A.; Pilati T.; Metrangolo P.; Resnati G. *Adv. Mater*. **2012**, *24*, OP 345.
(33) Desiraju G. R.; Ho P. S.; Kloo L.; Legon A. C.; Marquardt R.; Metrangolo P.; Politzer P.; Resnati G.; Rissanen K. *Pure Appl. Chem*. **2013**, *85*, 1711.
(34) Guthrie F. *J. Chem. Soc*. **1863**, *16*, 239.
(35) Benesi H. A.; Hildebrand J. H. *J. Am. Chem. Soc*. **1949**, *71*, 2703.
(36) Hassel O. *Science* **1970**, *170*, 497. (Nobel Lecture)
(37) Mulliken R. S.; Person W. B. *Molecular Complexes: a lecture and reprint volume* Wiley-Interscience, New York, **1969**.
(38) Dumas J-M.; Geron C.; Peurichard H.; Gomel M. *Chem. Res. (S)* **1978**, 54.
(39) Brinck T.; Murray J. S.; Politzer P. *Int. J. Quantum Chem.* **1992**, *19*, 57. ; Politzer P.; Lane P.; Concha M. C.; Ma Y.; Murray J. S. *J. Mol. Model*. **2007**, *13*, 305.
(40) Clark T.; Henneman M.; Murray J. S.; Politzer P. *J. Mol. Model*. **2007**, *13*, 291. ; Clark T. *WIRES Comput. Mol. Sci*. **2013**, *3*, 13.
(41) Awwadi F. F.; Willet D. R.; Peterson K. A.; Twamley B. *Chem. Eur. J*. **2006**, *12*, 8952.
(42) Shields, Z.; Murray J. S.; Politzer P. *Int. J. Quantum Chem.* **2010**, *110*, 2823.
(43) Legon A. C. *Angew. Chem. Int. Ed.* **1999**, *38*, 2686.
(44) Hohenstein G. E.; Sherrill C. D. *WIRES Comput. Mol. Sci*. **2012**, *2*, 304.
(45) Riley K. E.; Hobza P. *Phys. Chem. Chem. Phys*. **2013**, *15*, 17742.
(46) Einstein A. *Relativity: The Special and the General Theory* Henry Holt, New York, **1920**.
(47) I distinguish between *scalar relativistic* effects, i. e. those arising by the increase of the electron mass with velocity, and the *spin-orbit* interaction, generated by magnetic induction. Scalar relativity covers the largest part of relativistic effects and could be evaluated within the non-relativistic Schrödinger treatment with a (relatively!) little extra effort, while the *spin-orbit* and the higher order relativistic effects require a fully relativistic formalism. Here I consider only scalar relativistic effects. To the best of my knowledge fully relativistic calculations on non-covalent interactions have never been performed.
(48) Dyall K. G.; Faegri K. Jr. *Introduction to Relativistic Quantum Chemistry* Oxford University Press, Oxford, **2007**. ; Pyykkö P. *Ann. Rev. Phys. Chem*. **2012**, *63*, 45. ; Pyykkö P. *Chem. Rev.* **2012**, *112*, 371.
(49) Kozuch S.; Martin J. M. L. *J. Chem. Theory Comput.* **2013**, *9*, 1918.
(50) Řezáč J.; Riley K. E.; Hobza P. *J. Chem. Theory Comput.* **2012**, *8*, 4285.
(51) Desiraju G. R.; Vittal J. J.; Ramanan A. *Crystal Engineering A Textbook* World Scientific, Singapore, **2011**.

(52) Metrangolo P.; Resnati G.; Pilati T.; Biella S. *Struct. Bond.* **2008**, *126*, 105.

(53) Gavezzotti A. *Mol. Phys.* **2008**, *106*, 1473.

(54) Corradi E.; Meille S. V.; Messina M. T.; Metrangolo P.; Resnati G. *Angew. Chem. Int. Ed.* **2000**, *39*, 1782.

(55) Priimagi A.; Cavallo G.; Forni A.; Gorynsztejn-Leben M.; Kaivola M.; Metrangolo P.; Milani R.; Shishido A.; Pilati T.; Resnati G.; Terraneo G. *Adv. Funct. Mater*. **2012**, *22*, 2572.

(56) This was assessed by theoretical calculations at density functional level.

(57) Priimagi A.; Cavallo G.; Metrangolo P.; Resnati G. *Acc. Chem. Res*. **2013**, *46*, 2686.

Objectives.

Before presenting the work I did during my PhD it is useful to try to identify the objectives that motivated the studies I am going to present in this thesis work.

Encouraged by the work performed by Priimagi *et al*. on halogen bonded photoactive polymers, I tried to see if these system could tell something more to us. In particular if the prevalence of halogen bonding over hydrogen bonding in driving surface patterning phenomena is generalizable to systems featuring an extremely strong hydrogen bond such as perfluorophenols (Chapter 2). I was very satisfied when I discovered, together with Dr. Arri Priimagi, that this was really the case.

The objectives that lead to the discovery of the first photoactive halogen bonded liquid crystals were less obvious. I was inspired by the few halogen bonding liquid crystals reported and I tried to induce the liquid crystallinity in the iodo-azodye used by Priimagi *et al*. in their work about photoactive polymers, with known promesogenic molecules. The results were beyond our expectations. The resulting liquid crystalline complex showed not only a very efficient degree of photoalignment, but it was also very reliable in forming Surface Relief Gratings (Chapter 3). This is the first complex ever reported capable of doing this.

Highly fluorinated azobenzene and heterocyclic structures driven by halogen bonding were investigated with two main objectives. The azobenzenes were studied with the purpose of obtaining the first photomobile co-crystals, while the heterocyclic structures were prepared with the aim of obtaining supramolecular liquid crystals with improved properties (Chapter 4).

2 Halogen bonded photoactive polymers

2.1 Hydrogen is not forever.

As I anticipated in the introduction, halogen bonding is a high directional non-covalent interaction that shares many features with the much better known hydrogen bonding[1]. Recently many papers appeared in the literature about the coexistence or competition between halogen and hydrogen bonding in field such as crystal engineering[2], anion recognition and sensing[3], biochemistry[4], and even materials science[5]. Apart from the theoretical interest of this behavior, it is highly desirable to better understand the features of these intermolecular forces when they coexist or compete, because the highly technological applications in which supramolecular materials are expected to be involved, require more and more specialized structures, finely tuned to the desired function.

In the past 5-6 years, supramolecular photoresponsive side-chain polymers, where the photoactive azobenzene units have been attached to a passive polymer backbone via non-covalent intermolecular interactions, have emerged as a new class of SRG-forming materials[6], and are an excellent testing ground to assess the performances of hydrogen and halogen bonding. Some of the features of the first report on this comparison are reported in paragraph **1.5**. It has been shown that the efficiency of SRG formation increases with the strength of halogen bonding. Moreover, the directionality of the polymer-azobenzene noncovalent interaction seems to make a difference, as the SRG formation appeared more efficient in halogen-bonded complexes than in structurally related hydrogen-bonded complexes, the latter interaction being stronger but less directional. Although it was done a rigorous comparison between halogen bonded perfluorinated azobenzene derivatives, demonstrating that a single atom substitution makes the difference in the performance of the photoresponsive assemblies, the comparison was less perfect between halogen and hydrogen bonded systems: this is due to the fact that our reference hydrogen bonded azodye was not fluorinated, therefore its chemical and electronic properties differed from those of the other dyes considered (**Fig. 11**). The need for an unambiguous comparison between closely-related halogen and hydrogen bonded systems motivated me to extend the former study, in a way that I could compare the most efficient perfluoroiodo-azodye used in ref. 5 with one bearing a perfluorophenol

ring. In the present study, by comparing the SRG formation in complexes of poly(4-vinyl pyridine) and the fluorinated and non-fluorinated azobenzene derivatives shown in **Fig. 12** (**1**–**4**), we have shown that halogen-bonded polymer-azobenzene complexes unambiguously surpass their hydrogen-bonded counterparts in terms of SRG formation efficiency. This observation is important in view of supramolecular photoresponsive materials design as it confirms the hypothesis that in amorphous polymer-azobenzene complexes, the directionality rather than the strength of the non-covalent interaction dictates the macroscopic light-induced movements. Secondly, we point out through quantum-chemical calculations that fluorination plays a very distinct role in halogen-bonded and hydrogen-bonded complexes, greatly enhancing the polymer-azobenzene interaction strength (and the SRG formation efficiency) for the former while only slightly affecting that of the latter. Our results not only shed light to structure-function relationships of supramolecular SRG-forming materials – directionality makes a difference – but also highlight that the inherent tunability of halogen bonding through, e.g., fluorination cannot be transferred to hydrogen-bonding interaction because of the low polarizability of the hydrogen-bond donor moieties. The study is complemented by crystallographic investigations, which further enlighten the different performances displayed by halogen and hydrogen bonded systems.

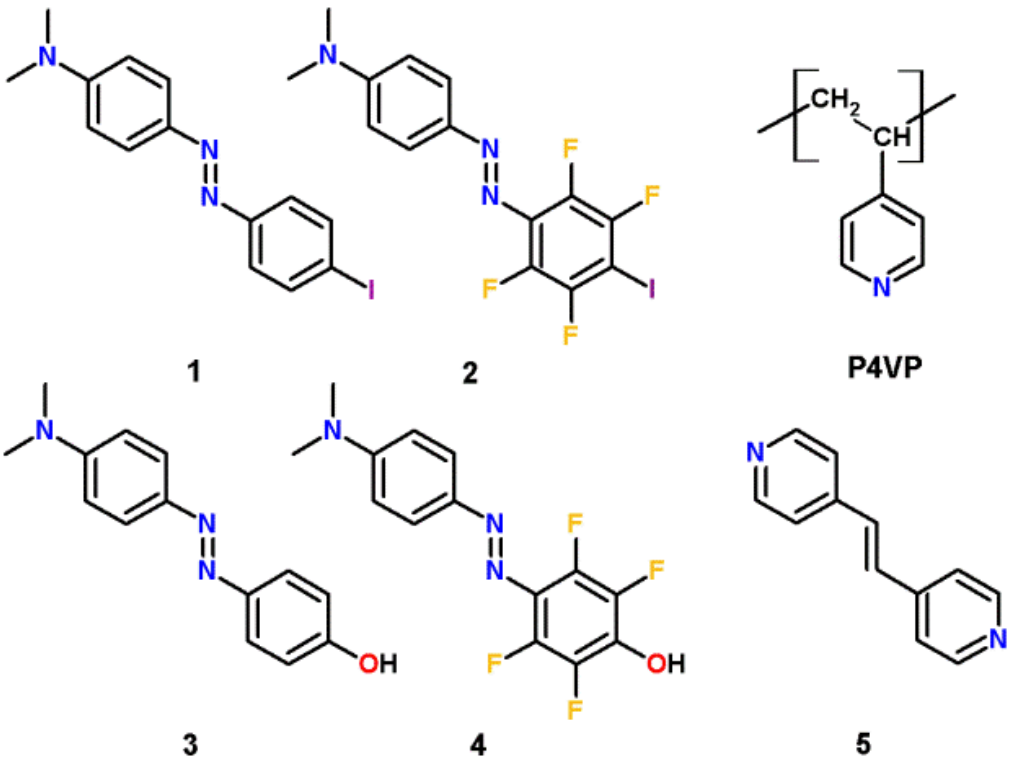

Fig. 12: The materials used in the present study.

2.2 Results and discussion.

Materials Design.

As a polymeric bond acceptor, we used poly(4-vinyl pyridine) (P4VP). It is a popular choice when constructing supramolecular polymeric complexes based on hydrogen bonding[7] or proton transfer[8], and it equally functions as a halogen-bond acceptor[9]. P4VP has also been used by several groups to prepare light-responsive polymeric complexes[10], rendering it the polymer of choice for the present study. We chose to work with low-molecular-weight P4VP (Mw 1000 g/mol, because long polymer chains tend to disrupt the photoinduced surface patterning phenomenon[11]. The azo compounds synthesized for the present work are shown in **Fig. 12** (These syntheses are discussed in the Experimental part). The series comprises a weak (**1**) and a strong (**2**) halogen-bond donor: herein the σ-hole and the polymer-azobenzene interaction strength are dictated by the fluorination of the bond-donating phenyl ring[12]. The iodoazo compounds **1** and **2** are compared to phenolic azo dyes **3** and **4** bearing nonfluorinated and fluorinated bond-donating phenyl rings, respectively. The perfluorinated ring with strong electron-withdrawing ability is often mandatory to have a strongly polarized halogen atom participating in halogen bonding[13], while the effect of fluorination on the strength of hydrogen bonding is much less studied[14]. Hence the compound **4** serves a dual purpose: (i) being structurally closely related, comparison of **2** and **4** allows us to study the role of halogen bonding versus hydrogen bonding in driving the SRG formation better than comparison between **2** and **3** which we carried out in ref. 5; (ii) the perfluorinated phenol could act as a very powerful hydrogen-bond donor that could give rise to extremely short contact and strong interaction[15], which would be interesting in its own right. Such extremely strong bonds are formed when the pK_a of the donor and the acceptor are similar[16]. For example, the shortest O-H$^{\cdots}$N hydrogen bond is found on the crystalline complex between pentachlorophenol (pKa 4.79) with 4-methyl pyridine (pKa 6.02). The pKa values for pentafluoro- and tetrafluorophenol are 5.33 and 5.41, respectively, comparable to that of pentachlorophenol.

The SRG formation was studied in polymer-azobenzene complexes, denoted P4VP(**X**)$_y$ where **X** is the azobenzene molecule (**1**-**4**) and y is the degree of complexation. Typically, we set y to 0.2, meaning that the systems contain one azobenzene moiety per five polymer repeat units. The low degree of complexation minimizes crystallization and macroscopic phase separation, which would compromise the comparison. In

quantum-chemical calculations and single-crystal x-ray analysis, we used small-molecule model compounds for P4VP, and chose for this purpose 4-methyl pyridine (computational studies) and the bis-pyridine derivative **5** (crystallographic characterization).

Theoretical analysis.

As stated, 4-methyl pyridine was used as a small-molecule model compound for the polymer to compute the stabilization energy with azobenzenes (**1**-**4**), $\Delta E = E_{complex} - (E_{4\text{-methyl pyridine}} + E_{dye})$. The energies computed for the complexes of 4-methyl pyridine with **1** / **2** were -2.546 / -5.135 kcal/mol, in good agreement with the CCSD(T) values computed at the complete basis set limit for complexes of pyridine with iodo- and iodopentafluorobenzene-, respectively. For the hydrogen-bonded complexes of 4-methyl pyridine and **3** / **4** the stabilization energies were -10.053 / -11.765 kcal/mol, corresponding to strong hydrogen bonds according to the Jeffrey classification[17]. The key observation here is that perfluorination of the benzene ring bonded to iodine or to the hydroxyl group is significantly much less effective in strengthening halogen bonding with respect to hydrogen bonding: the interaction strength doubles in the first case, whereas a minor, < 20 % enhancement takes place for the latter. It is also worth noting that, though weaker is the interaction more effective will be the perturbation due to fluorine atoms, the stabilization energy increases in absolute value definitely much more for halogen bonding than for hydrogen bonding. This difference can be rationalized by examining the changes in the local features of charge density distribution around iodine and the phenolic hydrogen in the isolated dyes upon fluorination. In fact, while the molecular dipole moment undergoes a greater increase for the phenolic with respect to the halogenated derivative (see **Table 1**), the electrostatic potential (see **Fig. 13**) is practically unaffected by fluorination near the phenolic hydrogens, though strongly positive (maximum values are 0.083 and 0.086 au for **3** and **4**, respectively). Conversely, the maximum value of the electrostatic potential around for the iodine atom, while less positive, yet doubles upon ring fluorination, ongoing from 0.018 au (1) to 0.035 au (2). This can be explained with polarizability arguments: it is well known that halogens are highly polarizable, the more the heavier is the halogen, as evidenced by the large dipole moments of **1** / **2** compared to **3** / **4**. As a result, the strength of halogen bonding significantly increases by introducing electron-withdrawing groups on the molecular moiety bonded to the halogen[12].

Compound	μ	λ	f	μ_{eg}	μ_e	$\Delta\mu$
1	9.28	466	1.48	12.13	16.53	7.25
2	10.22	486	1.60	12.85	17.31	7.09
3	5.65	455	1.35	11.42	11.62	5.97
4	7.63	467	1.20	10.91	12.94	5.31

Table 1: Computed data for the ground state and the dominant low-energy absorption band of compounds **1-4** in DMF: ground state dipole moments (μ, D), wavelengths (λ, nm), oscillator strengths (*f*), transition dipole moments (μ_{eg}, D), excited state dipole moments (μ_e, D) and difference between excited and ground state dipole moments ($\Delta\mu = \mu_e - \mu$, D). In all cases the absorption bands correspond to charge-transfer transitions from the Highest Occupied (HOMO) to the Lowest Unoccupied Molecular Orbitals (LUMO).

Here, we have further demonstrated that perfluorination is much more effective for iodine, compared to the OH group, in increasing the strength of the interaction with a Lewis base.

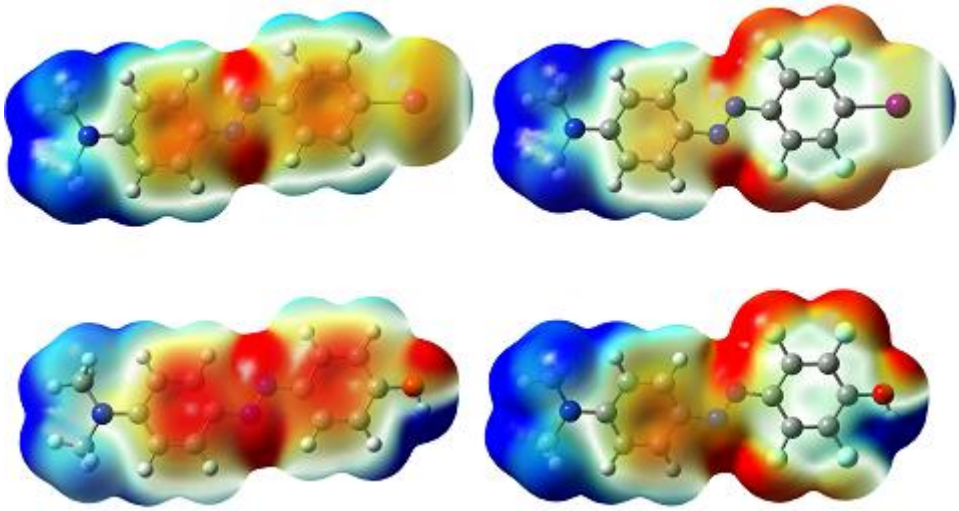

Fig. 13: Plots of the electrostatic potential of the compounds **1**–**4**: **1** top left, **2** top right, **3** bottom left, **4** bottom right. Potentials are mapped on the respective isosurfaces (0.001 a.u.) of electron density. Values of electrostatic potential range from –0.03 (red) to 0.03 (blue) a.u. Atom color scheme: C, gray; H, light gray; N, dark blue; O, red; F, sky blue, I, magenta.

Moreover, while, the hydrogen-bonded dimers are more stable than the analogous halogen-bonded ones, it is well evident from **Fig. 13** that halogen bonding is significantly more directional[18], because the positive region responsible for the noncovalent interaction is narrowly confined to the tip of the iodine atom whereas it is spread out hemispherically around the phenolic hydrogen. This very difference comprises the key of this study: we believe the directional noncovalent interaction to provide a more rigid junction between the photoactive units and the polymer backbone, which in turn enhances the light-induced macroscopic motions in the system. The

molecules **2** and **4** make a perfect pair to get further insights into this assumption. We also computed the UV-visible spectra for **1**-**4** by time-dependent DFT calculations (see **Table 1**), which showed that perfluorination red-shifts their absorption maximum in a greater extent for the iodine derivative with respect to the phenolic derivative, as was also verified experimentally by measuring the absorption spectra of the compounds in DMF solutions. Further details on these computations are given in the Experimental part.

Structural characterization.

Fluorophenols are extremely rare in crystal engineering, and a critical assessment of their interaction with suitable bond-accepting moieties is thus very important. Herein, we co-crystallized the compound **4** with the bis-pyridine derivative **5**, and obtained good-quality single crystals of trimers **6** by slow diffusion of diethyl ether in a 2:1 methanol solution (**Fig. 14**).

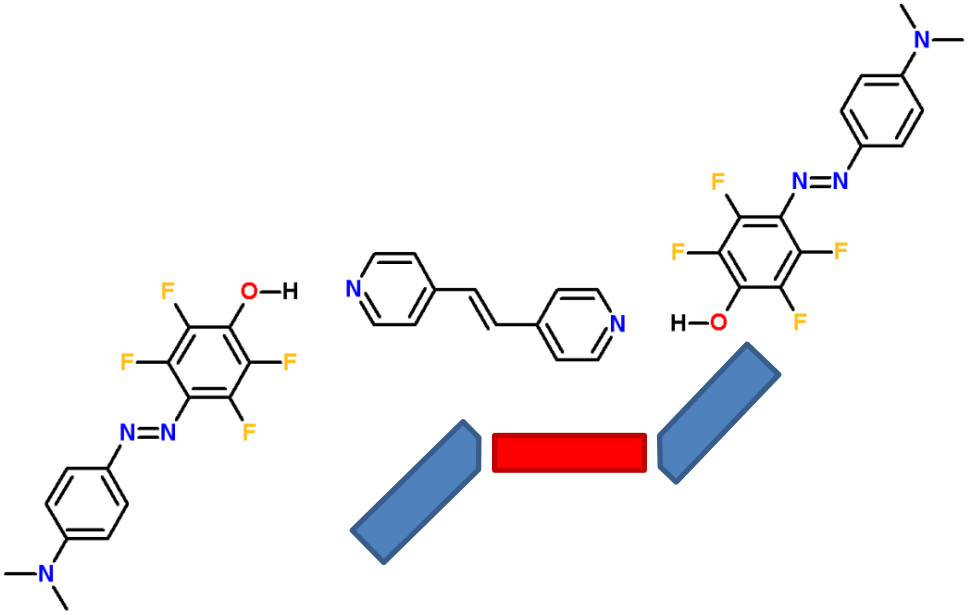

Fig. 14: The bent structure of the supramolecular complex **6** is directed by strong OH(Phen)-N(Pyr) hydrogen bonds.

As shown in **Fig. 15**, hydrogen bonding between the phenolic hydrogen of the azobenzene (**4**) and the pyridine nitrogen of the 1,2-Di(4-pyridyl)ethylene (**5**) drives the formation of the trimers. The O···N distance is 2.556 Å, the O···H distance is 0.979 Å and the N···H distance is 1.610 Å while the C-O···N angle is 127.93°.

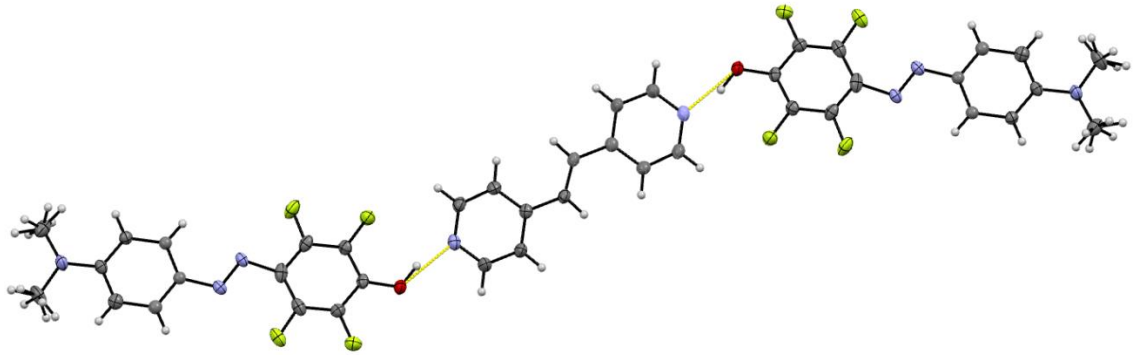

Fig. 15: The arrangement of compound **6** into hydrogen-bonded supramolecular trimers. O···N hydrogen bonds are in yellow. Ellipsoids are at 50% probability. Disorder is partially omitted.

Another motif that directs the packing of the trimers **6** is the perfluoroarene-arene quadrupolar interaction between the azobenzene tectons that are oriented in an antiparallel fashion (**Fig. 16**)[19]. The distance between the centroids of the fluorinated and non-fluorinated rings is 3.693 Å, almost the same observed in the benzene-hexafluorobenzene adduct[20]. These interactions are strong (3.7-5.6 kcal mol^{-1}) and very useful in crystal engineering[21] and in liquid-crystal self-assembly[22].

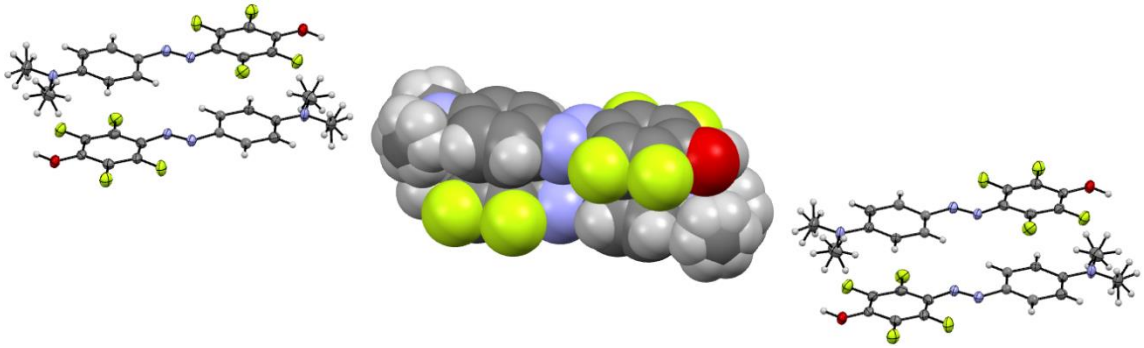

Fig. 16: Picture of the crystal structure of compound **6** showing the antiparallel orientation of the azobenzene molecules and the arene-perfluoroarene interactions. Disorder is partially omitted.

The hydrogen bond of **6** is shorter than in a co-crystal of the non-fluorinated compound **3** with a similar pyridine derivative[5] that is described in **Fig. 17**, in fact it approaches the already mentioned shortest hydrogen bond[16] that is in **Fig. 18** (see also **Table 2** for a detailed comparison). The bond lengths observed in the trimers bearing the azobenzene molecules **3** and **4** are well in line with the energy trend observed in the theoretical calculations of the complex formation between **3** or **4** with 4-methyl pyridine.

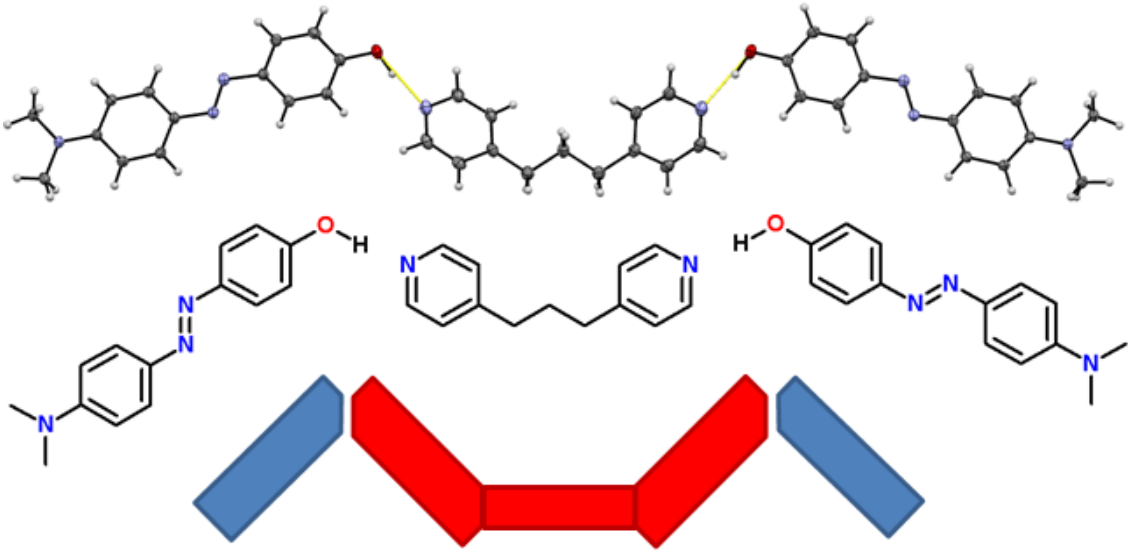

Fig. 17: Schematic representation and crystal structure of the hydrogen bonded complex described in ref. 5. The OH(Phen)···N(Pyr) hydrogen bonds are the major driving force of the crystal packing.

Herein I showed that the directional preferences of hydrogen bonding in phenol derivatives are towards bent structures (**Fig. 15**, **17**, **18**).

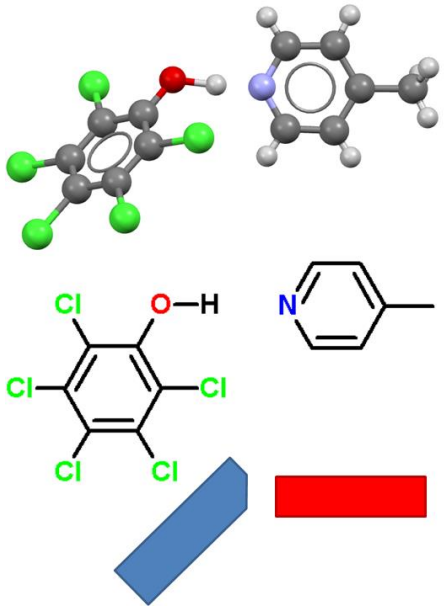

Fig. 18: Crystal structure of the complex featuring the shortest OH···N hydrogen bonding.

Halogen bonding instead has the tendency to form linear structures and furthermore to translate the tecton geometry into the self-assembled architecture geometry due to its directionality[23]. This is evident in **Fig. 19** showing **2** involved in halogen bonding with 1,2-Di(4-pyridyl)ethane.

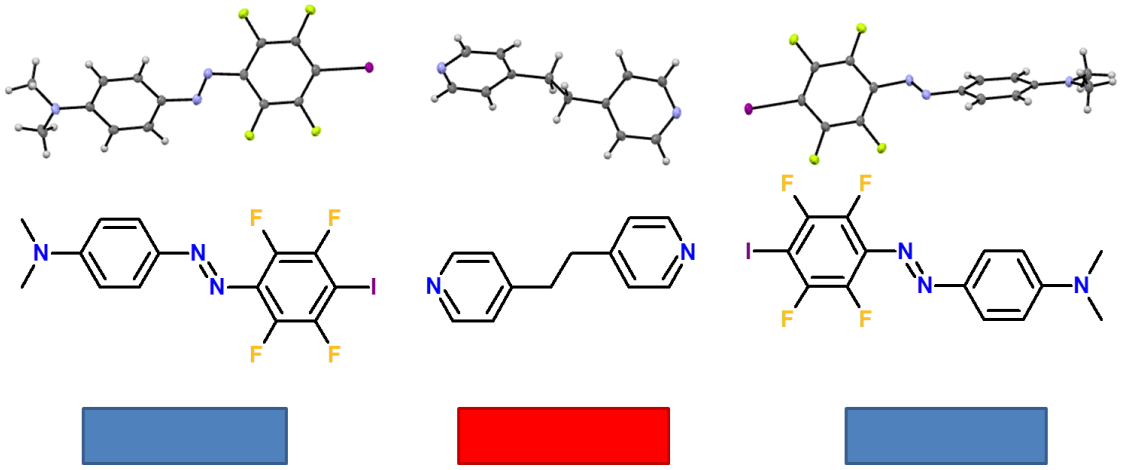

Fig. 19: Schematic representation and crystal structure of the halogen bonded complex described in ref. 5. As expected the N(Pyr)···I halogen bond is the main driving force of the packing. Quadrupolar interactions between arene-perfluoroarene rings are not present.

The noncovalent bonding between the tectons **4**, **3**, **2** and **5** was also probed by infrared spectroscopy. The pure 1,2-di(4-pyridyl)ethylene **5** has a symmetric ring stretching mode at 987 cm^{-1}, which exhibits a clear blue-shift of 26 cm^{-1}, 19 cm^{-1} and 7 cm^{-1} once complexed with **4**, **3** and **2**, respectively. The shift can be attributed to a reduced electron density over the N atom of the pyridine ring when it acts as a bond acceptor in hydrogen-/halogen-bond formation[5]. The larger the shift, the stronger the interaction, hence the infrared spectra further support the structural data and computations.

Crystal data				
Chemical formula	$C_{40}H_{32}F_4N_3O$ (**6**)	$C_{22}H_8F_8I_2N_4$ (**Fig 13**)	$C_{12}H_8Cl_5NO$ (**Fig 14**)	$C_{40}H_{32}N_8F_8I_2$ (**Fig 15**)
M_r	646.69	734.12	656.07	1000.45
Crystal system,	*Monoclinic,*	*Monoclinic,*	*Monoclinic,*	*Triclinic*
space group	*C2/c*	*P 21/c*	*C2/c*	*P-1*
Temperature	103(2)	103(2)	83(2)	103(2)
a, b, c (Å)	14.7987(6) 12.0088(6) 20.0244(11)	5.9388(10), 8.293(2), 22.160(4)	21.140(3), 10.0766(16), 9.5589(15)	5.9758(6) 13.998(2) 21.989(3)
α, β, γ (°)	90 90.598(3) 90	90 95.371(12) 90	90 111.347(12) 90	80.264(12) 88.694(12) 81.381(12)
V (Å^3)	3558.4(3)	1086.6(4)	1896.5(5)	1792.4(4)
Z	4	2	4	2
Radiation type	Mo *Kα*	Mo *Kα*	Mo *Kα*	Mo *Kα*
Crystal size (mm)	0.06 x 0.09 x 0.24	0.40 x 0.19 x 0.10	0.40 x 0.10 x 0.03	0.46 x 0.18 x 0.06
O···N distance (Å)	2.556	2.703	2.515	
O···H distance (Å)	0.979	0.990	1.222	
N···H distance (Å)	1.610	1.726	1.295	
I···N distance (Å)				2.818
Data collection				
Absorption correction	none	Multi-scan	Multi-scan	Multi-scan
No. of measured, independent and observed [$I > 2\sigma(I)$] reflections	33495, 3647, 2608	14181, 3840, 3177	12815, 1662, 1379	17334, 9283, 7497
R_{int}	0.0483	0.0208	0.0316	0.0201
$(\sin\theta/\lambda)_{max}$ (Å^{-1})	0.833	0.8	0.6	0.76
Refinement				
R [$F^2 > 2\sigma(F^2)$], $wR(F^2)$, S	0.0750, 0.1035, 1.096	0.0318, 0.0495, 1.059	0.0399, 0.0650, 1.076	0.0457, 0.0734, 1.047
No. of reflections	3647	3840	1662	9283
No. of parameters	287	163	1662	596
No. of restraints	338	0	137	509

Table 2: Crystal data for the complexes reported in this subchapter.

Surface patterning phenomena.

In order to study the SRG formation in halogen-bonded and hydrogen-bonded complexes, we prepared dimethyl formamide (DMF) solutions of the polymer–dye mixtures and spin-cast them as thin films on glass substrates. All the samples displayed high optical quality, having an average surface roughness of around 2 nm as measured by AFM. In order to prevent dye aggregation and phase segregation, we used the dye/polymer ratios of 0.2. The thin films are denoted as P4VP(i), where i corresponds to the dye molecule in question: I = **2**, OHSF = **3**, OH = **4**. The thin films exhibited similar absorption spectra as measured for the dyes in dilute solutions (**Fig. 20**), showing that no excessive dye aggregation took place in the films[8].

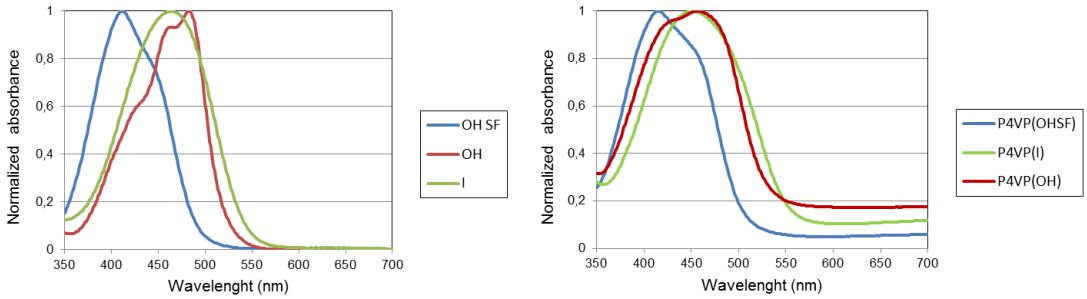

Fig. 20: Normalized UV-Vis spectra of the dyes **2**, **3** and **4** in (left) dilute DMF solution, and (right) thin films of P4VP(i)$_{0.2}$ complexes.

It is desirable that there are no difference in the *cis* isomer lifetime among the different dyes for meaningful comparison of their SRG formation efficiencies, to probe this, we studied the photochemistry of the P4VP-dye complexes. For the rate of thermal *cis*–*trans* isomerization of the dyes and complexes we obtained indeed very similar values for all the dyes considered. The films afforded high-quality SRGs upon irradiation with an interference pattern produced with circularly polarized light. The diffraction efficiencies and grating modulation depths for the complexes are shown in **Fig. 21**.

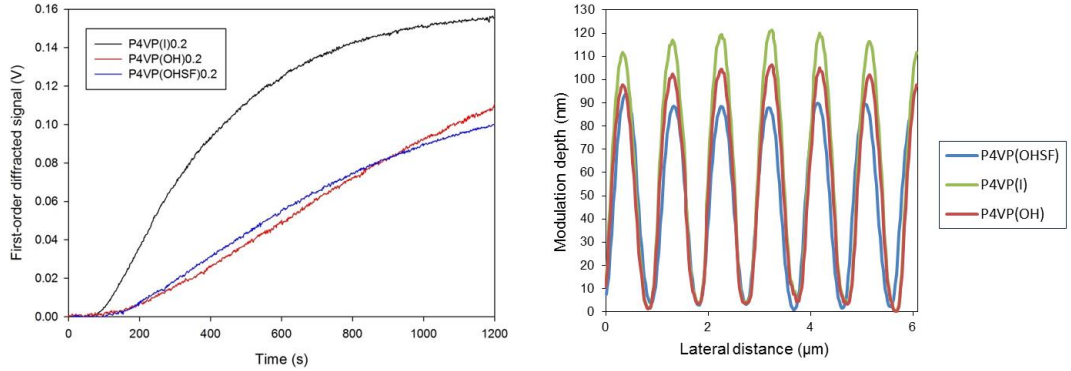

Fig. 21: Time evolution of the first-order diffraction efficiency of a He–Ne probe beam upon SRG formation (left) and the surface-modulation depth of the gratings (right).

The complex with **1** is not present in the figure because it yields essentially no diffraction and no surface modulation, whereas in the complexes of P4VP with **2**, **3** and **4** the first-order diffraction efficiency in transmission mode is approximately 3.8%, 2.1% and 2% after 20 min of irradiation, respectively. Even if their overall diffraction efficiencies are comparable (essentially the same for P4VP (**3**) and P4VP (**4**)), the SRG inscription rate of the two hydrogen bonded complexes P4VP (**3**) and P4VP (**4**) is slower than for the P4VP (**2**) complex, with the fluorophenol being slightly faster than the phenol. The diffraction efficiencies correlate excellently with the surface profiles (**Fig. 21**), which show that the modulation depths are ca. 110 nm, 90 nm, and 80 nm for the **2** , **4** , and **3** based complexes, respectively. However, the most striking difference between the halogen- and hydrogen-bonded samples lies in the time evolution of first-order diffraction efficiency, which is commonly used to monitor the build-up of the SRG. In the case of the halogen-bonded film, the initial slope of the curve, i.e., the SRG inscription efficiency, is significantly higher than for the hydrogen-bonded film, We note here that when the inscription was performed using s -polarized light, essentially no gratings were formed. This evidences the fact that under the experimental conditions used (inscription wavelength 488 nm, irradiation intensity 150 mW cm^{-2} , irradiation time 20 min), the grating formation is driven by light-induced mass transport, as opposed to thermal effects, ablation, and photodegradation, which start playing a role at higher irradiation intensities and are polarization-independent[24].

2.3 Conclusions.

From the present measurement it is clear that the perfluoroiodo azodye **2** is the most efficient in driving the SRG formation, and the performance of the perfluorophenol dye **4** is quite inferior and similar to that of **3** despite it is bound to the polymer matrix considerably stronger than **2**. Here we can safely rule out the possibility that the superior efficiency of **2** is due to the higher absorption at the irradiation wavelenght compared to **4**, because this is not the case (**Fig. 20**). Also the difference in the chemical structure due to the presence of a perfluorinated ring, which was invoked in the previous report[5] to explain the better performance of **2** compared to **3**, seems not to be the driving force of the grating formation. **3** and **4** display a similar efficiency, despite relevant structural differences. This is probably due to the higher absorption of **4** at the irradiation wavelenght. Indeed the superior directionality of the halogen bonding compared to hydrogen bonding, is the most convincing explanation for this behaviour. It has been demonstrated that halogen bonding involving iodoperfluorobenzenes can successfully compete with hydrogen bonding involving phenols in driving the crystal packing of bis-pyridine derivatives with aromatic tectons[2]. On the other hand theoretical calculations show that simple iodobenzenes are weak halogen bonding donors and a stable complex with the polymer matrix is not formed in the solid state. The non-fluorinated iodobenzene is thus the least efficient dye of those examined.

References and notes:

(1) Politzer P.; Murray J. S.; Clark T. *Phys. Chem. Chem. Phys*. **2013,** *15*, 11178.

(2) Aakeroy C. B.; Fasulo M.; Schultheiss N.; Desper J.; Moore C. *J. Am. Chem. Soc*. **2007**, *129*, 13772. ; Corradi E.; Meille S. V.; Messina M. T.; Metrangolo P.; Resnati G. *Angew. Chem. Int. Ed.* **2000**, *39*, 1782.

(3) Chudzinski M. G.; McClary C. A.; Taylor M. S. *J. Am. Chem. Soc.* **2011**, *133*, 10559.

(4) Voth A. R.; Khuu P.; Oishi, K.; Ho P. S. *Nature Chem*. **2009**, *1*, 74.

(5) Priimagi A.; Cavallo G.; Forni A.; Gorynsztejn-Leben M.; Kaivola M.; Metrangolo P.; Milani R.; Shishido A.; Pilati T.; Resnati G.; Terraneo G. *Adv. Funct. Mater*. **2012**, *22*, 2572.

(6) Priimagi A.; Shevchenko A. *J. Polym. Sci. Part B. Polym. Phys*. **2013**, DOI: 10.1002/polb.23390.

(7) Brinke G. ten; Ikkala O. *Chem. Rec*. **2004**, *4*, 219.

(8) Priimagi A.; Cattaneo S.; Ras R. H. A.; Valkama S.; Ikkala O.; Kauranen M. *Chem. Mater*. **2005**, *17*, 5798.

(9) Bertani R.; Metrangolo P.; Moiana A.; Perez E.; Pilati T.; Resnati G.; Rico-Lattes I.; Sassi A. *Adv. Mater*. **2002**, *14*, 1197.

(10) Priimagi A.; Lindfors K.; Kaivola M.; Rochon P. *ACS Appl. Mater. Interfaces* **2009**, *1*, 1183.

(11) You F.; Paik M. Y.; Häckel M.; Kador L.; Kropp D.; Schmidt H. W.; Ober C. K. *Adv. Funct. Mater*. **2006**, *16*, 1577.

(12) Riley K. E.; Murray, J. S.; Fanfrlik J.; Rezac J.; Sola R. J.; Concha M. C.; Ramos F. M.; Politzer P. *J. Mol. Model*. **2011**, *17*, 3309.

(13) Metrangolo P.; Pilati T.; Resnati G.; Biella S. *Struct. Bond*. **2008**, *126*, 105.

(14) Wong J. P. W.; Whitwood A. C.; Bruce D. W. *Chem. Eur. J*. **2012**, *18*, 16073.

(15) Steiner T. *Angew. Chem. Int. Ed*. **2002**, *41*, 48.

(16) Majerz I.; Malarski Z.; Sobczyk L. *Chem. Phys. Lett*. **1997**, *274*, 361 ; Steiner T.; Majerz I.; Wilson C. C. *Angew. Chem. Int. Ed*. **2001**, *40*, 2651.

(17) Jeffrey G. A. *An introduction to hydrogen bonding* Oxford University Press, Oxford, **1997**.

(18) Politzer P.; Murray J. S. *Chemphyschem* **2013**, *14*, 278.

(19) Meyer E. A.; Castellano R. K.; Diederich F. *Angew. Chem. Int. Ed*. **2003**, *42*, 1210.

(20) Williams J. H.; Cockcroft, J. K.; Fitch N. *Angew. Chem. Int. Ed. Engl*. **1992**, *31*, 1655.

(21) Yoon M.-H.; Facchetti, A.; Charlotte E. S.; Marks T. J. *J. Am. Chem. Soc*. **2006**, *128*, 5792.

(22) Kishikawa K. *Isr. J. Chem*. **2012**, *52*, 800.

(23) Saccone M.; Cavallo G.; Metrangolo P.; Pace A.; Pibiri I.; Pilati T.; Resnati G.; Terraneo G. *CrystEngComm* **2013**, *15*, 3102.

(24) Yager K. G.; Barrett C. J. in *Smart Light-Responsive Materials*, edited by Zhao Y. and Ikeda T. John Wiley & Sons, Hoboken, NJ **2009**.

3 Halogen bonded photoactive liquid crystals.

3.1 Not separate and not equal.

Liquid crystals (LCs), sometimes coined as “the fourth state of matter”, are ubiquitous in our present-day lives. Lying in between isotropic liquids and crystalline solids, LCs combine the mobility of the former and the orientational order of the latter. Examples of liquid crystals in which the mesophase formation is driven by specific non-covalent interactions such as arene-perfluoroarene quadrupolar interactions[1] or hydrogen bonding[2] are widespread in the literature and, as I wrote in the first chapter, halogen bonding shares many features with the much well known hydrogen bonding: indeed this similarity was used to exploit its full potential in materials science[3]. Inspired by this similarity, halogen bonded liquid crystals have been demonstrated 10 years ago[4] and recently reviewed in great detail[5]. Almost all these systems (exceptions do exist)[6] features iodoperfluorobenzene rings interacting with pyridine derivatives that are known to induce a liquid crystalline phase in hydrogen bonded systems[7]. Due to the presence of perfluorinated and non-fluorinated rings one could expect that some kind of arene-perfluoroarene stacking could be the driving force of the mesophase formation or the crystal packing. Analysis of the many single-crystal structures obtained does not show them to be dominated by such an interaction and indeed explicit experiments[4] using C_6F_6 show that quadrupolar interactions are not factors in the mesomorphism of these materials. Halogen bonding thus makes the difference, being the driving force of the self-assembly of these materials and it is also responsible for the stability of the mesophases. Encouraged by the great performance of halogen bonded photoactive polymers, I tried to design a small molecule complex featuring the photoactive azo group and useful liquid crystalline properties. Azobenzene derivatives, due to their large structural change upon photoisomerization, are versatile photochromic units that are considered as the ultimate photoswitches for many applications[8]. Indeed, azobenzenes can act as “master” molecules that control, through collaborative movements, the orientation of neighboring “slave” molecules[9]. This property makes azobenzenes highly attractive for photoalignment control (either when doped into a material system of interest or through so called “command surfaces”[10] (also see Gelbaor et al.[11] as an example of inorganic photoalignment layer) and for the design of rewritable photoresponsive optical elements[9,12]. The potential of azobenzene-based

materials is further boosted by their unique photomechanical response[13] the most-pronounced examples of which are photoinduced threedimensional motion and mass transport. The latter takes place upon irradiating azobenzene thin films with light bearing an intensity/polarization gradient: for instance, a sinusoidal interference pattern at the sample surface can lead to a sinusoidal surface corrugation, often referred to as a surface-relief grating (SRG)[14]. It is noteworthy that *efficient photoalignment and SRG formation usually occur in very distinct molecular environments*, the former being boosted by collaborative effects and the existence of LC phases[15]. Conversely, SRG formation can be severely suppressed by LC behavior, particularly at high spatial frequencies[16] even if detailed structure– performance relations of the process are not completely understood. Majority of azobenzene-based photoalignment and SRG materials studied to date are polymeric, due to their desirable film-forming and mechanical properties. However, SRG formation is a highly complex process involving the motions of both light-responsive units and polymer chains. Hence, issues related to polydispersity and polymer-chain entanglement may compromise the efficiency and reproducibility of the mass-migration process, rendering the grating formation efficiency strongly dependent on, for example, the molecular weight of the polymer[17]. In 2002, Nakano et al. demonstrated that amorphous low- M w photochromic materials can also undergo photoinduced mass transport, and soon after they showed that the SRG formation in such molecular glasses can, in fact, be more efficient than in corresponding polymeric materials[18]. Later on, the SRG formation in amorphous low- M w glasses has been studied by several other research groups, with the particular aim of understanding the structure–performance relationships governing this complicated photomechanical process[19], and photoinduced SRG formation on a single crystal has also been reported[20]. At the same time, photoactive low- M w glasses were investigated in a number of other applications[21], but being amorphous, they are not suitable candidates for efficient photoalignment. The best low- M w materials for photoalignment have been reported by Zakrevskyy et al. who have shown that ionic self-assembled LC complexes can exhibit exceptionally high values of photoinduced anisotropy with dichroic ratios as high as 50[22]. However, no SRG formation occurred in their complexes.

Herein, we show that halogen-bonded low- Mw LC complexes can exhibit both high degree of photoinduced anisotropy upon irradiation with polarized light (promoted by liquid crystallinity)[15,23] and efficient photoinduced mass transport upon irradiation with an interference pattern (promoted by the directionality of halogen bonding)[24]. The

strategy we adopted was to synthesize a halogen-bond-donor molecule incorporating an azo group and assemble it with an alkoxystilbazole, which is a known promesogenic molecule[7] and has proven particularly reliable for the construction of new halogen-bonded, supramolecular mesogens[4]. This design strategy allowed us to obtain an order parameter of molecular alignment exceeding 0.5 upon excitation with linearly polarized light, as well as to inscribe an SRG with surface-modulation depth exceeding the initial sample thickness by a factor of 2.4.

3.2 Results and discussion.

Supramolecular Complex Design and Structural Characterization.

The halogen-bonded complex **3** was prepared by self-assembly of the *N*, *N* -dimethyl-4-[(2,3,5,6-tetrafluoro-4-iodophenyl) diazenyl]aniline (**1**) and 4-[(*E*)-2-(4-methoxyphenyl)-ethenyl]-pyridine (**2**), as shown in **Fig. 22**.

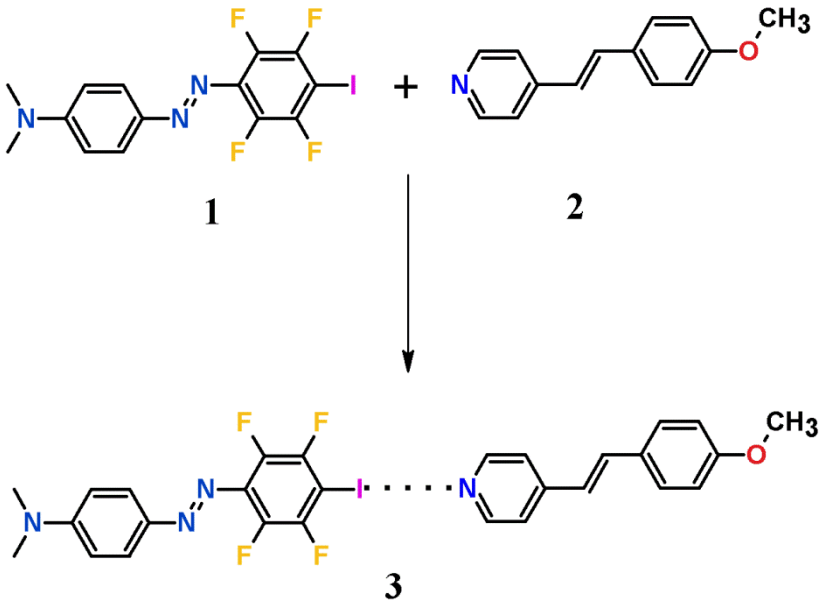

Fig. 22: Chemical structures of the azobenzene **1** and the stilbazole **2** modules, and their halogen-bonded complex **3**.

Generally, the number of carbon atoms (*n*) in the flexible alkoxy chain of the stilbazole module affects the type of the given mesophase: Nematic phases are seen for complexes with *n* = 1–5, while longer alkoxy chains (*n* = 6–10) promote smectic phases[25]. Since long alkyl chains have been reported to suppress the formation of SRGs in LC polymers[16], we decided to use the methoxy-substituted stilbazole (**2**). The structure of the azobenzene compound is optimized for efficient SRG formation, due to the presence of the dimethylamino group that promotes efficient trans–cis–trans cycling upon photoirradiation[26]. Moreover, the iodine atom on the tetrafluorobenzene ring is a very good halogen bond-donor site and it is possible to foresee the formation of a quite strong interaction with the pyridyl moiety of the stilbazole module[24]. Therefore, the rod-like structure of the dimeric complex, driven by the highly directional halogen bond, is anticipated to promote liquid crystallinity, and as a result photoalignment[15,22], while the lack of long flexible chains and the presence of the dimethylamino group would promote SRG formation. To investigate the supramolecular organization of the

halogen- bonded complex in the crystal lattice, single crystals of **3** were grown by slow isothermal evaporation of an equimolar solution of the starting components in tetrahydrofuran (THF). To investigate the supramolecular organization of the halogen-bonded complex in the crystal lattice, single crystals of **3** were grown by slow isothermal evaporation of an equimolar solution of the starting components in tetrahydrofuran. As expected, halogen bonding between the pyridyl nitrogen atom and the iodine atom of the azobenzene module is the structure-determining factor that drives the self-assembly of the dimeric complex between **1** and **2** (**Fig. 23**).

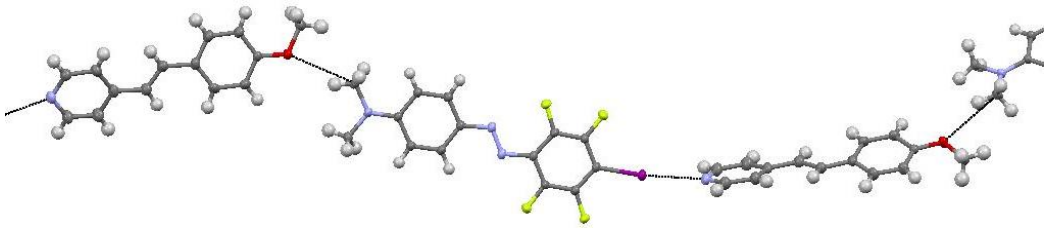

Fig. 23: Halogen bonding drives the self-assembly of the azobenzene **1** and the stilbazole **2** into the dimeric supramolecular complex **3**. A weak hydrogen bond involving the methoxyl oxygen atom and a methyl hydrogen of the dimethylanilino group promotes the self-assembly of these dimers into infinite polar chains.

The N···I distance is 2.860(2) Å, corresponding to *ca*. 19 % contraction of the sum of the van der Waals radii for N and I. The C–I···N angle is 173.64(7)°, which is perfectly consistent with the expected high directionality of halogen bonding. The halogen-bonded dimers self-assemble head-to-tail into highly undulated polar chains as a consequence of a much weaker hydrogen bond involving the methoxyl oxygen atom and a methyl hydrogen of the dimethylanilino group ($C21_{met}$···O1 distance: 3.316(3) Å). In the crystal lattice these polar chains stack in an antiparallel manner through *π*-*π* interactions between the tetrafluorophenyl ring and the methoxybenzene ring (the distance between benzene centroids (C1-C6)···(C22-C27) is about 3.57 Å; **Fig. 24**) and residual crystal packing interactions (mainly H···F contacts), resulting in an overall centrosymmetric structure. In order to verify that the 1:1 ratio of the starting compounds observed in the single crystal was also representative of the entire bulk sample, we performed ^{1}H NMR experiments. By calculating the ratio between the integral of the –$N(CH_3)_2$ signal of the azobenzene compound at 3.15 ppm and the –OCH_3 signal of the stilbazole at 3.85 ppm, we were able to confirm the 1:1 bulk stoichiometry of the azobenzene–stilbazole complex.

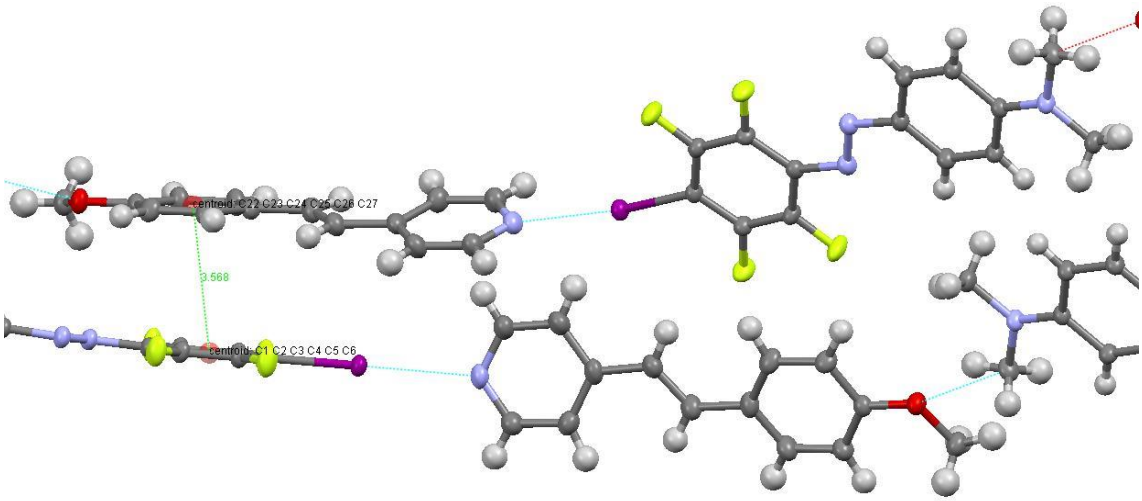

Fig. 24: Crystal packing of the supramolecular complex **3** formed upon XB driven self-assembly of **1** and **2**.

Moreover, powder X-ray diffraction analysis (**Fig. 25**) confirmed that the crystalline bulk sample had the same crystal structure as determined on one single crystal of **3**.

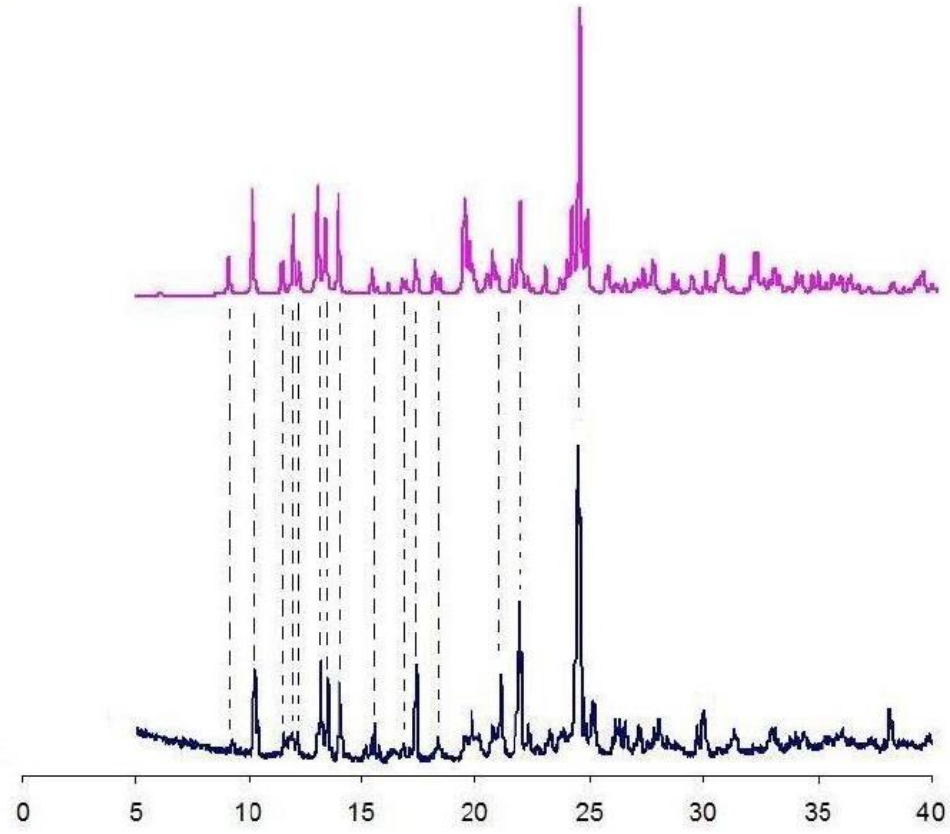

Fig. 25: Simulated from single crystal data (top) and experimental (bottom) PXRD patterns of **3**.

The halogen bond-driven complex formation was also verified using infrared (IR) spectroscopy. It is well-established that halogen bonding between pyridine and iodo-

perfluoroarene moieties leads to a blue-shift and intensity decrease in the pyridine bands in the region 3000-3100 cm^{-1} and a red-shift of the bands associated with the tetrafluorophenyl ring[27]. This is clearly evident in the infrared spectrum of the complex **3** (see **Table 3**). The ν_{C-H} absorption of the pure stilbazole at 3021 cm^{-1} becomes less intense upon complexation and shifted to 3025 cm^{-1} as a result of a higher positive charge on the pyridyl hydrogens in the complex. A blue-shift is also observed for the four bands associated with the pyridine ring breathing vibrations at 1585, 1572, 1507, and 1415 cm^{-1}. Similar shifts have been observed in hydrogen-bonded adducts and attributed to increased stiffness of the pyridine ring when it behaves as a hydrogen bond-acceptor[28]. A same increased stiffness can also be anticipated for pyridine rings working as halogen bond-acceptors. On the other hand, due to an increased electron density of the fluorinated ring upon XB formation, the vibrations related to the fluorophenyl moiety at 1476, 940, and 806 cm^{-1} for the *p*-iodo-tetrafluorophenyl ring in pure **1** are red-shifted to 1472, 933, and 799 cm^{-1}, respectively, upon complex formation.

	1	**3**		**2**
		bulk	**film**	
Pyridine ν_{C-H} *stretching*		3025	3027	3021
Pyridyl *ring breathing*		1589	1590	1585
Pyridyl *ring breathing*		1575	1576	1572
Pyridyl *ring breathing*		1510	1511	1507
Pyridyl *ring breathing*		1417	1420	1415
Fluorophenyl ν_{C-F} *stretching*	1476	1472	1474	
Fluorophenyl ν_{C-F} *bending*	940	933	931	
Fluorophenyl ν_{C-F} *bending*	806	799	798	

Table 3: Selected FT-IR absorptions (cm^{-1}) of **1**, **2**, and their halogen-bonded complex **3**.

The liquid-crystalline properties of the complex **3** were examined by hot-stage polarized optical microscopy (POM). Despite the non-mesogenic nature of the starting materials, the halogen-bonded complex **3** showed a nematic LC phase. On heating, the complex melted directly to the isotropic liquid at 423 K. Upon cooling from the isotropic phase, a monotropic nematic phase was observed (**Fig. 26**a) with an isotropic-to-nematic phase-transition temperature of 404.8 K (cooling rate: 5 K/min; mesophase temperature range: 18.2 K). The thermal behavior was reproducible, even after several excursions into the isotropic phase.

Thin film characterization and phoresponsive behavior.

In order to study the photoresponsive behavior of the halogen-bonded complex **3**, we prepared non-annealed spin-coated thin films on glass substrates (thickness *ca*. 250 nm). The films were crystalline at room temperature (**Fig. 26**b), and exhibited relatively high optical scattering.

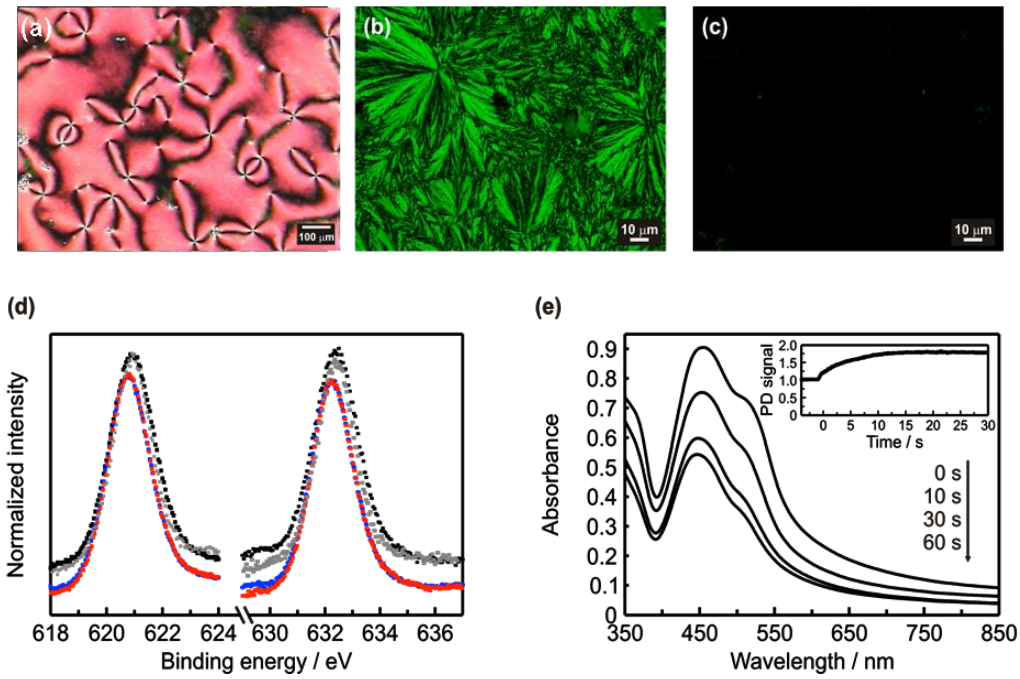

Fig. 26: (a) POM image of the nematic LC phase shown by **3** on cooling from the isotropic state. (b) POM image of a spin-coated (crystalline) thin film of **3**. (c) Upon irradiation with circularly polarized light (488 nm, 30 s, 100 mW/cm^2), the crystal structure is destroyed and the film becomes opaque when imaged between crossed polarizers. (d) Normalized I3d core-level XPS spectra of the starting compound **1** (black and gray curves), **3** (blue curve), and **3** after irradiation with circularly polarized light (red curve). The red-shift in the binding energy in **3** as compared to **1** is an indication of halogen-bond formation between **1** and **2**. (e) Light irradiation induces significant changes to the absorption spectrum of **3**, and reduces optical scattering of a 633 nm He–Ne probe beam (inset).

Their average surface roughness was approximately 30 nm, as determined by atomic-force microscopy (AFM). **Fig. 26**b displays a POM image of the spin-coated crystalline thin film. The texture shown is reproducible, and the films are stable at ambient conditions for several months. The occurrence of halogen bonding in spin-cast thin films of **3** was verified by X-ray photoelectron (XPS) and IR spectroscopy. XPS is a powerful tool for studying halogen bonding in supramolecular complexes as the I3d binding energies are sensitive to noncovalent interactions and shift to slightly lower

energies upon complexation[29]. The spectra of the I3d doublet are shown in **Fig. 26**d. For the starting azobenzene molecule, the doublet binding energies are 620.94 eV/632.33 eV; for the spin-coated thin film of the azobenzene–stilbazole complex these values are 620.81 eV/632.26 eV. These shifts are small but repeatable, indicating that halogen-bonded species exist also in the spin-coated films. This was further confirmed by IR analysis: The thin films exhibited blue-shifts for several bands of the stilbazole moiety and corresponding red-shifts for the bands attributable to the fluorinated aromatic ring, identical to the bulk samples, as reported in the **Table 2**. Even a short irradiation with a 488 nm laser beam (30 s, 100 mW/cm^2, circular polarization; the wavelength was chosen to induce both *trans–cis* and *cis–trans* photoisomerization of the azobenzene) transforms the pristine crystalline film (**Fig. 26**b) into an amorphous film. As a consequence, the film appears as opaque when imaged between crossed polarizers (**Fig. 26**c), *i.e.*, it becomes macroscopically isotropic. Such *photoinduced isotropization* results in various changes in the absorption spectrum of the complex (**Fig. 26**e). The gradual decrease in absorbance is an indication of the *trans–cis* photoisomerization of the azobenzene moiety. The low-energy shoulder in the absorption spectrum becomes less pronounced, most likely due to changes in the molecular packing upon photoirradiation, and the optical scattering, seen as a relatively large extinction in the NIR-region, decreases significantly. Equivalently, the reduced scattering can be seen as increased transmittance of a non-resonant (633 nm) He–Ne probe beam through the sample (**Fig. 26**e, inset), based on which we can observe that 30 s irradiation suffices to reach saturation, *i.e.*, to break the crystal structure. Due to the reduced scattering, the irradiated isotropic films were used as a basis for further optical measurements, although similar results were also obtained using non-irradiated pristine crystalline films. Importantly, the irradiated isotropic film displayed I3d binding energies identical to those seen in the pristine crystalline sample, confirming that irradiation does not disrupt the halogen bonding within the film (see **Fig. 26**d). Upon irradiating the spin-coated thin films with linearly polarized light (488 nm) at room temperature, they became highly anisotropic (**Figure 27**). Based on the example spectra are shown in **Fig. 27**a, 2 min irradiation at moderate intensity (100 mW/cm^2) leads to a 49 % decrease in the absorbance parallel to the polarization direction of the excitation beam, and a 38 % increase in the absorbance in the perpendicular direction. This result is a clear evidence of a photoinduced reorientation of the supramolecular complex **3**. Prior to irradiation, the molecular alignment is random, but excitation with

linearly polarized light causes the molecules to align preferentially in the direction perpendicular to the polarization plane, which is seen as an increase in $A_{\perp}$[22].

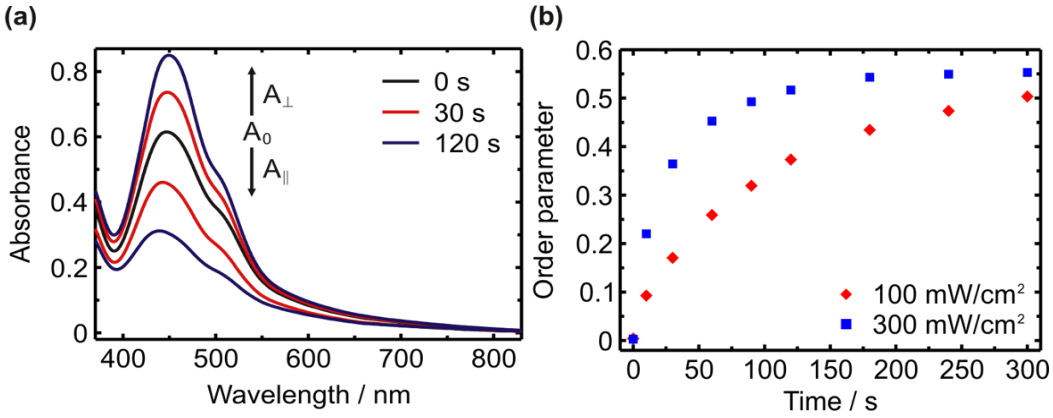

Fig. 27: (a) Selected polarized absorption spectra of a spin-coated thin film of **3** after irradiation with linearly polarized light (488 nm, 100 mW/cm^2). Black curve: initial spectrum (same for both polarizations). The red and blue curves correspond to the polarized absorption spectra in the directions parallel ($A_{||} < A_0$) and perpendicular ($A_{\perp} > A_0$) to the polarization plane, taken after 30 s and 120 s of irradiation time, respectively. (b) The time evolution of the order parameter of molecular alignment at different irradiation intensities.

Based on the polarized absorption spectra, the order parameter of molecular alignment can be determined as $S = (A_{\perp} - A_{||})/(A_{\perp} + 2A_{||})$, which is plotted at different time instances in **Fig. 27**b. If the irradiation intensity is increased, the reorientation dynamics is speeded up, and for 300 mW/cm^2 irradiation intensity the order parameter of molecular alignment exceeds 0.5 already after 2 min of irradiation. The order parameter of 0.5 is quite typical for nematic liquid crystals and sufficiently high for many purposes: for instance typical nematic liquid-crystal displays have an order parameter of 0.4[30] .The anisotropic alignment order remains stable over, at least, a period of several months at ambient conditions. However, unlike for many azobenzene-containing polymers[9], the alignment order could not be satisfactorily randomized with circularly polarized light even if slow decrease in order parameter upon circularly polarized irradiation was observed.

The efficient photoalignment of the low-M_w supramolecular complex **3** can be attributed to its high-temperature liquid crystallinity[31], even if further investigations are required to comprehensively understand the connection between the molecular-level properties, structural properties, and the optical response. In spite of the fact that the photoalignment experiments are carried out at room temperature, the LC nature, which enhances the molecular cooperative motions, allows both the acceleration and

stabilization of the photoinduced anisotropic molecular alignment. This was recently demonstrated by Kodar, Schmidt and coworkers using low-M_w tris-azobenzene derivatives[31]. Moreover, even if the dichroic ratio of 50 reported by Faul, Stumpe *et al*. in their self-assembled ionic LCs[22] is beyond our reach, the present complex possesses an important and unique advantage compared to previously reported low-M_w photochromic materials, which is combining efficient photoalignment and SRG inscription.

The essence of the SRG inscription investigations is summarized in the **Fig. 28**. Upon irradiating the thin film (**Fig. 28**a) with a polarization interference pattern generated using a two-beam interferometer setup with counter-circularly polarized beams and a period of 2 μm, the complex underwent pronounced photoinduced surface deformation (**Fig. 28**b). The SRG formation is driven by *polarization modulation* (in case of two counter-circularly polarized beams intersecting at small angle the intensity profile within the interference pattern is essentially flat) rather than intensity modulation, which was verified by the observation that when *s*-polarized input beams were used (producing intensity-modulated interference pattern with no polarization modulation), no gratings were formed. The troughs of the surface pattern appear as flat, which indicates that *all material is removed from the troughs of the grating*.

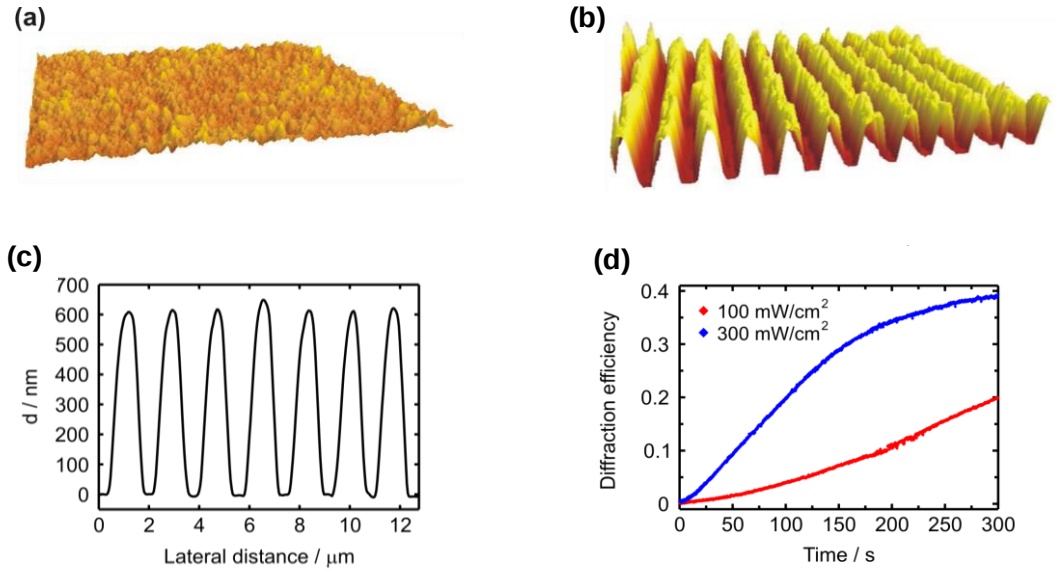

Fig. 28: Atomic-force microscope views of the spin-coated thin film of **3** (a) before, and (b) after the SRG inscription (5 min, 300 mW/cm^2). (c) The surface-modulation depth of the grating shown in (b); (d) The time evolution of the first-order diffraction efficiency of a He–Ne probe beam upon SRG formation using different irradiation intensities.

This is confirmed by the AFM surface-profile (**Fig. 28**c): The surface-modulation depth is 600 nm, which is 2.4 times higher than the initial sample thickness of 250 nm. We used first-order diffraction to monitor the surface-deformation dynamics, as shown in **Fig. 28**d. Being driven by subsequent *trans–cis–trans* photoisomerization cycles, SRG formation dynamics is highly intensity dependent: 300 mW/cm^2 irradiation (for both beams) results in 40% diffraction efficiency within 5 min exposure whereas the dynamics is significantly slower when irradiation intensity of 100 mW/cm^2 is used. By increasing the inscription intensity to 500 mW/cm^2, 40 % diffraction efficiency is obtained within 2 min exposure.

The most sensitive SRG materials reported to date are based on the so-called "phototriggered mass migration" phenomenon occurring in LC polymers, as introduced by Seki *et al*.[32] In such materials, however, the mechanism of the grating formation is completely different than in amorphous molecular glasses or in the supramolecular complex **3**, as attested by their distinct polarization dependence[32] as well as their limitation to relatively thin films and low spatial frequencies. Hence, the overall diffraction efficiency and modulation depth of the "phototriggered LC materials" are limited, although the surface-modulation depth can be as high as twice the film thickness. In case of photochromic molecular glasses, modulation depth exceeding 500 nm has been reported on several instances, but only for thicker films (> 500 nm) than in the present case (250 nm)[19]. In fact, to the best of our knowledge we report here on the first example of photoinduced SRG with modulation depth significantly higher than twice the film thickness.

3.3 Conclusions.

The results shown in **Fig. 27** and **Fig. 28** imply that halogen bonding may provide unique possibilities in the design of photoresponsive and multifunctional supramolecular complexes. In fact the halogen-bonded complex **3** reported in this paper has a unique capability of combining efficient photoalignment (order parameter of molecular alignment > 0.5) with exceptional surface-relief grating formation efficiency (modulation depth of at least 2.4 times the initial film thickness). This unique combination may be attributed to the following features: (i) the presence of a high-temperature nematic LC phase (presumably enabled by the high directionality of halogen bonding), which enhances and stabilizes the photoalignment; (ii) the lack of flexible alkyl spacers and the presence of the dimethylamino group, which enhance the SRG formation efficiency. The films are crystalline, which compromises their optical quality, however even short irradiation with circularly polarized light destructs the crystal structure and makes the samples amorphous. We also note here that the relatively high surface roughness of the fluorine-containing thin films may be beneficial for designing photocontrollable superhydrophobic surfaces. This latter topic, in combination with (i) detailed structure–performance characterization and (ii) studying the feasibility of halogen-bonded complexes as photoalignment layers for liquid crystals, will be investigated in detail in the near future.

This study highlights the potential of halogen bonding in the design of photoresponsive supramolecular complexes, even if detailed understanding on the connection between the molecular-level properties, structural properties, and the optical response requires further detailed studies. Like no other non-covalent interactions, halogen bonding combines high directionality and controllable interaction strength, hence providing a facile platform for the design of photocontrollable suprastructures, with potential use in both fundamental studies as well as in applications ranging from liquid-crystal photoalignment to the design of diffractive optical elements and novel classes of smart functional materials.

References and notes:

(1) Kishikawa K. *Isr. J. Chem*. **2012**, *52*, 800.

(2) Paleos C. M.; Tsiourvas D. *Liq. Cryst*. **2001**, *28*, 1127.

(3) Priimagi A.; Cavallo G.; Metrangolo P.; Resnati G. *Acc. Chem. Res*. **2013**, *46*, 2686.

(4) Nguyen H. L.; Horton P. N.; Hursthouse M. B.; Legon A. C.; Bruce D. W. *J. Am. Chem. Soc*. **2004**, *126*, 16.

(5) Bruce D. W. *Liquid Crystals Formed from Specific Supramolecular Interactions* in *Supramolecular Chemistry: From Molecules to Nanomaterials*. edited by Gale P. A. and Steed J. W. John Wiley & Sons, Ltd. **2012**.

(6) Liquid crystals in which the halogen bonding donor is a iodoperfluoroalkane, iodoethinylbenzene, or even molecular iodine, have recently been reported.

(7) Bruce D. W. *Adv. Inorg. Chem*. **2001**, *52*, 151.

(8) Russew M.-M.; Hecht S. *Adv Mater*. **2010**, *22*, 3348.

(9) Natansohn A.; Rochon P. *Chem. Rev*. **2002**, *102*, 4139.

(10) Ichimura K. *Chem. Rev*. **2000**, *100*, 1847.

(11) Gelbaor M.; Klebanov M.; Lyubin V.; Abdulhalim I. *Appl. Phys. Lett*. **2011**, *98*, 071909.

(12) Shishido A. *Polym. J*. **2010**, *42*, 525.

(13) Lee S.; Kang H. S.; Park J. K. *Adv. Mater*. **2012**, *24*, 2069. ; Mahimwalla Z.; Yager K. G.; Mamiya J.; Shishido A.; Priimagi A.; Barret C. J. *Polym. Bull*. **2012**, *69*, 967.

(14) Rochon P.; Batalla E.; Natansohn, A. *Appl. Phys. Lett*. **1995**, *66*, 136. ; Priimagi A.; Shevchenko A. *J. Polym. Sci. Part B. Polym. Phys*. **2013**, DOI: 10.1002/polb.23390.

(15) Han M.; Morino S.; Ichimura K. *Macromolecules* **2000**, *33*, 6360.

(16) You F.; Paik M. Y.; Häckel M.; Kador L.; Kropp D.; Schmidt H. W.; Ober C. K. *Adv. Funct. Mater*. **2006**, *16*, 1577.

(17) Priimagi A.; Lindfors K.; Kaivola M.; Rochon P. *ACS Appl. Mater. Interfaces* **2009**, *1*, 1183.

(18) Nakano H.; Takahashi T.; Kadota T.; Shirota Y. *Adv. Mater*. **2002**, *14*, 1157.

(19) Ishow E.; Lebon B.; He Y.; Wang X.; Bouteiller L.; Galmiche L.; Nakatani K. *Chem. Mater.* **2006**, *18*, 1261. ; Walker R.; Audorff H.; Kador L.; Schmidt H. W. *Adv. Funct. Mater*. **2009**, *19*, 2630.

(20) Nakano H. *J. Phys. Chem. C* **2008**, *112*, 16042.

(21) Shirota Y. *J. Mater. Chem.* **2005**, *15*, 75.

(22) Zakrevskyy Y.; Stumpe J.; Faul C. F. J. *Adv. Mater*. **2006**, *18*, 2133.

(23) Hernández-Ainsa S.; Alcalá R.; Barberá J.; Marcos M.; Sánchez C.; Serrano J. L. *Macromolecules* **2010**, *43*, 2660.

(24) Priimagi A.; Cavallo G.; Forni A.; Gorynsztejn-Leben M.; Kaivola M.; Metrangolo P.; Milani R.; Shishido A.; Pilati T.; Resnati G.; Terraneo G. *Adv. Funct. Mater*. **2012**, *22*, 2572.

(25) Kato T.; Kihara H.; Uryu T.; Fujishima A.; Frechet J. M. J.; *Macromolecules* **1992**, *25*, 6836.

(26) Rau H.; in *Photoreactive Organic Thin Films* (Eds: Z. Sekkat , W. Knoll), Academic Press , San Diego, CA, USA **2002**.

(27) Bruce D. W.; Metrangolo P.; Meyer F.; Präsang C.; Resnati G.; Terraneo G.; Whitwood A. C. *New J. Chem*. **2008**, *32*, 477.

(28) Cesteros L. C.; Isasi J. R.; Katime I. *Macromolecules* **1993**, *26*, 7256.

(29) Xu J.; Liu X.; Ng J. K.; Lin T.; He C. *J. Mater. Chem.* **2006**, *16*, 3540.

(30) Yeh P.; Gu C. *Optics of Liquid Crystal Dispalys*, Wiley, Hoboken, NJ, USA **2010**.

(31) Kreger K.; Wolfer P.; Audorff H.; Kador L.; Stingelin-Stutzmann N.; Smith P.; Schmidt H. W. *J. Am. Chem. Soc*. **2010**, *132*, 509.

(32) Zettsu N.; Ubukata T.; Seki T.; Ichimura K. *Adv. Mater.* **2001**, *13*, 1693. ; Zettsu N.; Fukuda T.; Matsuda H.; Seki T. *Appl. Phys. Lett*. **2003**, *83*, 4960.

4 Highly fluorinated azobenzene and heterocyclic supramolecules assembled by halogen bonding.

4.1 Fluorine strikes back.

The importance of fluorinated organic molecules in all aspects of the chemicals industry is growing year by year and is one of the emerging topics in fields such as pharmaceutical science[1], crystal engineering[2], or even materials[3]. The success of fluorine in organic chemistry is mainly due to the peculiar features of the C-F bond[4].

First of all the C-F bond is highly polarized compared for example to the common C-H bond. This happens because of the electronegativity of the fluorine atom that is the highest in the periodic table[5], and leads to a high electrostatic character of the bonding. Perhaps unexpectedly the polarized bond does not result in a good donor ability of the fluorine. The three lone pairs on fluorine are held tightly due to the high electronegativity of the atom and, they are reluctant to get involved in resonance or interact as hydrogen bonding acceptors[6].

Second, the C-F bond is extremely strong, indeed it is the strongest in organic chemistry (105.4 kcal mol^{-1}). The particular strength of the bond can be attributed to significant electrostatic attraction between $F^{\delta-}$ and $C^{\delta+}$ rather than the more classical electron sharing of a covalent bond[7]. This argument can be used to rationalize the progressive bond shortening as we proceed from fluoromethane through to tetrafluoromethane (**Fig. 29**).

Third, the fluorine atom (and C-F bond length) is intermediate in size (and length) between hydrogen and oxygen. The atomic radius of fluorine is 1.47 Å or 1.30 Å, that of hydrogen is 1.2 Å or 1.17 Å and that of oxygen is 1.50 Å or 1.40 Å (I quote Bondi[8] and Gavezzotti[9] respectively). For this reason fluorine is often used to replace hydrogen in medicinal chemistry and such a replacement has significant electronic consequences, dramatically changing the properties of a molecule, e.g. pK_as of adjacent functional groups. A C–F for C–OH replacement involves the loss of the acidic hydrogen and its potential hydrogen bonding donor ability. This is the reason why the substitution of C–F for C–OH has emerged as an excellent tool in exploring the roles of

C–OH hydrogen bonding relative to the inherent polarity of the C–O bond in biological systems.

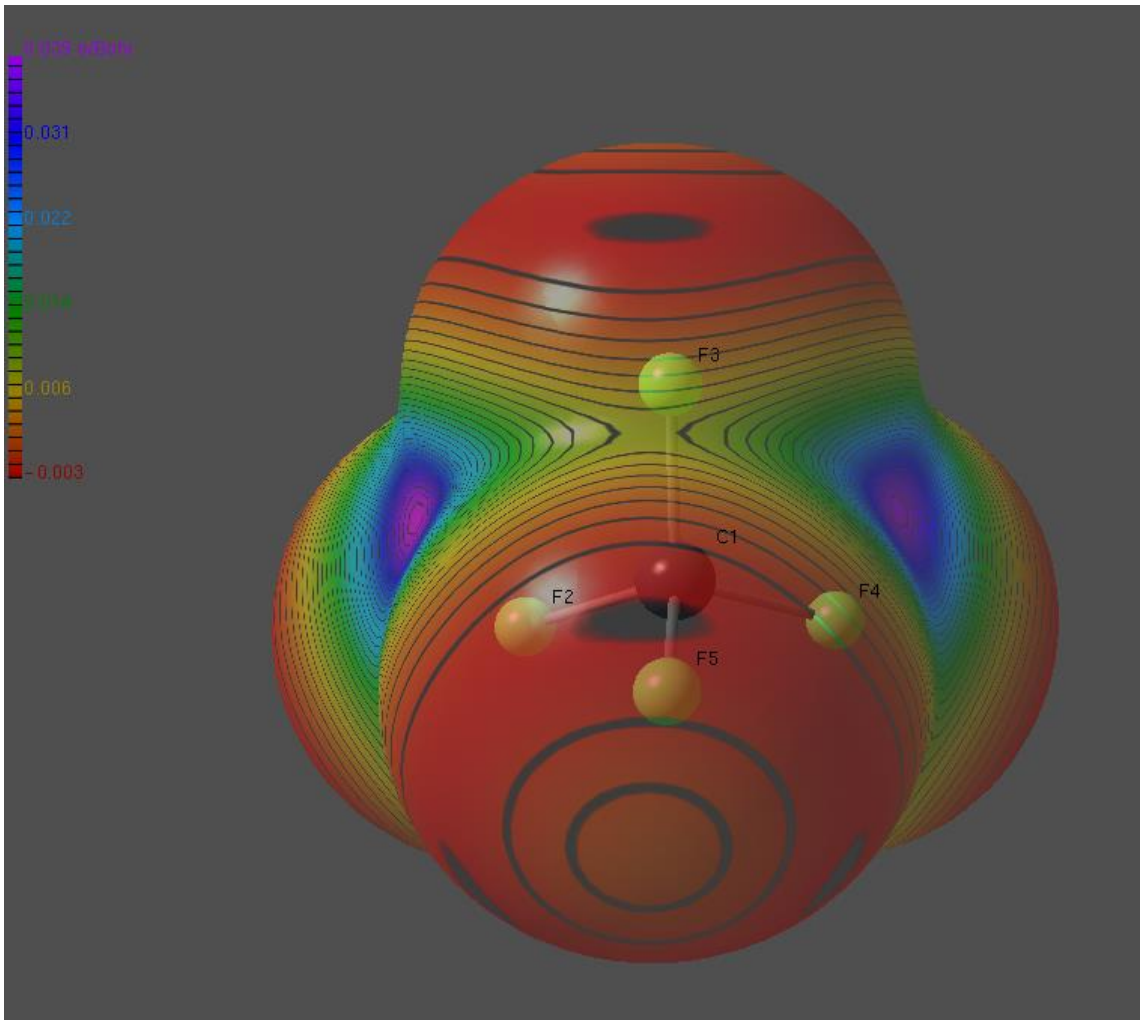

Fig. 29: Molecular electrostatic potential of CF_4 (All electron MP2 aug-cc-pCV5Z wavefunction) mapped on the 0.001 au contour of the electron density. The computed C-F bond length is 1.316 Å compared to 1.392 Å of CH_3F.

This chapter of the thesis is focused on the role of fluorinated building blocks in the halogen bonding driven self-assembly in the solid state of new molecules conceived for optoelectronics applications and is organized as follows: In the first part it is demonstrated that the directionality of halogen bonding is able to promote the self-assembly of fluorinated and non-fluorinated molecules and to translate the tecton geometry in the geometry of the desired supramolecular structure. In the second part the potential of a new perfluorinated azobenzene in driving the formation of co-crystals is discussed, these could be the first photomobile co-crystals.

4.2 Old molecules, new concepts: Oxadiazoles as halogen bonding acceptors.

Among the constituents of supramolecular assemblies based on halogen bonding, the presence of fluorinated synthons is common[2]. In fact, fluorine atoms and perfluorinated residues are among the most powerful electron withdrawing groups[10], thus enhancing the halogen bonding strength with respect to the corresponding hydrocarbon derivatives (e.g. halo-perfluoroalkanes vs halo-alkanes). In this context, factors affecting the strength of the halogen bond have been investigated by considering also the nature of the XB acceptors, which could be either neutral (aliphatic and aromatic amines, carbonyls, ethers, etc.) or anionic (halides, N-oxides, perchlorate, etc…)[11].

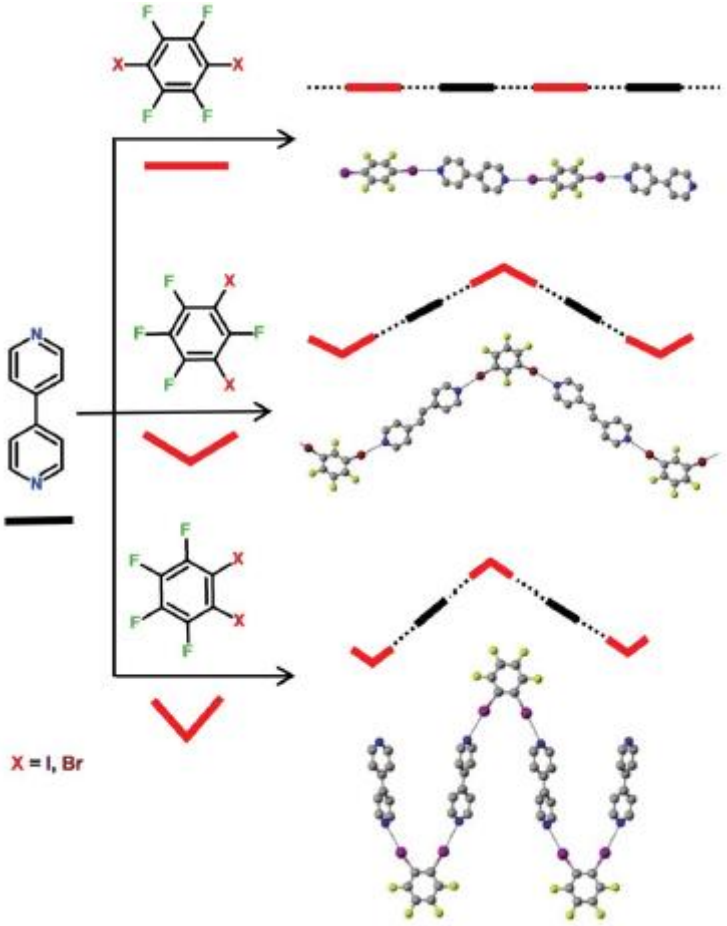

Fig. 30: Schematic representation of structures showing how the angle between the two XBs formed by a bidentate XB donor is strictly similar to the angle between its two C-halogen covalent bonds. Ball and stick representation (Mercury 3.0) of selected structures are also given.

Depending on the electronic nature of both the XB acceptor and donor, the structural diversity of bi- and tridimensional supramolecular XB-based networks has been

achieved through a variety of spacers in polyfunctional tectons. Often, *halogen bonding directionality is maintained throughout the network*, by means of rigid spacers such as multiple bonds or aromatic rings. For this reason, pyridine and its derivatives have been used as the acceptor moiety in many XB-based structures[12] (**Fig. 30**)

Multiple bonds and six-membered aromatic ring spacers offer the possibility to access typical 60, 120, and 180 degrees of inter-XB angles, leading to hair-pin, bent (or hockey stick), and linear structures, respectively. On the other hand, regular five-membered ring spacers would give access to bent core structures with approximately 72 and 144 degrees directionality angles, with small variations given to the actual identity of the five membered ring. Despite the wide variety of potentially accessible geometries, studies on supramolecular structures based on spaced bis-pyridyl halogen bonding acceptors are mostly limited to systems with 180 degrees directionality, bearing 4'-pyridyl moieties[13].

In this context, a systematic study on the XB-accepting potential of ter(aryl) systems, based on a five-membered ring core spacing two six-membered ring terminals, would cover a wide variety of geometries. To the best of my knowledge, no study has been performed on the geometrical diversity of XB-based supramolecular structures accessible by using an Azine-Azole-Azine (**AAA**) heteroaromatic triad (**Fig. 31**). Therefore, we decided to explore the feasibility of our approach by testing the halogen bonding acceptor potential of a 3,5-bis(pyrid-4'-yl)-1,2,4-oxadiazole, chosen as a model compound for **AAA** systems.

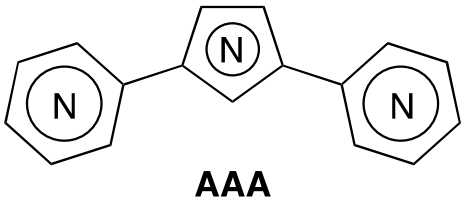

Fig. 31. General representation of an Azine-Azole-Azine heteroaromatic triad.

1,2,4-Oxadiazoles[14], are promising compounds for their applications in materials[15] as well as pharmaceutical science[16] and heterocyclic syntheses[17]. From a structural point of view, the choice of the 1,2,4-oxadiazole as a five-membered heteroaromatic spacer was based on the peculiar features of this heterocycle compared to its symmetric isomer 1,3,4-oxadiazole. In fact, the peculiar exocyclic bond angle of 140° between the C(3) and the C(5) substituted positions of 1,2,4-oxadiazole has been claimed to be responsible for a better molecular organization in the mesophase of 1,2,4-oxadiazole bent core liquid crystals[18].

Due to the asymmetric distribution of the oxadiazole ring heteroatoms, the bis(pyridyl)-1,2,4-oxadiazole scaffold is composed by nine compounds which, by considering only quasi-planar conformers, would give access to as much as twenty five different conformers where halogen bonding acceptor atoms point in different directions (**Fig. 32**). Additionally, the presence of three heteroatoms in the central core would allow to assess also the site selectivity of XB formation. Indeed, the strong electron withdrawing capability of the 1,2,4-oxadiazole ring would decrease the electron density on the pyridyl nitrogen atoms. Therefore, before pursuing the synthesis of **AAA** libraries of halogen bonding acceptors, the capability of bis(pyridyl)-oxadiazoles in forming stable XB supramolecular interactions needed to be assessed on a model compound.

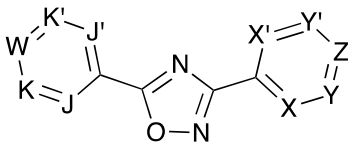

X or X'	Y or Y'	Z	J or J'	K or K'	W	n. of planar conformers
N	CH	CH	N	CH	CH	4
CH	N	CH	N	CH	CH	4
CH	CH	N	N	CH	CH	2
N	CH	CH	CH	N	CH	4
CH	N	CH	CH	N	CH	4
CH	CH	N	CH	N	CH	2
N	CH	CH	CH	CH	N	2
CH	N	CH	CH	CH	N	2
CH	CH	N	CH	CH	N	1

Fig. 32. General structure of bis(pyridyl)-1,2,4-oxadiazoles.

Here I reported the site-selective self-assembly of two fluorocarbon/heteroaromatic co-polymers driven by halogen bonding among compound **1** (XB acceptor) and diiodoperfluoroalkanes **2** and **3** (XB donors). In the formed cocrystals **4** and **5** both the XB donors **2** and **3** and acceptor **1** work as bidentate tectons and the relative geometry between the two pyridyl rings is strictly similar to the bent geometry of two formed XBs. The compounds used here are reported in **Fig. 33**. Solvents were slowly evaporated (3 days at room temperature) from systems obtained on mixing separately prepared solutions (MeOH/THF, 10:90) of **1** and either **2** or **3**. The formed co-crystals **4** or **5** melt at 174 and 176 °C, namely higher than starting oxadiazole **1** (m.p. 165-167 °C) and diiodoperfluoroalkanes **2** and **3** (m.p. -9 and +25 °C, respectively).

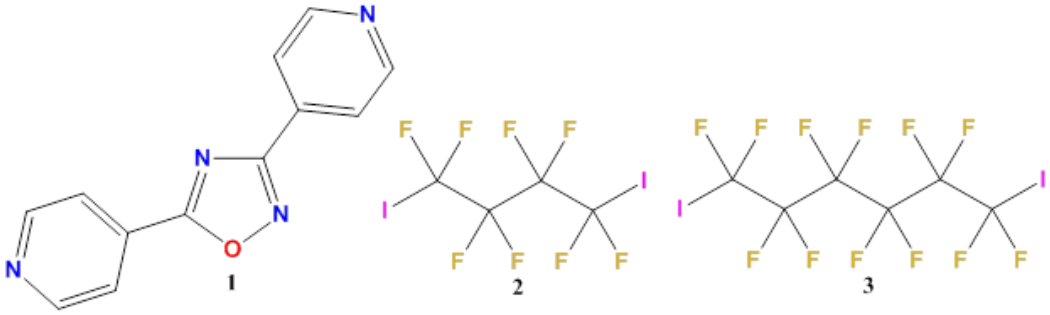

Fig. 33: Building blocks used for the synthesis of XB-based co-crystals **4** and **5**.

Although the relationship between intermolecular interactions in a crystalline solid and its melting point can be hardly analysed in terms of the role of single interactions, the observed behaviour suggests the formation of a new chemical species with well defined identity rather than an aspecific mixture of starting components.

The infrared spectra of cocrystals **4** and **5** suggest the presence of halogen bonds. The vC–H absorptions of the pyridine rings are centred at 3045 cm^{-1} in the pure oxadiazole **1**. In **4** and **5** are blue shifted to 3047 and 3051 cm^{-1}, respectively, and also become less intense than in pure **1** consistent with a higher positive charge on the pyridyl hydrogens in the complexes[19]. A blue-shift is observed also for the bands associated with the pyridine ring breathing vibrations (at 1543 and 1487 cm^{-1} in pure **1**, at 1545 and 1489 cm^{-1} in **4**, at 1549 and 1492 cm^{-1} in **5**). Such shifts have been attributed to increased stiffness of the pyridine ring when behaving as a XB acceptor[20]. The vC-F stretching for pure 1,4–diiodotetrafluorobutane **2** at 1190 and 1130 cm^{-1} are red-shifted to 1175 and 1124 cm^{-1} in **4**, in keeping with an increased electron density on the perfluoroalkane moiety in the co-crystal due to the charge transfer component of the halogen bonding.

^{1}H and ^{19}F NMR spectra of **4** and **5** in $CDCl_3$ and in the presence of $(CF_3CH_2)_2O$ as an internal standard indicated that the oxadiazole and diiodoperfluoroalkane components were present in a 1:1 ratio and this confirmed that the crystals used for single crystal x-ray analyses (see onwards) are representative of the batch sample. The -CF_2I signal in ^{19}F NMR spectrum of **4** (0.1 molar solution in $CDCl_3$) is shifted 1.97 ppm upfield with respect to pure **3**. A smaller shift is shown by the signal of -CF_2CF_2I and a similar behavior is presented by **5**. Clearly the halogen bonding is present also in solution[21].

Single crystal x-ray analyses of **4** and **5** reveal that short I···N halogen bonding involving pyridyl nitrogen atoms are the attractive non covalent interactions largely responsible for the cocrystals formation (**Fig. 34**).

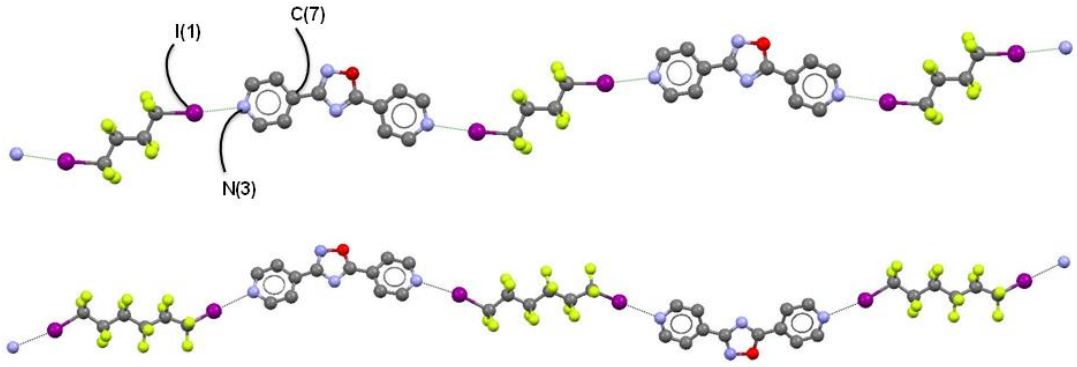

Fig. 34: Ball and stick representation (Mercury 3.0) of X-bonded infinite chains in **4** (top) and **5** (bottom). Hydrogen atoms have been omitted.

In fact, while the nitrogen atom in position four of the oxadiazole ring has a nucleophilic or weakly basic character and the nitrogen in position two has an amphiphilic character, no halogen bond is involving the azole ring. Halogen bonding formation selectively involves the two pyridyl nitrogen atoms of **1** which give I···N contacts in the range 2.77-2.88 Å. These values, corresponding to normalized contacts in the range 0.78-0.82, are quite short despite the strong electron withdrawing capability of the 1,2,4-oxadiazole ring may decrease the ability of the pyridine to function as halogen bonding acceptor. The C-I···N angles are in the range 170.2(3)-174.62(6)° namely nitrogen atoms enter approximately the elongation of the C-I bonds. Also diiodoperfluoroalkanes **2** and **3** work as bidentate tectons and undulated infinite chains are formed. In the two complexes, the weakness of π–π interactions between the heteroaromatic rings (only present in **5**), the disorder in the oxadiazole core (leading to exchange of the contiguous oxygen and nitrogen atoms which occupy the two positions with nearly the same population factor), and the disorder in the perfluorohexyl chain of **5** (refined with two equi-populated models having in common only the iodine atoms) confirm that the I···N halogen bonds are by far the most relevant attractive interaction present and are largely responsible for the co-crystals formation. The only short contacts, below the sum of van der Waals radii, other than the I···N halogen bonds are some $F^{\cdots}C_{aromatic}$ (in the range 3.106-3.141 Å) and $F^{\cdots}H_{pyridine}$ (between 2.40 and 2.66 Å) present in complex **4** as well as F···F contacts (in the range 2.89-2.94 Å) and $C_{azole}{}^{\cdots}O$ or $C_{azole}{}^{\cdots}N$ (3.19 Å) present in complex **5** and related to the segregation of the hydrocarbon and fluorocarbon components which form twin columns running along the b crystallographic axis (**Fig. 35**).

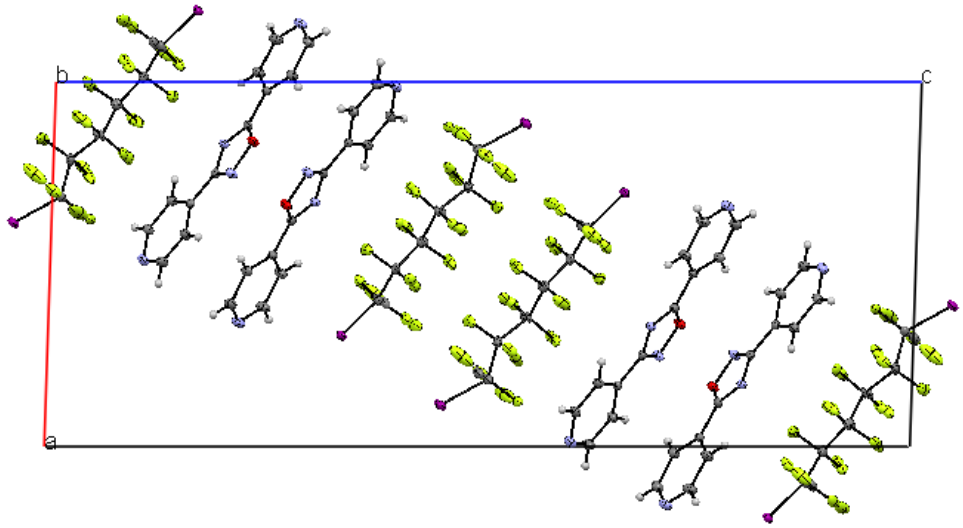

Fig. 35: A view of the unit cell of the complex **5** along the b axis, showing the segregation of the perfluoroalkyl chains and the stacking of the heterocyclic cores.

In conclusion, the single-crystal structure determinations carried out on **4** and **5** are the first example of co–crystals involving a symmetrically substituted 1,2,4–oxadiazole. Both structures feature infinite halogen bonded chains in which the nitrogen atoms of the two pyridine rings act selectively as halogen bonding acceptors, while the oxadiazole core is not involved in halogen bonding. The observed site selectivity in XB formation parallels the relative basicity of the competing sites[22-23] and is favored by the greater steric accessibility of the pyridine nitrogen relative to the oxadiazolic core. Exploitation of this site selectivity is currently under investigation to construct novel oxadiazole-based bent core liquid crystalline materials[15]. The pyridine lone pairs enter the σ-hole of the iodine atoms and the bend of the azine–azole–azine heteroaromatic triads is translated into the angle between the two formed halogen bonds. The use of bis(4-pyridyl) heteroaromatics with different bend angles will allow for the preparation of a library of halogen bonded adducts wherein the curvature along the infinite chain is systematically changed. The use of α,ω-diiiodoperfluoroalkanes of different length will allow for a fine tuning of the metric along the chains[24].

4.3 The return of azobenzenes.

In the second and third chapter of this thesis I discussed about the light induced processes that occur in halogen-bonded supramolecular azobenzene complexes when exposed to interference irradiation. We demonstrated that the directionality of the polymer–dye noncovalent interaction enhances the mass-transport efficiency, and the same directionality allows for the liquid crystalline behavior that enhances the photoalignment of the small complex described in chapter 3.

A very important point of the latter work is that we were able to merge together two very different photoisomerization-triggered processes such as photoalignment (that occur at the *molecular level*) and SRG formation (that is a *macroscopic* effect).

These two studies pointed out that halogen bond is a highly promising noncovalent interaction in the context of photoresponsive materials design. However, examples of azobenzene molecules containing halogen-bond-donor groups are scarce[20,25-27] and clearly a wider set of such molecules is needed in order to elaborate the photoresponsive behaviour and to understand the full potential of halogen bonded supramolecules.

Photoinduced bending is another process that occurs at the *macroscopic* level: it takes place predominantly in crosslinked liquid-crystalline polymers and is based on isomerization-triggered dimensional changes upon light irradiation[28]. Interestingly, it can occur also in supramolecular material systems[29] and even in crystalline materials[30] despite the general conception that photoisomerization, and hence the photomechanical response is suppressed in crystals. As pointed out by Barrett[31], a very long cis-isomer half-life is necessary to achieve the photoinduced bending in single cystals of organic materials and a very productive strategy to obtain such long half-lives is the fluorination of the benzene positions that are *ortho* to the azo-link[26].

Photoinduced bending or SRG formation in cocrystals has not been reported up to date. As (i) cocrystal strategy could allow for facile optimization of the constituent compounds to yield efficient photomechanical response, and (ii) halogen bonding appears as a promising design tool for efficient photoresponsive materials[20,25], there is a need for difunctional halogen-bond-donor fluorinated azobenzenes with capability of crystallizing into infinite chains or acting as noncovalent crosslink points. For this reason I prepared and studied the crystal structure of the complexes formed by a new symmetrically substituted iodoperfluoro azobenzene with different halogen bonding donors (**Fig. 36**). The structural studies have shown that the iodine atoms on the fluorinated azobenzene **IoFAZO** function as very strong and effective halogen-bond

donors, highlighting its great flexibility in the construction of different supramolecular architectures: linear infinite chains as well as discrete adducts.

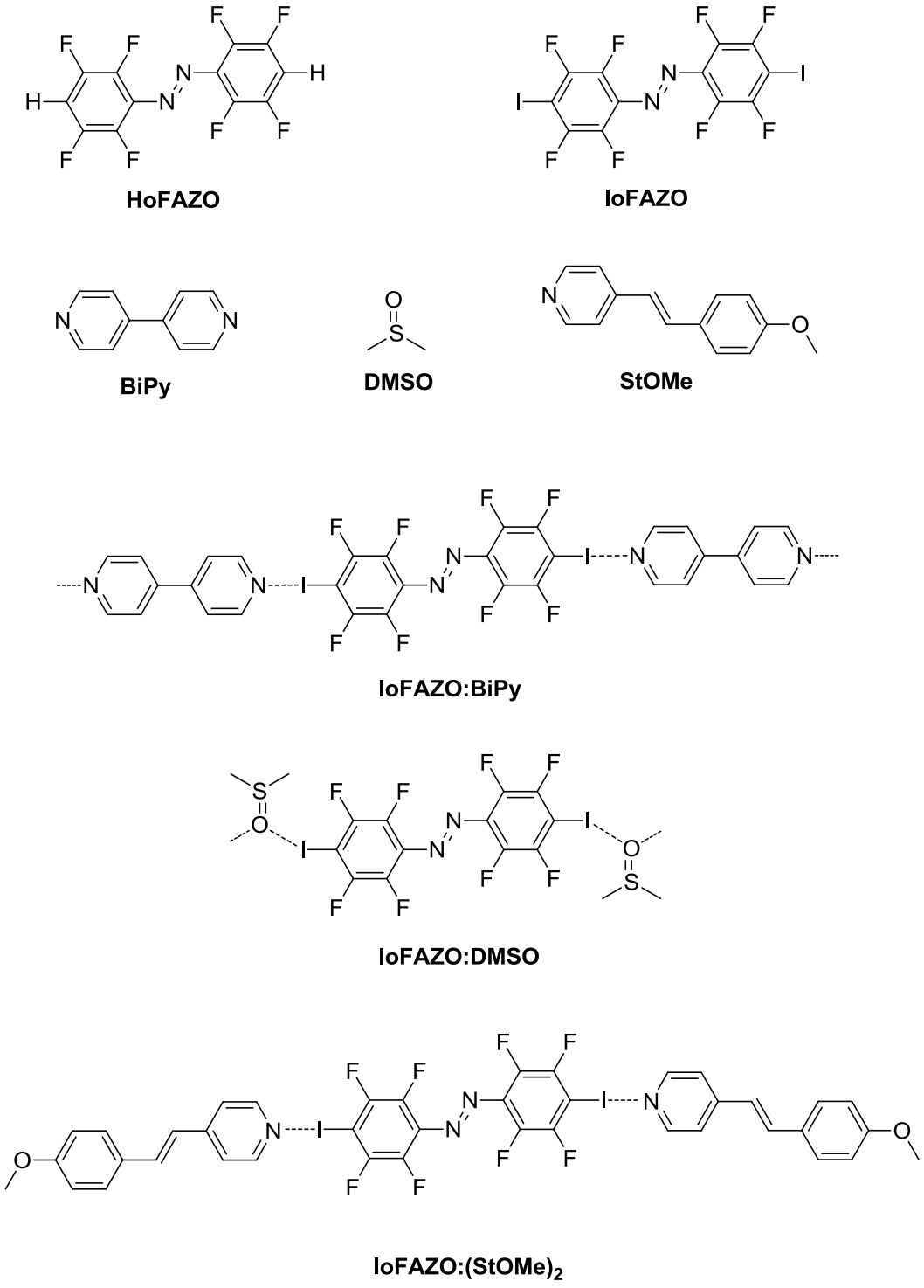

Fig. 36: Chemical structures of the starting tectons and corresponding halogen-bonded adducts.

Full details of the synthesis and spectroscopic characterization of **HoFazo**, **IoFAZO** as well as the co-crystals are provided in the Experimental part. The synthesis of **IoFAZO** started from 4-iodo-2,3,5,6-tetrafluoroaniline. 4-Methoxyl-4'-stilbazole (**StOMe**) was synthesized according to the procedure reported by Bruce[32]. Single crystals of **HoFAZO** suitable for X-ray diffraction studies were obtained by slow evaporation from a $CHCl_3$ solution. The crystal of **IoFAZO:DMSO** was obtained after 3 months from a dimethylsulfoxide solution. For the other co-crystals, compound **IoFAZO** and the appropriate halogen-bond acceptor were separately dissolved in THF at room temperature in a 1:1 (for **IoFAZO:BiPy**) or 1:2 (for **IoFAZO:(StOMe)$_2$**) stoichiometric ratio. The two saturated solutions were then mixed in a clear borosilicate glass vial, which was left open in a closed cylindrical wide-mouth bottle containing paraffin oil. The solvent was allowed to evaporate slowly at room temperature for three days until good-quality single crystals were formed.

(E)-bis(2,3,5,6-tetrafluorophenyl)diazene (HoFAZO).

Compound **HoFAZO** is the bis-deiodinated analogue of **IoFAZO**, which is the main target of this study. The molecule has been crystallized in order to study the determinants of its crystal packing and establish how the introduction of I atoms into its structure, resulting in **IoFAZO**, modifies the crystal packing. The **HoFAZO** molecule crystallizes as a monoclinic system with space group $P2_1/n$. The molecule is located at the center of symmetry, and the azo group exclusively adopts the trans isomer. The two tetrafluorobenzene rings are not coplanar and the angle between them is 25.3(2)°. The crystal packing is mainly driven by hydrogen bonds between the hydrogen atom in *para* position on the tetrafluorobenzene ring and two fluorine atoms of the adjacent **HoFAZO** molecules (**Fig. 37**). This intermolecular interaction is known to be one of the two modes of a bifurcated hydrogen bond[33], namely a three-centered hydrogen bond (THB), adopting an arrangement where the hydrogen atom, which is covalently bonded to an electronegative group (the tetrafluorobenzene ring) is hydrogen bonded to two electron-density donor sites (the fluorine atoms)[34]. The distances and angles between the donors and the acceptor in **HoFAZO** are: H4···F3^{i} = 2.56 Å, C4-H4···F3^{i} = 145.5°; H4···F4 = 2.54 Å, C4-H4···F4 = 145.4°. [symmetry code: (i) 1/2-x, 1/2+y, 3/2-z]. THBs are quite common in organic molecules[35] and biomolecules[36] however majority of the electron density donor sites are oxygen atoms. Fluorine atoms involved in THBs are quite rare and in Cambridge Structural Database (CSD)[37] there are only six structures

with fluorine atoms bound to sp^2-carbon atoms which are involved in such a supramolecular synthon.

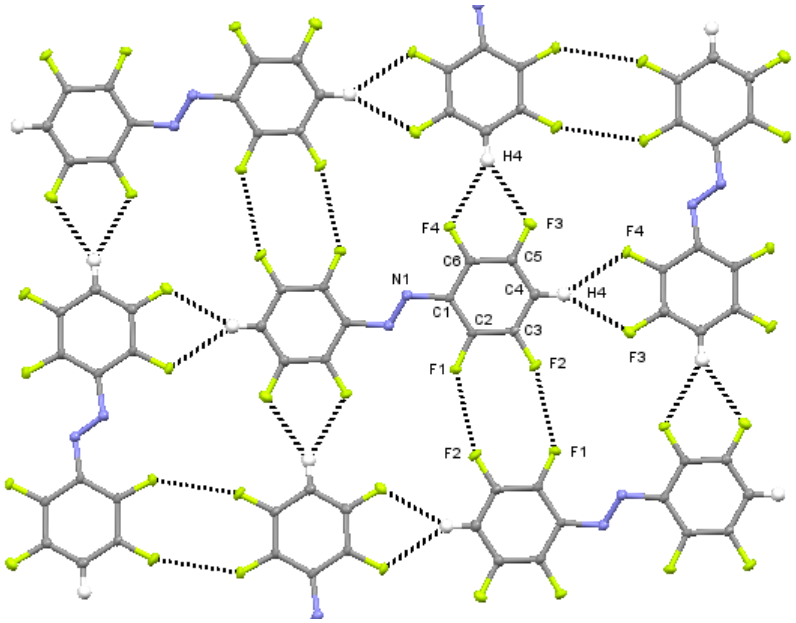

Fig. 37: Ellipsoid representation (50% probability) of supramolecular layer of **HoFAZO** assembled by three-centered hydrogen bonds and fluorine-fluorine contacts.

The bifurcated hydrogen bonds in combination with contacts between F1···F2^{ii} [symmetry code: 2-x, 1-y, 2-z] (and its centrosymmetric equivalent) drive the formation of supramolecular corrugated layers that propagate along the [010] direction (**Fig. 37**).

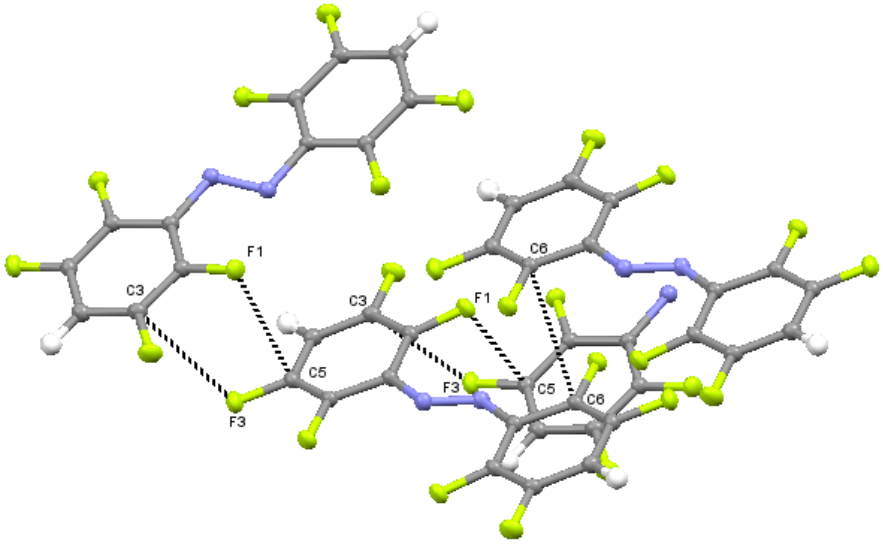

Fig. 38: Ellipsoid representation (50% probability) of the crystal packing of **HoFAZO**, C···C and F···F interactions are pictured as black lines.

The crystal packing of **HoFAZO** is further stabilized through weak C···C and C···F contacts between adjacent layers (**Fig. 38**): C6···C6^{iii} = 3.3144 (14), C3···F3^{iv} = 3.1620 (10) and C5···F1^{v} = 3.1101 (10) Å [symmetry codes: (iii) 1-x, -y, 2-z; (iv) 1/2+x, 1/2-y, 1/2+z; (v) -1/2+x, 1/2-y, -1/2+z].

From crystal engineering point of view it is interesting to compare the supramolecular arrangement seen in **HoFAZO** with those observed in the related fully hydrogenated and fully fluorinated azobenzenes. The trans-azobenzene unit cell parameters have been known since 1939[38] and during the years several research groups have studied its solid-state structure in detail[39]. In all crystal structures of trans-azobenzene reported in the CSD, the unit cells contain two independent molecules, both on inversion centres, and the non-covalent interactions responsible for the crystal packing of the trans-azobenzene molecules are weak C-H···π contacts occurring between the aromatic rings (**Fig. 39A**).

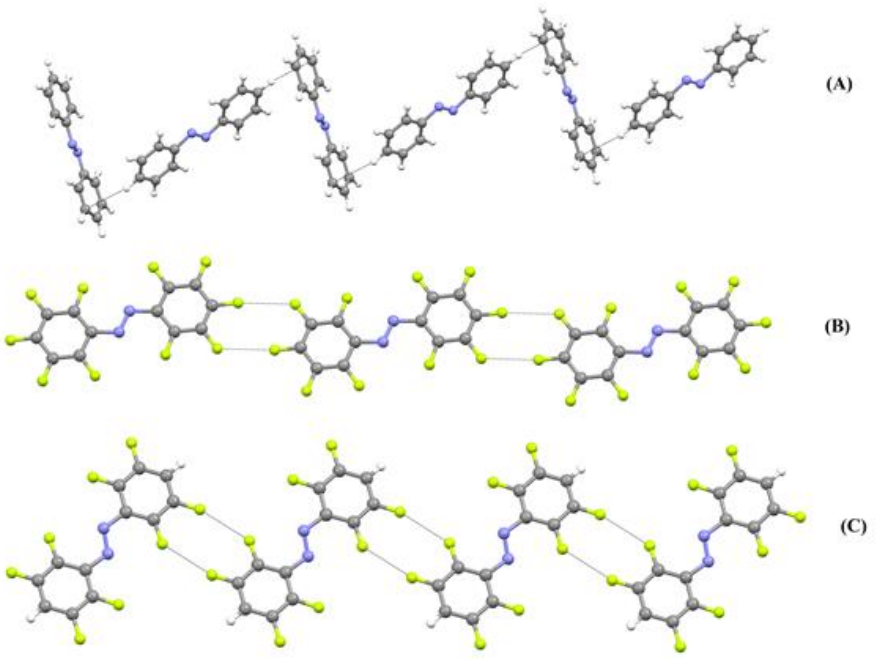

Fig. 39: Supramolecular motif in *trans* azobeneze (CSD code: AZOBEN01), *trans* decafluoroazobenzene (CSD code: WACHAJ) and **HoFAZO**. C-H···π and F···F synthons are in black lines.

The resulting supramolecular motif is very undulated, and no layer organization is present in the *trans*-azobenzene crystal structures. The crystal structure of the *trans*-decafluoroazobenzene is also reported in CSD[40]. The substitution of hydrogen atoms with fluorine atoms establishes the formation of fluorine-fluorine contacts between the fluorine atoms in *para* and *meta* positions of two adjacent molecules (**Fig. 39B**). This

supramolecular motif allows the construction of infinite ribbons propagating along the molecular long axis, but, even in this case, no layer structure is observed. The **HoFAZO** molecule is a hydrocarbon/fluorocarbon hybrid system with a high content of fluorine atoms and also acidic hydrogen atoms. The F···F synthon in **HoFAZO** resembles the one observed in decafluoroazobenzene, but here the non-covalent interactions involve the *ortho* and *meta* fluorines as opposed to *para* and *meta* fluorines in decafluorobenzene. This geometrical modification of the interacting sites gives rise to the formation of a *zigzag* supramolecular ribbon rather than a linear chain (**Fig. 39C**). This difference is clearly due to the presence of the hydrogen-bond donor in the *para* position of the aromatic ring, which forms three-centered hydrogen bond with the other two fluorine atoms. The mutual cooperation between THB and F···F contacts allows for the in-plane connection between the ribbons.

(E)-bis(4-iodo-2,3,5,6-tetrafluorophenyl)diazene:dimehylsulfoxide (IoFAZO:DMSO).

Compound **IoFAZO** was synthesized so that an azobenzene based difunctional halogen-bond donor could be used for the self-assembly of photoresponsive co-crystals. Iodine was selected since it is the most polarizable halogen atom and (as stated previously) when it is bound to a fluorinated aromatic ring it behaves as a strong halogen-bond donor. Several solvents and various crystallization techniques were utilized in order to crystallize **IoFAZO**, but only slow evaporation of a dimethylsulfoxide solution afforded good quality single crystals.

The 1:1 adduct **IoFAZO**:**DMSO** crystallizes in the space group *C*2/*c*, with the unit cell containing one molecule of **IoFAZO** lying on the inversion centre, and one **DMSO** molecule on the twofold rotation axis. In this co-crystal, the diazene derivative is not planar, and the angle formed by the benzene plane and the plane described by atoms C3, N1 and $N1^{i}$ [symmetry code: (i) 3/2-x, 3/2-y, 1-z] is 28.7 (3)° (**Fig. 40**), resembling the geometry of molecule **HoFAZO**. The supramolecular assembly is driven by strong halogen bonds between the O atom of **DMSO** and the I atoms of **IoFAZO** (**Fig. 40**). Both the halogen-bond donor and acceptor molecules behave as bidentate modules forming a chain of alternating **IoFAZO** and **DMSO** molecules. The ability of the O atom in **DMSO** to function as an electrondensity donor site has already been proven in several halogen-bonded complexes involving either I[41] or the less polarizable Br[42] as bond donor sites.

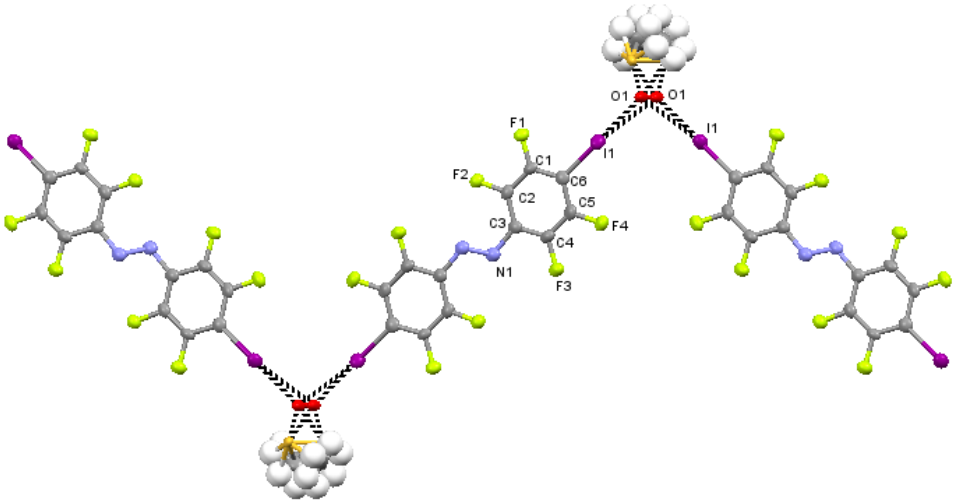

Fig. 40: Ellipsoid representation (50% probability) of the halogen bonded chain in **IoFAZO:DMSO** cocrystal. XBs are pictured as black lines.

The halogen bond is highly directional and capable of translating the geometrical features of the starting modules into the geometrical features of the supramolecular entity. In **IoFAZO:DMSO**, the angle between the two lone pairs on the O atom imposes the formation of an undulating halogen-bonded chain where the molecules of **IoFAZO** function as rigid and linear spacers between the bent halogen-bond acceptor sites.

In **IoFAZO:DMSO** the C-I···O halogen bonds are short and directional with the following geometrical parameters: I1···O1^{ii} = 2.630 (9) Å, C6-I1···O1^{ii} = 178.2 (2)°; I1···O1^{iii} 2.962 (8) Å, C6- I1···O1^{iii} = 166.2 (2)° [symmetry codes: (ii) 1/2+x, 1/2+y, 1+z; (iii) 3/2-x, 1/2+y, 1.5-z]. The I···O distances correspond to *ca* 25 and 16% reduction with respect to the sum of the van der Waals radii of the interacting atoms (I, 1.98 Å; O, 1.52 Å)[8]. It is interesting to note that in the crystal packing of pure **DMSO**[43], the O atoms form four hydrogen bonds leading to the assembly of homomeric layers composed of chains wherein the **DMSO** molecules are arranged in a head-to-tail fashion. Within the **IoFAZO:DMSO** cocrystal, the halogen bonds replace these hydrogen bonds, resulting in channels that are defined by four molecules of **IoFAZO** running parallel to the crystallographic c-axis, which confine the **DMSO** molecules (**Fig. 41**). The channels contain crystallographic inversion centres, but adjacent **DMSO** molecules within a single channel cannot be related by these centres because the S···S distance [3.266 (1) Å] is too short. Instead the **DMSO** molecules must adopt the *c*-glide relationship, with S···S distances of 1/2 *c* = 4.784 (1) Å. However, the overall distribution of the DMSO molecules in the channels is disordered, and hence the average structure is centrosymmetric. Weak hydrogen bonds between H atoms of the

methyl groups and F atoms of the aromatic ring stabilize the **DMSO** molecules within the channels: F1···H7*F*^{iv} = 2.56, F4···H7*A*^{iii} = 2.50, F4···H7*E*^{iii} = 2.62 Å [symmetry code: (iv) 3/2-x, 5/2-y, 1-z].

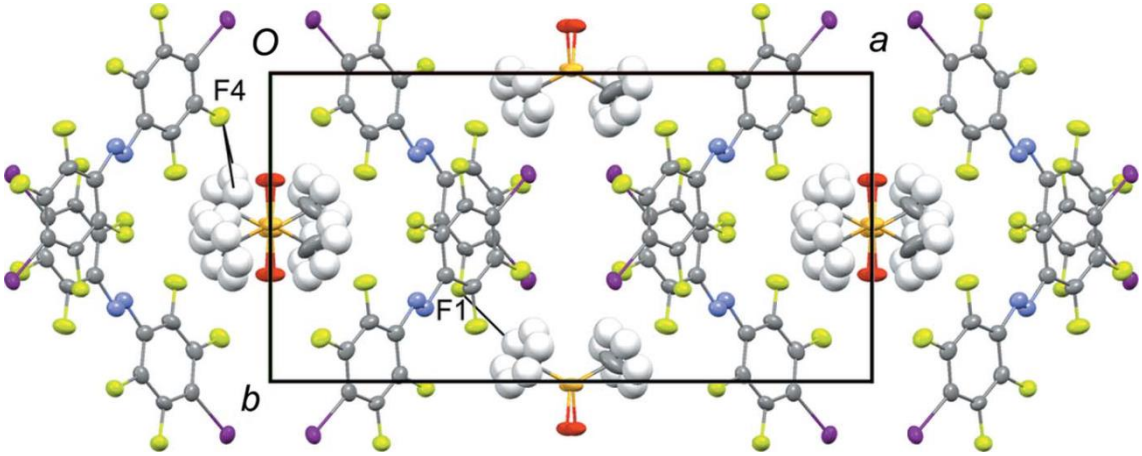

Fig. 41: View along the *c*-axis of the channel arrangement in **IoFAZO:DMSO**. The channels are filled with **DMSO** molecules. HBs are pictured as black lines.

(E)-bis(4-iodo-2,3,5,6-tetrafluorophenyl)diazene:4,4'-bipyridine (IoFAZO:BiPy).

A confirmation of the very good propensity of molecule **IoFAZO** to become involved in halogen bonding came from the obtainment of its co-crystal with 4,4'-bipyridine (**BiPy**), which is a standard difunctional halogen-bond acceptor module. The co-crystal **IoFAZO:BiPy** crystallizes in the space group $P2_1/c$, with both the halogen-bond donor and acceptor units lying on inversion centres. The two interacting modules are ditopic tectons bearing two monodentate interaction sites, *i.e*. the I atoms for **IoFAZO** and the N atoms for **BiPy**, which pair with each other and form a halogen-bonded adduct with a 1:1 stoichiometric ratio. The supramolecular arrangement is controlled by halogen bonds between the I and N atoms, leading to the formation of a chain propagating along the [201] direction (**Fig. 42**).

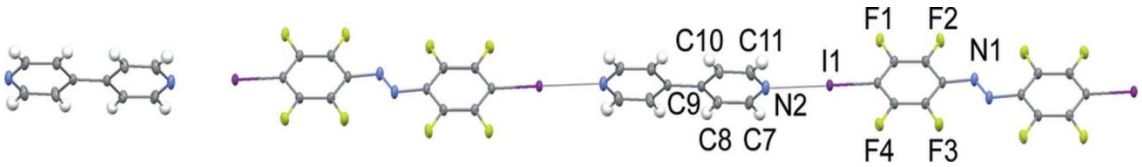

Fig. 42: Ellipsoid representation (50% probability) of a halogen-bonded chain in the **IoFAZO:BiPy** co-crystal.

The halogen-bond donor–acceptor distance in the supramolecular chain is 2.8149 (18) Å, corresponding to ca 20% contraction with respect to the sum of the van der Waals

radii for N and I[8]. The C1-I1···N2 angle is 179.03 (7)°, consistent with the expected directionality of the halogen bond[44].

Both **IoFAZO** and **BiPy** are flat molecules, and their aromatic rings are coplanar. However, along the halogen-bonded chain, the two tectons adopt a non-planar arrangement, with the angle between the tetrafluorobenzene and the pyridyl rings being 72.5° (**Fig. 43**). The molecules of **IoFAZO** and **BiPy** are connected along the [210] direction by weak hydrogen bonds between the H atoms on the pyridyl rings and the F atoms (C7-H7···F2, C8-H8···F3 and C10-H10···F4; **Fig. 43**). The geometrical parameters for the hydrogen bonds are reported in **Table 4**.

D-H···A	*d*(H···A) (Å)	*d*(D···A) (Å)	∠ D-H···A (°)
C7-H7···F2^{i}	2.53	3.429(2)	158.8
C8-H8···F3^{ii}	2.43	3.204(2)	138.2
C10-H10···F4^{iii}	2.46	3.316(2)	150.2
C11-H11···F1^{iv}	2.46	3.359(2)	158.3

Table 4: Hydrogen-bond geometry (Å, °) for **IoFAZO:BiPy**.

These H···F contacts generate a supramolecular tape where the alternating halogen-bond donors and acceptors are quasi-coplanar; the angle defined by the plane of the benzene rings in **IoFAZO** and the plane of the pyridyl rings in **BiPy**^{i} is 1.1° [symmetry code: (i) x, 1/2+y, 1/2-z].

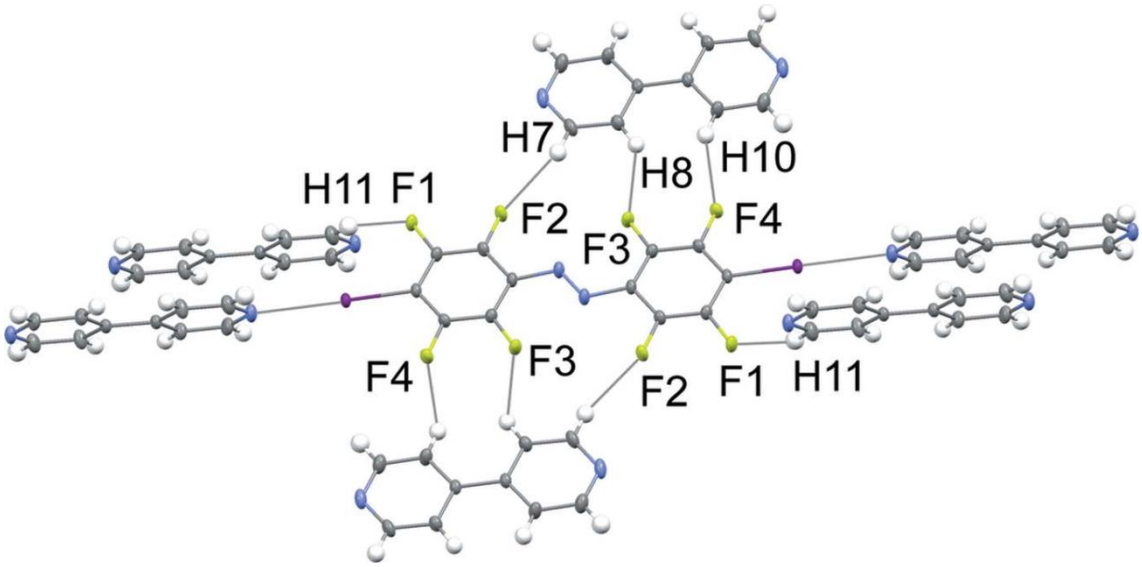

Fig. 43: Hydrogen bonding pattern in the **IoFAZO:BiPy** co-crystal.

The halogen-bonded chains interact through short C···C contacts: C3···C7^{ii} = 3.388 (3), C8···C8^{ii} = 3.388 (4) Å [symmetry code: (ii) 1-x, -1/2+y, 1/2-z; (iii) 1-x, -y, -z], while no π- π interactions are observed. Finally, the chains are also connected by additional H···F hydrogen bonds between the *ortho* H atom of the pyridyl ring (H11) and the F atom (F1) in the *meta* position of **IoFAZO** molecule.

(E)-bis(4-iodo-2,3,5,6-tetrafluorophenyl)diazene: 4-methoxyl-4-stilbazole [IoFAZO:(StOMe)$_2$].

As stated previously, **StOMe** is a very interesting promesogenic molecule and has already been used to construct efficient halogen bonded photoresponsive supramolecules[25]. Under the hypothesis that an eventual co-crystal between **IoFAZO** and **StOMe** may show interesting photoresponsive liquid crystallinity, we studied the reaction between **IoFAZO** and **StOMe**. The two compounds were mixed in THF in a 1:2 ratio, since StOMe is a monodentate halogen-bond acceptor. As expected, the trimeric adduct **IoFAZO:(StOMe)$_2$** was obtained, which crystallized in space group P11. The unit cell comprises two trimeric complexes labelled hereafter as trimer-1 (TR1) and trimer-2 (TR2; **Fig. 44**).

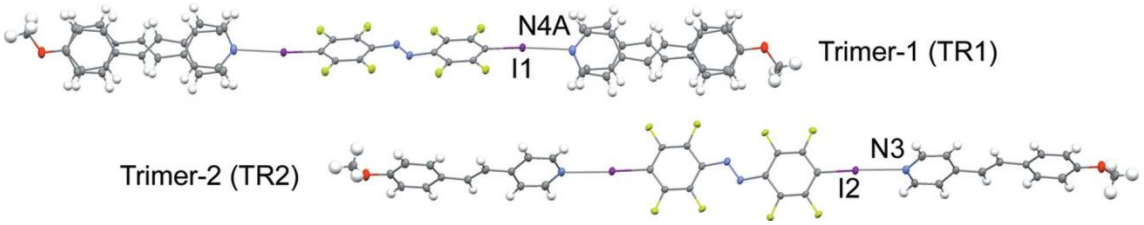

Fig. 44: Ellipsoid representation (50% probability) of the two halogen bonded trimeric systems of the **IoFAZO:StOMe** adduct. The **StOMe** in TR1 is disordered over two positions [refined ratio 0.767 (1):0.233 (1)].

In the trimers the stilbazole molecules are complexed to **IoFAZO** through halogen bonds: I1···N4*A*/N4*B*^{i} = 2.812 (4), I2···N3^{ii} = 2.776 (2) Å, and C3-I1···N4*A*/N4*B*^{i} = 174.71 (10), C9-I2···N3^{ii} = 174.75 (10)° [symmetry codes: (i) -2+x, y, z; (ii) 2-x, -y, 1-z]. Similar to the **IoFAZO:BiPy** co-crystal, the halogen bonds in **IoFAZO:(StOMe)$_2$** are strong and directional, confirming the general ability of **IoFAZO** to function as a good halogen-bond donor. In both trimers the centrosymmetric tetrafluoroaromatic rings are coplanar as also observed in the **IoFAZO:BiPy** co-crystal. The **StOMe** molecules in TR1 are disordered over two positions that are related by 180° rotation approximately along the long axis of the stilbazole molecule. Only the stilbazole core is disordered, while the methoxyl group appears to be ordered. Similar to **IoFAZO:BiPy**, the

iodotetrafluorobenzene and pyridyl rings of the **IoFAZO:(StOMe)$_2$** trimers are not coplanar, the angles between the planes described by the tetrafluorobenzene and pyridyl rings being 60.9° in TR1 and 62.5° in TR2. Each molecule of **IoFAZO** is also bound, in the plane defined by the tetrafluoroaromatic rings, to two neighbouring alkoxystilbazole molecules by several weak hydrogen bonds. In TR1 the F···H contacts involve the aromatic H atoms of the pyridyl and benzene rings but not those on the ethylene group. Conversely, in TR2 the hydrogen bonds occur specifically between the F atoms on the tetrafluorobenzene ring and one aromatic H atom on the benzene ring, and one H atom on the ethylene group in **StOMe** (**Fig. 45**).

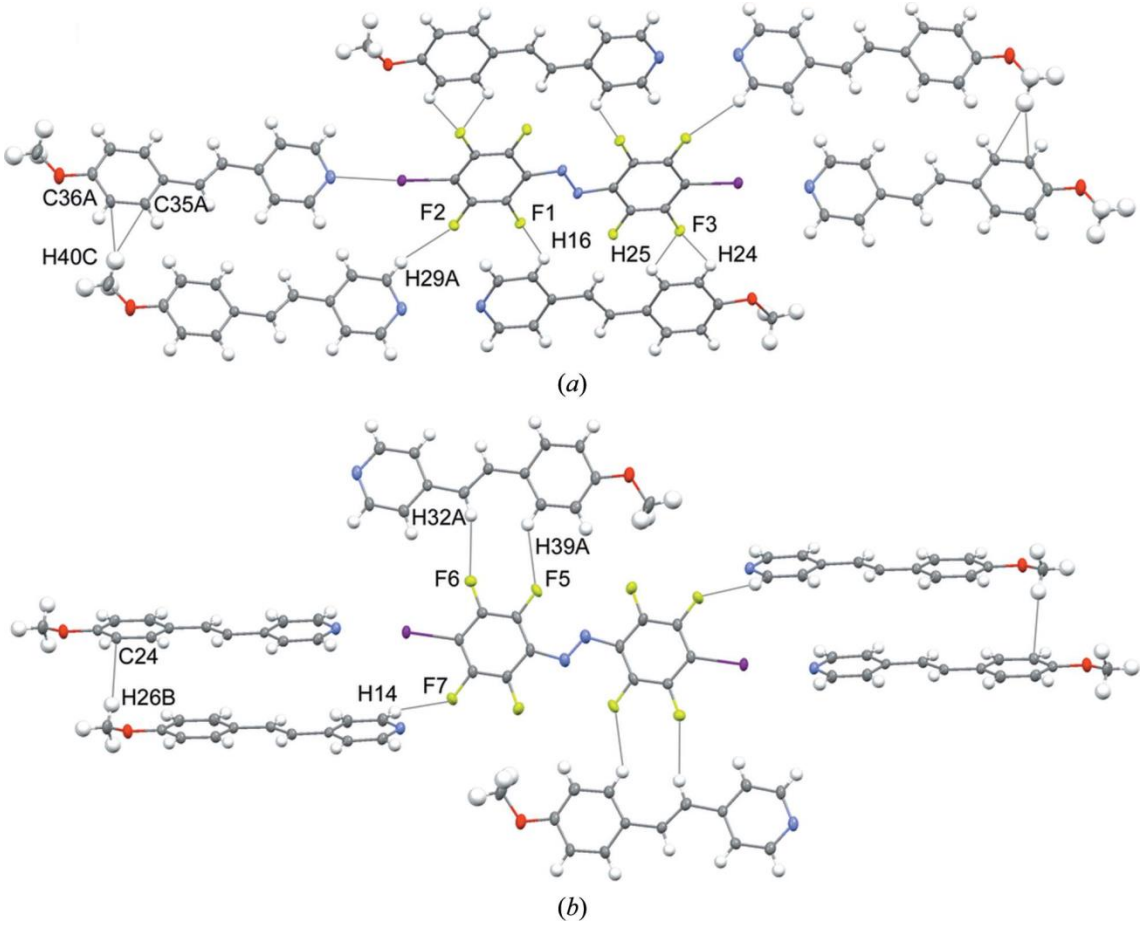

Fig. 45: Hydrogen bonds and C-H···π contacts in TR1 (top) and TR2 (bottom). The disorder of the **StOMe** molecule has been omitted for clarity.

The trimers are connected to nearby trimers by additional weak F···H interactions that occur out of the plane described by the diazene molecules. Relevant geometrical parameters are reported in **Table 5**.

Alkoxystilbazole molecules have been recently used in the construction of trimeric halogen-bonded liquid crystals[45]. In terms of distances and angles between the

halogen-bond donor and acceptor, the **IoFAZO:(StOMe)$_2$** trimers share strong similarity with those reported in ref. 45. Investigations of the liquid crystalline properties of the **IoFAZO:(StOMe)$_2$** complex are currently in progress.

D-H···A	H···A	D···A	D-H···A
C14-H14···F7^{I}	2.63	3.491(3)	151.5
C16-H16···F1^{II}	2.61	3.276(3)	127.4
C24-H24···F3^{III}	2.54	3.145(3)	121.9
C25-H25···F3^{III}	2.51	3.132(3)	123.0
C29A-H29A···F2^{IV}	2.56	3.451(4)	156.0
C39A-H39A···F5	2.61	3.382(5)	138.7
C32A-H32A···F6	2.58	3.503(4)	162.6

Table 5: Hydrogen-bond geometry (Å, °) for **IoFAZO:(StOMe)$_2$**.

Here I assessed the ability of (E)-bis(4-iodo-2,3,5,6-tetrafluorophenyl)diazene to drive molecular recognition and self-assembly processes through C-I···X supramolecular interactions (X = N and O). The structural studies have shown that the iodine atoms on the fluorinated azobenzene **IoFAZO** function as very strong and effective halogen bond donors, highlighting their great flexibility in the construction of different supramolecular architectures, both linear and highly corrugated infinite chains as well as discrete adducts. The halogen-bonded structures reported have further proved that the **IoFAZO** molecule is able to drive the formation of the supramolecular complexes independently the bond acceptor modules. This highlights the potential of **IoFAZO** from the crystal-engineering point of view. Due to the photoisomerizable azo moiety, **IoFAZO** and even its no-iodinated homologue, **HoFAZO** (due to its acidic hydrogen atoms that work as hydrogen-bond donors), may prove interesting in photoresponsive materials design, particularly in view of photomechanical crystals[31] and noncovalently crosslinked elastomers[29]. Finally, yet another interesting observation is that in the halogen-bonded cocrystals studied, the azo group is never involved in any intermolecular interactions. This self-sorting process renders the azo group completely “free”, which presumably facilitates the photoisomerization process even in the crystalline state.

References and notes:

(1) Müller K.; Faeh C.; Diederich F. *Science* **2007**, *317*, 1881. ; O'Hagan D. *J. Fluorine Chem*. **2010**, *131*, 1071.

(2) Reichenbächer K.; Süss H. I.; Hulliger J. *Chem. Soc. Rev*. **2005**, *34*, 22. ; Chopra D.; Guru Row T. N. *CrystEngComm* **2011**, *13*, 2175.

(3) Babudri F.; Farinola G. M.; Naso F.; Ragni R. *Chem. Commun*. **2007**, 1003.

(4) O'Hagan D. *Chem. Soc. Rev*. **2008**, *37*, 308.

(5) Pauling L. *The Nature of the Chemical Bond and the Structure of Molecules and Crystals: An Introduction to Modern Structural Chemistry*, Cornell University Press, Ithaca, NY, **1939**.

(6) Dunitz J. D.; Taylor R. *Chem. Eur. J*. **1997**, *3*, 89.

(7) Wiberg K. B.; Rablen P. R. *J. Am. Chem. Soc*. **1993**, *115*, 614.

(8) Bondi A. *J. Phys. Chem*. **1964**, *68*, 441.

(9) Gavezzotti A. *J. Am. Chem. Soc*. **1983**, *105*, 5220.

(10) Bratsch S. G. *J. Chem. Educ*. **1985**, *62*, 101.

(11) Metrangolo P.; Pilati T.; Terraneo G.; Biella S.; Resnati G. *CrystEngComm* **2009**, *11*, 1187.

(12) Metrangolo P.; Resnati G.; Pilati T.; Biella S. *Struct. Bond.* **2008**, *126*, 105.

(13) Crihfield A.; Hartwell J.; Phelps D.; Walsh R. B.; Harris J. L.; Payne J. F.; Pennington W. T.; Hanks T. W. *Cryst. Growth Des*. **2003**, *3*, 313. ; Getmanenko Y. A.; Tongwa P.; Timofeeva T. V.; Marder S. R. *Org. Lett*. **2010**, *12*, 2136.

(14) Pace A.; Pierro P. *Org. Biomol. Chem*. **2009**, *7*, 4337.

(15) Lo Celso F.; Pibiri I.; Triolo A.; Triolo R.; Pace A.; Buscemi S.; Vivona N. *J. Mater. Chem*. **2007**, *17*, 1201. ; Pibiri I.; Pace A.; Buscemi S.; Causin V.; Rastrelli F.; Saielli G. *Phys. Chem. Chem. Phys*, **2012**, *14*, 14306.

(16) Bostrom J.; Hogner A.; Llinas A.; Wellner E.; Plowright A. T. *J. Med. Chem*. **2012**, *55*, 1817. ; Palumbo Piccionello A.; Musumeci R.; Cocuzza C.; Fortuna C. G.; Guarcello A.; Pierro P.; Pace A. *Eur. J. Med. Chem*. **2012**, *50*, 441.

(17) Palumbo Piccionello A.; Guarcello A.; Buscemi S.; Vivona N.; Pace A. *J. Org. Chem*. **2010**, *75*, 8724. ; Palumbo Piccionello A.; Pace A.; Buscemi S. *Org. Lett*. **2011**, *13*, 4749.

(18) Gallardo H.; Cristiano R.; Vieira A. A.; Neves Filho R. A. W.; Srivastava R. M.; Bechtold I. H. *Liq. Cryst*. **2008**, *35*, 857. ; Torgova S.; Geivandova T.; Francescangeli O.; Strigazzi A. *Pramana* **2003**, *61*, 239.

(19) Corradi E.; Meille S. V.; Messina M. T.; Metrangolo P.; Resnati G. *Tetrahedron Lett.* **1999**, *40*, 7519.

(20) Priimagi A.; Cavallo G.; Forni A.; Gorynsztejn-Leben M.; Kaivola M.; Metrangolo P.; Milani R.; Shishido A.; Pilati T.; Resnati G.; Terraneo G. *Adv. Funct. Mater*. **2012**, *22*, 2572.

(21) Metrangolo P.; Panzeri W.; Recupero F.; Resnati G. *J. Fluorine Chem.* **2002**, *114*, 27.

(22) Trifonov R. E.; Volovodenko A. P.; Vergizov S. N.; Shirinbekov N. I.; Gindin V. A.; Koren A.O. Ostrovskii V. A. *Helv. Chim. Acta* **2005**, *88*, 1790.

(23)Volovik S. V.; Staninets V. I.; Zefirov N. S. *Theor. Exp. Chem*. **1991**, *26*, 390.

(24)Metrangolo P.; Pilati T.; Resnati G.; Stevenazzi A. *Chem. Commun*. **2004**, 1492.

(25)Priimagi A.; Saccone M.; Cavallo G.; Shishido A.; Pilati T.; Metrangolo P.; Resnati G. *Adv. Mater*. **2012**, *24*, OP 345.

(26)Bleger D.; Schwarz J.; Brouwer A. M.; Hecht S. *J. Am. Chem. Soc*. **2012**, *134*, 20597.

(27)Walter S. M.; Jungbauer S. H.; Kniep F.; Shindler S.; Herdtweck E.; Huber S. M. *J. Fluorine Chem*. **2013**, *150*, 14.

(28)Ikeda T.; Mamiya J.; Yu Y. *Angew. Chem. Int. Ed*. **2007**, *46*, 506.

(29)Kulikovska O.; Goldenberg L. M.; Stumpe, J. *Chem. Mater*. **2007**, *19*, 3343. ; Zettsu N.; Ogasawara T.; Mizoshita N.; Nagano S.; Seki T. *Adv. Mater*. **2008**, *20*, 516. ; Mamiya J.; Yoshitake A.; Kondo M.; Yu Y.; Ikeda T. *J. Mater. Chem*. **2008**, *18*, 63.

(30)Nakano H. *J. Phys. Chem. C* **2008**, *112*, 1042. ; Koshima H.; Ojima, N.; Uchimoto H. *J. Am. Chem. Soc*. **2009**, *131*, 6890. ; Bushuyev O. S.; Singleton T. A.; Barrett C. J. *Adv. Mater*. **2013**, *25*, 1796.

(31)Bushuyev O. S.; Tomberg A.; Friščić T.; Barrett C. J. *J. Am. Chem. Soc*. **2013**, *135*, 12556.

(32)Bruce D. W.; Dunmur D. A.; Lalinde E.; Maitlis P. M.; Styring P. *Liq. Cryst.* **1988**, *3*, 385.

(33)Jeffrey G. A. *An introduction to hydrogen bonding* Oxford University Press, Oxford, **1997**.

(34)Rozas I.; Alkorta I.; Elguero J. *J. Phys. Chem. A* **1998**, *102*, 9925.

(35)Taylor R.; Kennard O.; Versichel, W. *J. Am. Chem. Soc*. **1984**, *106*, 244.

(36)Jeffrey G. A.; Mitra, J. *J. Am. Chem. Soc*. **1984**, *106*, 5546. ; Preißner R.; Egner U.; Saenger W. *FEBS Letters* **1991**, *288*, 192.

(37)Allen F. H. *Acta Cryst*. *B* **2002**, *58*, 380.

(38)de Lange J. J.; Robertson J. M.; Woodward I. *Proc. R. Soc. London Ser. A* **1939**, *171*, 398.

(39)Brown, C. J. *Acta Cryst*. **1966**, *21*, 146. ; Harada J.; Ogawa K. *J. Am. Chem. Soc*. **2004**, *126*, 3539.

(40)Chinnakali K .; Fun H.-K.; Shawkataly O. B.; Siang-Guan T. *Acta Cryst. C* **1993**, *49*, 615.

(41)Britton D. *Acta Cryst*. E **2003**, **59**, O1332. ; Ostermeier M.; Berlin M.-A.; Meudtner R. M.; Demeshko S.; Meyer F.; Limberg C.; Hecht, S. *Chem. Eur. J*. **2010**, *16*, 10202.

(42)Bertolotti F.; Cavallo G.; Metrangolo P.; Nayak S. K.; Resnati G.; Terraneo G. *Supramol. Chem*. **2013**, *25*, 718.

(43)Hartmann F.; Dahlems T.; Mootz, D. *Z. Kristallogr.-New Cryst. Struct*. **1998**, *213*, 639.

(44)Saccone M.; Cavallo G.; Metrangolo P.; Pace A.; Pibiri I.; Pilati T.; Resnati G.; Terraneo G. *CrystEngComm* **2013**, *15*, 3102.

(45) Bruce D. W.; Metrangolo P.; Meyer F.; Prasang C.; Resnati G.; Terraneo G.; Whitwood A. C.; *New J. Chem*. **2008**, *32*, 477.

5 Experimental part.

5.1 Materials and methods.

The starting materials were purchased from Sigma-Aldrich, Acros Organics, Apollo Scientific and TCI Europe.

Commercial high-performance liquid chromatography (HPLC)-grade solvents were dried and distilled following the standard purification procedures[1] before use.

^{1}H, ^{13}C and ^{19}F NMR spectra were recorded at room temperature on a Bruker AV400 or AV500 spectrometer, using $CDCl_3$ as solvent. ^{1}H and ^{13}C NMR chemical shifts were referenced to tetramethylsilane (TMS) using the residual proton or carbon impurities of the deuterated solvents as standard reference, while ^{19}F NMR chemical shifts were referenced to an internal $CFCl_3$ standard.

Attenuated total reflectance FTIR (ATR-FTIR) spectra were obtained with a Nicolet Nexus FTIR spectrometer. The values were given in wave numbers and were rounded to 1 cm^{-1} upon automatic assignment.

Mass spectra were recorded on a BRUKER Esquire 3000 PLUS.

DSC analysis was performed on a Mettler Toledo DSC823e instrument, using aluminium light 20 µL sample pans and Mettler STARe software for calculation.

The melting points were also determined on a Reichert instrument by observing the melting process through an Olympus BH-2 optical microscope. The phase transition of the liquid crystals were studied with the same instrumentation.

The UV-vis spectra were collected using Perkin Elmer Lambda 950 spectrophotometer.

The XPS measurements were performed using an ULVAC-PHI Inc. 1700R ESCA spectrometer equipped with a Mg K_α X-ray source (1253.6 eV) and a hemispherical analyzer. The resolution used was 0.05 eV. All of the spectra were referenced to the C1s neutral carbon peak at 284.6 eV.

AFM images used for surface profile characterization were taken with a Veeco Dimension 3000 scanning force microscope in tapping mode.

The theoretical calculations were performed using the GAUSSIAN program suite[2], the rendering of the electrostatic potential in **Fig. 29** was performed with *MolIso*[3]. Further details about a specific calculation are given in the appropriate section.

X-ray powder diffraction experiments were carried out on a Bruker D8 Advance diffractometer operating in reflection mode with Ge-monochromated Cu K_α radiation (λ

= 1.5406 Å) and a linear position-sensitive detector. Powder X-ray diffraction data were recorded at ambient temperature, with a 2θ range of 5−40 °, a step size 0.016 ° and exposure time of 1.5 s per step.

The single-crystal X-ray structure was determined using a Bruker Kappa Apex II CCD diffractometer with Mo *Kα* radiation (λ = 0.7107 Å) and a Bruker Kryoflex low-temperature device. Crystals were mounted in inert oil on glass fibres. Data collection and reduction were performed by SMART[4] and SAINT[4] and absorption correction, based on multi-scan procedure, by SADABS[4]. The structures were solved by SIR92[5] and refined on all independent reflections by full-matrix least-squares based on F_o^2 by using SHELX-97[6]. Further details about a specific crystal structure determination are given in the appropriate section.

The optical experiments are described in the appropriate section.

5.2 Halogen bonded photoactive polymers.

Synthetic procedures.

Compound **3** was purchased by TCI Europe, while compound **2** was prepared as previously reported[7].

Compound **1** was synthetized as follows: 4-iodoaniline (1.31 g, 6 mmol) was dissolved in freshly distilled acetonitrile (10 ml) and added dropwise to a solution of nitrosonium tetrafluoborate (6 mmol) in acetonitrile (10 ml) at -30 °C. The resulting solution was stirred at -30 °C for 1h and then 24 mmol of *N,N*-dimethylaniline were added dropwise. After 12h of additional stirring at room temperature, 30 ml of distilled water were added. The mixture was extracted three times with CH_2Cl_2 . The organic layers were collected and dried over anhydrous Na_2SO_4. The solvent was removed under reduced pressure and the residue was purified by recrystallization from chloroform to yield 2.5 mmol of **1** (42%) as an orange powder.

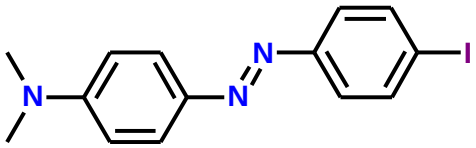

Melting point: 153° (DSC onset) decomposes.
FT-IR ν_{max} = 2901, 2812, 1598, 1561, 1514, 1471, 1440, 1418, 1409, 1385, 1357, 1310, 1294, 1228, 1154, 1119, 1095, 1066, 1049, 998, 943, 837, 819, 735, 725, 670, 647, 637.
^{1}H NMR (400 MHz, δ): 7.91 (d, *J* = 4 Hz, 2H), 7.82 (d, *J* = 3 Hz, 2H), 7.62 (d, *J* = 4 Hz, 2H), 6.79 (d, *J* = 4.5 Hz, 2H), 3.11 (s, 3H)
MS/ESI m/z 351.2 found 352.2 ($M+H^+$).

Compound **4** was synthetized as follows: Pentafluoroaniline (300 mg, 1.639 mmol.) was dissolved in 70% w/w sulphuric acid (2 ml) and treated with sodium nitrite (181 mg). After being stirred for 2 h. the solution was rendered alkaline by the addition (over 4 h.) of a solution of anhydrous sodium carbonate (2.65 g) in distilled water (13 ml) with vigorous stirring, the temperature being kept at 0° C. After a further 30 min., the mixture was acidified with 70% w/w sulphuric acid (1 ml) and treated with dimethylaniline (2 ml). One hour later the orange-red precipitate which had formed was filtered off, washed with water, and dried. The filtrate was extracted two times with

diethyl ether, and the combined extracts dried over anhydrous Na_2SO_4 and evaporated. The residue was than triturated and stirred with anhydrous acetic acid, filtered with a sintered glass funnel and recrystallized from methanol to obtain 247 mg (48% 0.79 mmol.) of **4** as orange crystals.

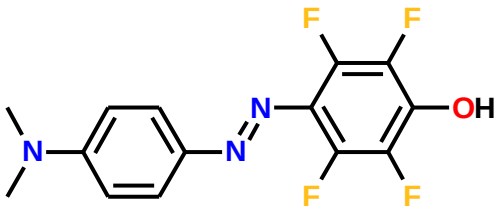

Melting point: 157° C (DSC onset) decomposes.

FT-IR ν_{max} = 2913, 1635, 1597, 1556, 1526, 1503, 1444, 1401, 1365, 1305, 1271, 1241, 1230, 1139, 1066, 1012, 945, 887, 743, 731, 718, 663, 632, 593 cm^{-1}.

^1H NMR (500 MHz, DMSO-d_6, δ): 7.72 (d, J = 5 Hz, 2H), 6.83 (d, J = 5 Hz, 2H), 3.07 (s, 3H).

^{19}F NMR (470 MHz, DMSO-d_6, δ): -155.31 (m, 2F), -163.95 (bs, 2F).

MS/ESI m/z 313.2 found 312.2 ($M\text{-}H^+$).

Elementar analysis: calcd. C 53.7, H 3.5, N 13.4 %. Found C 53.6, H 3.4, N 13.6 %.

Computational studies.

The molecular structures of dyes **1**-**4** were optimized for vacuum and for DMF solution using density functional (DFT) theory by applying the PBE0[8] functional and the 6-311++G** basis set for all atoms. Absorption spectra were computed by time-dependent DFT. Accurate interaction energies for the molecular dimers composed of the dyes and 4-methylpyridine were computed at PBE0/6-311++G** level as the difference between the energy of the dimer and the sum of the energies of the single monomers and were corrected for basis set superposition error (ΔE_{BSSE})[9].

The solvation effects have been included by means of the Polarizable Continuum Model (PCM)[10]. To determine the absorption wavelengths, standard vertical Time Dependent DFT (TDDFT) calculations have been carried out, using the so-called non-equilibrium approach, while the equilibrium solvation was used for TDDFT excited state geometry optimizations.

Co-crystallization Experiments.

The azobenzene derivative **4** and the bis-pyridine derivative **5** were separately dissolved in methanol at room temperature in a 2:1 ratio, under saturated conditions.

The two saturated solutions containing the HB-donor and the HB-acceptor were then mixed in a clear borosilicate glass vial, which was left open in a closed cylindrical wide-mouth bottle containing diethyl ether. The ether was allowed to slowly diffuse in the methanol solution at room temperature for two weeks, until the formation of good-quality single crystals of **6** occurred.
Melting point: 188° C (DSC onset) decomposes.
FT-IR ν_{max} = 1643, 1597, 1558, 1494, 1444, 1407, 1359, 1299, 1229, 1116, 1013, 963, 948, 888, 819, 789, 733, 663.

Optical experiments.

The optical experiments were carried out for thin films (250 nm) spin-coated from DMF solution on clean microscope slides.
SRG inscription were performed using a spatially filtered and collimated Ar^+ laser beam at wavelength of 488 nm. The gratings were inscribed by intersecting two counter-circularly polarized laser beams on the film surface. The incidence angle of the beams was 7°, which yielded a polarization-modulated interference pattern with a 2 μm period. The time evolution of the resulting diffraction gratings was monitored by collecting the transmitted first-order diffraction of a normally incident 633 nm He-Ne laser beam using an oscilloscope. The diffraction efficiency of the gratings was defined as $\eta = I_1 / I_0$, where I_1 and I_0 are the intensities of the first-order diffracted and the transmitted beam, respectively.

5.3 Halogen bonded photoactive liquid crystals.

Synthetic procedures.

Compounds **1**[7] and **2**[11] were prepared as previously reported.

Co-crystallization Experiments.

The azobenzene derivative **1** and the stilbazole **2** were separately dissolved in THF at room temperature in a 1:1 ratio, under saturated conditions. The two saturated solutions containing the XB-donor and the XB-acceptor were then mixed in a clear borosilicate glass vial, which was left open in a closed cylindrical wide-mouth bottle containing paraffin oil. The solvents were allowed to slowly evaporate at room temperature for three days until the formation of good-quality single crystals of **3** occurred.

3: melting point = 150° C.

^{1}H NMR (500 MHz, *δ*): 8.55 (d, *J* = 3 Hz, 2H), 7.88 (d, *J* = 9 Hz, 2H), 7.48 (d, *J* = 9 Hz, 2H), 7.34 (d, *J* = 4 Hz, 2H), 7.25 (d, *J* = 13 Hz, 1H), 6.92 (d, *J* = 8 Hz, 2H), 6.88 (d, *J* = 16 Hz, 1H), 6.73 (d, *J* = 9 Hz, 2H), 3.84 (s, 3H), 3.12 (s, 6H).

^{19}F NMR (470 MHz, *δ*): − 122.55 (q, *J* = 14 Hz, 2F), − 151.10 (q, *J* = 14 Hz, 2F).

FT-IR ν_{max} = 3025, 2896, 2835, 1589, 1575, 1510, 1472, 1417, 1394, 1361, 1308, 1282, 1175, 1146, 1066, 1045, 1024, 996, 975, 964, 933, 886, 821, 799, 736 cm^{-1}.

Elemental analysis: calcd. for $C_{14}H_{13}NO \cdot C_{14}H_{10}N_3F_4I$: C 53.01, H 3.65, N 8.83; found: C 52.8, H 3.5, N 8.6.

Thin-film characterization and optical experiments.

The optical experiments were carried out for thin films (250 nm) spin-coated from dichloromethane solution on clean microscope slides.

FT-IR (film): ν_{max} = 3027, 2897, 2835, 1590, 1576, 1511, 1474, 1420, 1395, 1364, 1310, 1281, 1177, 1147, 1066, 1045, 1023, 995, 975, 964, 931, 886, 822, 798, 736 cm^{-1}.

The POM images of the thin films were taken using an Olympus BH-2 optical microscope equipped with a Mettler–Toledo hot stage. The XPS measurements were performed using an ULVAC-PHI Inc. 1700R ESCA spectrometer equipped with a Mg K_α X-ray source (1253.6 eV) and a hemispherical analyzer. The resolution used was 0.05 eV. The spectra of **1** and **2** were measured from powders mounted on double-

sided carbon tape. The spectra of **3** were measured from the spin-coated thin film. All of the spectra were referenced to the C1s neutral carbon peak at 284.6 eV.

The photoalignment and SRG inscription were performed using a spatially filtered and collimated Ar^+ laser beam at wavelength of 488 nm. The photoalignment was carried out using a vertically polarized laser beam. In order to determine the order parameters at different stages of irradiation, the sample was mounted to a holder containing a 1 mm aperture through which it was irradiated. The aperture size was smaller than the size of the irradiation beam, which ensured uniform photoalignment throughout the whole aperture area. The irradiation was ceased at time instances of 10 s, 30 s, 60 s, 90 s, 120 s, 180 s, 240 s, and 360 s, and the sample was inserted into a polarizer-equipped spectrophotometer (Jasco V-650); also the polarized absorption spectra were measured through the 1 mm aperture. Since the photoinduced anisotropy is temporally stable, such a two-step procedure was justified.

The order parameter is determined at different time instances from the polarized absorption spectra using the equation $S = (A_\perp - A_{||})/(A_\perp + 2A_{||})$, where $A_{||}$ and $A_\perp$ are the absorbances parallel and perpendicular (the uniaxial direction) to the writing beam polarization, respectively. The absorbance values were obtained in each case by averaging over a wavelength range of 440 nm – 460 nm. The gratings were inscribed by intersecting two counter-circularly polarized laser beams on the film surface. The incidence angle of the beams was 7°, which yielded a polarization-modulated interference pattern with a 2 μm period. The time evolution of the resulting diffraction gratings was monitored by collecting the transmitted first-order diffraction of a normally incident 633 nm He–Ne laser beam using an oscilloscope. The diffraction efficiency of the gratings was defined as $\eta = I_1 / I_0$, where I_1 and I_0 are the intensities of the first-order diffracted and the transmitted beam, respectively. AFM images used for surface profile characterization were taken with a Veeco Dimension 3000 scanning force microscope in tapping mode.

Crystal data.

Chemical formula: $C_{28}H_{23}F_4ION_4$; M_r = 634.40; monoclinic, $P2_1/n$; crystal color: dark-red; shape: wedge; dimensions: 0.12×0.25×0.32 mm^3, a = 10.2984(15), b = 8.8606(12), c = 28.157(4) Å, β = 94.345(12)°, Z = 4, d_{calc} = 1.645 g cm^{-3}, μ(Mo-$K\alpha$) = 1.309 mm^{-1}, temperature 103(2) K.

Data collection range 2.06 < θ < 36.23° (completeness = 1.00 for θ < 32.00°), θ/2θ scan mode, 97266 collected reflections, 10581 independent, 9057 with $I > 2\sigma(I)$, multi-scan absorption correction: 0.6606 $\leq T \leq$ 0.7471, R_{ave} = 0.0297. All the heavy atoms were refined anisotropically. H atoms were localized in a difference Fourier map and refined with soft restraints, imposing similar distance on chemically equivalent C-H distances and on H-C-H methyl angles; 412 parameter refined, 178 restraints; final disagreement factors based on all (and 'observed') independent reflections *R* = 0.0511 (0.0415) and w*R* = 0.0991(0.0947), *GOF* = 1.134.

5.4 Highly fluorinated azobenzene and heterocyclic supramolecules assembled by halogen bonding.

Synthetic procedures.

Synthetic efforts towards 3,5-bis(pyridyl)-1,2,4-oxadiazoles started some years ago[12] and the current synthetic strategy greatly benefited of such efforts.
0.500 g (3.66 mmol) of isonicotinamidoxime[12] were placed in a closed tube, 1.525 g (14.6 mmol) of 4-cyano-pyridine were added respectively, and put in an oil bath at 150° C for 8 h. The reaction mixture was purified by column chromatography using hexane/ethyl acetate as eluent to give 0.635 mg of **1** (yield 77%).

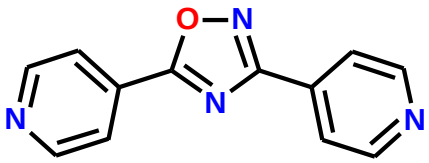

Melting point: 165–167 °C.
^{1}H NMR (500 MHz, *δ*): d 8.07 (m, 4H), 8.85 (d, J=5.7 Hz, 2H), 8.93 (d, J=5.5 Hz, 2H).
FTIR vmax = 3045, 1603, 1579, 1543, 1520, 1487, 1414, 1365, 1338, 1313, 1289, 1209, 1142, 1092, 1062, 988, 980, 904, 863, 838, 752, 725, 714, 683 cm^{-1}.

(*E*)-bis(2,3,5,6-tetrafluorophenyl)diazene (**HoFAZO**) was synthesized as follows: 2,3,5,6-tetrafluoroaniline (4 mmol) was dissolved in an ethanol-water (1:1) mixture. A solution of potassium hydroxide (10 mmol) in a 1:1 ethanol-water mixture was added, followed by slow addition of solid potassium ferricyanide (20 mmol). The mixture was refluxed overnight, filtered to remove the excess of oxidant and extracted with chloroform. The organic phase was washed twice with water, dried with anhydrous sodium sulfate and evaporated under reduced pressure. The resulting solid was *chromatographed* over silica gel using hexane/ethyl acetate (9/1) as the eluent, to obtain 0.22 mmol (11%) of **HoFAZO** as orange powder.

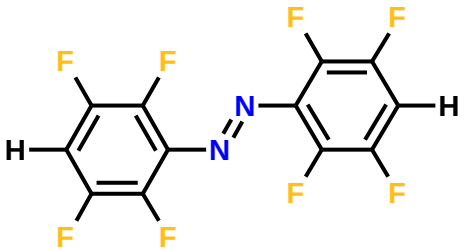

Melting point 124-126°C.

FTIR ν_{max} = 3095, 1709, 1607, 1499, 1409, 1378, 1278, 1257, 1178, 1130, 1068, 1036, 951, 855, 745, 716, 700 cm^{-1}.

^{1}H NMR (400 MHz, *δ*): 7.2-7.1 (m 2H).

^{13}C NMR (100 MHz, *δ*): 146.3 (d, $^{1}J_{CF}$ = 251 Hz, 4C), 140.2 (d, $^{1}J_{CF}$ = 264 Hz, 4C), 132.9-132.7 (m, 2C), 107.8 (t, *J* = 16Hz, 2C).

MS/ESI *m/z* 326.1 found 327.1 ($M+H^{+}$).

(*E*)-bis(4-iodo-2,3,5,6-tetrafluorophenyl)diazene (**IoFAZO**) was synthesized as follows: 4-iodo-2,3,5,6-tetrafluoroaniline (2.5 mmol) was dissolved in an ethanol-water (1:1) mixture. A solution of potassium hydroxide (5 mmol) in a 1:1 ethanol-water mixture was added, followed by slow addition of solid potassium ferricyanide (10 mmol). The mixture was refluxed overnight, filtered to remove the excess of oxidant and extracted with chloroform. The organic phase was washed twice with water, dried with anhydrous sodium sulfate and evaporated under reduced pressure. The resulting solid was *chromatographed* over silica gel using hexane/ethyl acetate (95/5) as the eluent, to obtain 0.06 mmol (5%) of **IoFAZO** as orange powder.

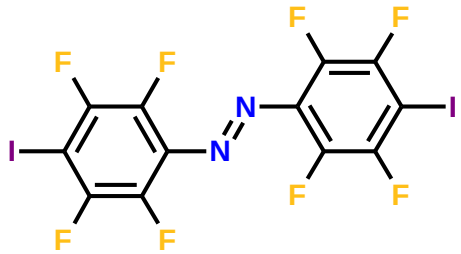

Melting point 203-207 °C (dec.).

FTIR ν_{max} = 1621, 1583, 1468, 1405, 1380, 1279, 1135, 1034, 973, 802, 762, 634 cm^{-1}.

^{13}C NMR (100 MHz, *δ*) 148.4 (d, $^{1}J_{CF}$ = 246 Hz, 4C), 140.3 (d, $^{1}J_{CF}$ = 265 Hz, 4C), 133.1 (t, *J* = 8.2 Hz, 2C), 76.9 (t, *J* = 28.4 Hz, 2C).

^{19}F NMR (471 MHz, *δ*) -120.2 (m, 4F), -148.6 (m, 4F).

MS/ESI m/z 578, found 579 ($M+H^{+}$).

Co-crystallization Experiments.

The 1,2,4-oxadiazole derivative **1** and the appropriate halogen bonding donor were separately dissolved in a 10%-90% MeOH-THF solution at room temperature in a 1:1 ratio, under saturated conditions. The two saturated solutions containing the XB-donor and the XB-acceptor were then mixed in a clear borosilicate glass vial, which was left open in a closed cylindrical wide-mouth bottle containing paraffin oil. Solvents were

allowed to slowly evaporate at room temperature for three days until the formation of good-quality single crystals occurred. A similar approach was used to obtain the azobenzene-based co-crystals.

4: Melting point: 172–174 °C.
^{1}H NMR: d 8.07 (m, 4H), 8.85 (d, J=5.7 Hz, 2H), 8.93 (d, J=5.5 Hz, 2H).
FTIR vmax = 3047, 1580, 1545, 1520, 1489, 1466, 1414, 1365, 1313, 1288, 1229, 1209, 1175, 1142, 1124, 1090, 1064, 1048, 989, 905, 863, 838, 816, 798, 753, 714, 692, 683, 631 cm^{-1}.
Elemental analysis: calcd for $C_{12}H_8N_4O.C_4F_8I_2$: C, 28.34; H, 1.18; N, 8.26%. Found: C, 28.11; H, 1.31; N, 8.38%.

5: Melting point: 175–176 °C.
^{1}H NMR: d 8.07 (m, 4H), 8.85 (d, J=5.7 Hz, 2H), 8.93 (d, J=5.5 Hz, 2H).
FTIR vmax = 3051, 1608, 1584, 1549, 1522, 1492, 1464, 1417, 1371, 1337, 1314, 1287, 1119, 1134, 1083, 1035, 995, 983, 933, 881, 862, 841, 804, 754, 718, 725, 685, 615 cm^{-1}.
Elemental analysis: calcd for $C_{12}H_8N_4O.C_6F_{12}I_2$: C, 27.78; H, 1.04; N, 7.20%. Found: C, 27.95; H, 1.27; N, 7.31%.

IoFAZO:BiPy (1:1): Melting point 236-240 °C (dec.).
FTIR vmax = 3038, 1619, 1592, 1536, 1464, 1406, 1463, 1368, 1273, 1214, 1063, 993, 974, 807, 794, 760, 732 cm^{-1}.

IoFAZO:DMSO (1:1): Melting point 210-212 °C (dec).
FTIR vmax = 3000, 2921, 2850, 1621, 1581, 1466, 1420, 1375, 1276, 1034, 979, 913, 792, 793, 726, 534 cm^{-1}.

IoFAZO:StOMe (1:2) : Melting point 210-214 °C (dec.).
FTIR vmax = 3026, 1620, 1590, 1576, 1510, 1463, 1420, 1405, 1361, 1308, 1282, 1175, 1146, 1066, 1045, 1024, 964, 933, 886, 799, 762, 635 cm^{-1}.

NMR experiments.

The experiments were carried out on diluted solutions (0.1 M in $CDCl_3$) of both complexes and starting materials. The ^{19}F data are given in **Table 6**.

Compound	$\Delta\delta_{CF2I}$ (ppm)	$\Delta\delta_{CF2CF2I}$ (ppm)	$\Delta\delta_{CF2CF2CF2I}$ (ppm)
4	1.97	0.12	-
5	2.03	0.16	0.05

Table 6: ^{19}F chemical shift changes observed in solutions of **4** and **5**. $\Delta\delta = \delta_{pure\ dioiodide} - \delta_{cocrystals}$. For compound **2** we obtained $\delta_{(CF2CF2I)2} = -60.07$, $\delta_{(CF2CF2I)2} = -113.39$, for compound **3** we obtained $\delta_{(CF2CF2CF2I)2} = -60.24$, $\delta_{(CF2CF2CF2I)2} = -114.27$, $\delta_{(CF2CF2CF2I)2} = -122.13$.

Crystal data (compounds 4 and 5).

All the non-hydrogen atoms were refined anisotropically. Hydrogen atoms of **5** were assigned to idealized positions and were allowed to ride, while in **4**, they were localized in a difference Fourier map and refined isotropically. Relevant data are in **Table 7**.

	4	**5**
Chemical Formula	$C_{16}H_8F_8I_2N_4O$	$C_{18}H_8F_{12}I_2N_4O$
Formula weight	678.06	778.08
Temperature K	103(2)	103(2)
Crystal system	Monoclinic	Monoclinic
Space group	$P2_1/n$	$P2_1/n$
***a* (Å)**	8.0406(12)	13.1606(12)
***b* (Å)**	22.942(3)	5.5451(6)
***c* (Å)**	11.6153(15)	31.302(3)
α (°)	90.00	90.00
β (°)	108.400(12)	91.877(10)
γ (°)	90.00	90.00
Volume (Å^3)	2033.1(5)	2283.1(4)
Z	4	4
Crystal size	0.04 x 0.22 x 0.35	0.10 x 0.35 x 0.42
Crystal description and colour	Table, colourless	Prism, colourless
Density (g cm^{-3})	2.215	2.264
μ (mm^{-1})	3.182	2.873
***F* (000)**	1272	1464
ABS T_{min}, T_{max}	0.3687, 0.5233	0.4482, 0.7470
$\theta_{min,\ max}$ (°)	2.73, 34.74	2.45, 35.61
No. of reflections measured	29563	139794
No. of independent reflections	7828	9494
R_{int}	0.0281	0.0736
No of parameters	305	460
No of restraints	0	262
Final R_1 values ($I > 2\sigma(I)$),	0.0242	0.0327
Final $wR(F^2)$ values ($I > 2\sigma(I)$)	0.0532	0.0821
Final R_1 values (all data)	0.0340	0.0375
Final $wR(F^2)$ values (all data)	0.0573	0.0841
G.o.F	1.034	1.122
$\Delta\rho_{max,\ min}$ (eÅ^{-3})	1.00, -0.53	1.04, -1.49
CCDC No.	915396	915397

Table 7: Crystal data for compounds **4** and **5**.

Crystal data (Azobenzene co-crystals).

For **HoFAZO**, the one H atom was localized in the difference Fourier map and refined isotropically without restraint. For **IoFAZO:DMSO**, the **DMSO** molecule lies on a

twofold axis. The H atoms on the one independent methyl group of **DMSO** were modelled in two orientations rotated from each other by 60°. For **IoFAZO:(StOMe)$_2$**, one of the two independent **StOMe** molecules is modelled as disordered in two orientations, with refined site occupancy 0.767 (1):0.233 (1), and equivalent bond lengths in the two disorder components were restrained to be similar (**Table 8**).

	HoFAZO	**IoFAZO:BiPy**	**IoFAZO:DMSO**	**IoFAZO:(StOMe)$_2$**
Crystal data				
Chemical formula	$C_{12}H_2F_8N_2$	$C_{22}H_8F_8I_2N_4$	$C_{14}H_6F_8I_2N_2OS$	$C_{40}H_{26}F_8I_2N_4O_2$
M_r	326.16	734.12	656.07	1000.45
Crystal system, space group	*Monoclinic,* *P 21/n*	*Monoclinic,* *P 21/c*	*Monoclinic,* *C2/c*	*Triclinic* *P-1*
Temperature	103(2)	103(2)	103(2)	103(2)
a, b, c (Å)	6.2100(8), 9.7294(13), 9.2163(13)	5.9388(10), 8.293(2), 22.160(4)	21.140(3), 10.0766(16), 9.5589(15)	5.9758(6), 13.998(2), 21.989(3)
α, β, γ (°)	90, 98.019(6), 90	90, 95.371(12), 90	90, 111.347(12), 90	80.264(12), 88.694(12), 81.381(12)
V (Å^3)	551.40(13)	1086.6(4)	1896.5(5)	1792.4(4)
Z	2	2	4	2
Radiation type	Mo $K\alpha$	Mo $K\alpha$	Mo $K\alpha$	Mo $K\alpha$
μ (mm^{-1})	0.214	2.983	3.510	1.840
Crystal size (mm)	0.44 x 0.22 x 0.16	0.40 x 0.19 x 0.10	0.40 x 0.10 x 0.03	0.46 x 0.18 x 0.06
Data collection				
Absorption correction	none	Multi-scan	Multi-scan	Multi-scan
T_{min}, T_{max}	-	0.3720, 0.4423	0.5181, 0.6022	0.2935, 0.3984
No. of measured, independent and observed [$I > 2\sigma(I)$] reflections	20442, 2342, 2030	14181, 3840, 3177	12815, 1662, 1379	17334, 9283, 7497
R_{int}	0.0290	0.0208	0.0316	0.0201
(sin $\theta/\lambda)_{max}$ (Å^{-1})	0.833	0.8	0.6	0.76
Refinament				
R [$F^2 > 2\sigma(F^2)$], $wR(F^2)$, S	0.0379, 0.1035, 1.096	0.0318, 0.0495, 1.059	0.0399, 0.0650, 1.076	0.0457, 0.0734, 1.047
No. of reflections	2342	3840	1662	9283
No. of parameters	104	163	1662	596
No. of restraints	0	0	137	509
H-atom treatment	Difference Fourier map	Not refined	Not refined	Not refined
$\Delta\rho_{max}$, $\Delta\rho_{min}$ (e Å^{-3})	0.664, -0.236	1.604, -0.771	0.834, -1.191	1.530, -0.636

Table 8: Crystal data for the azobenzene compounds.

References and notes:

(1) Armarego W. L. F.; Chai C. L. L. *Purification of Laboratory Chemicals* Butterworth-Heinemann, Oxford, **2009**.

(2) *Gaussian 09, Revision D.01*, Frisch M. J.; Trucks G. W.; Schlegel H. B.; Scuseria G. E.; Robb M. A.; Cheeseman J. R.; Scalmani G.; Barone V.; Mennucci B.; Petersson G. A.; Nakatsuji H.; Caricato M.; Li X.; Hratchian H. P.; Izmaylov A. F.; Bloino J.; Zheng G.; Sonnenberg J. L.; Hada M.; Ehara M.; Toyota K.; Fukuda R.; Hasegawa J.; Ishida M.; Nakajima T.; Honda Y.; Kitao O.; Nakai H.; Vreven T.; Montgomery J. A., Jr.; Peralta J. E.; Ogliaro F.; Bearpark M.; Heyd J. J.; Brothers E.; Kudin K. N.; Staroverov V. N.; Kobayashi R.; Normand J.; Raghavachari K.; Rendell A.; Burant J. C.; Iyengar S. S.; Tomasi J.; Cossi M.; Rega N.; Millam N. J.; Klene M.; Knox J. E.; Cross J. B.; Bakken V.; Adamo C.; Jaramillo J.; Gomperts R.; Stratmann R. E.; Yazyev O.; Austin A. J.; Cammi R.; Pomelli C.; Ochterski J. W.; Martin R. L.; Morokuma K.; Zakrzewski V. G.; Voth G. A.; Salvador P.; Dannenberg J. J.; Dapprich S.; Daniels A. D.; Farkas Ö.; Foresman J. B.; Ortiz J. V.; Cioslowski J.; Fox D. J. Gaussian, Inc., Wallingford CT, **2009**.

(3) Hübschle C. B.; Luger P. *J. Appl. Cryst*. **2006**, *39*, 901.

(4) *SMART*, *SAINT*, and *SADABS*, Bruker Analytical X-ray Systems; Bruker AXS Inc.: Madison, WI, **1999**.

(5) Altomare A.; Cascarano G.; Giacovazzo C.; Guagliardi A.; Burla M. C.; Polidori G.; Camalli M. *J. Appl. Crystallogr*. **1994**, *27*, 435.

(6) Sheldrick G. M. *SHELXL-97, Program for the Refinement of Crystal Structures*; University of Gottingen: Germany, **1997**.

(7) Priimagi A.; Cavallo G.; Forni A.; Gorynsztejn-Leben M.; Kaivola M.; Metrangolo P.; Milani R.; Shishido A.; Pilati T.; Resnati G.; Terraneo G. *Adv. Funct. Mater*. **2012**, *22*, 2572.

(8) Adamo C.; Barone V. *J. Chem. Phys*. **1999**, *110*, 6158.

(9) Boys S. F.; Bernardi F. *Mol. Phys*. **1970**, *19*, 553.

(10) Tomasi J.; Mennucci B.; Cammi R. *Chem. Rev*. **2005**, *105*, 2999.

(11) Bruce D. W.; Dunmur D. A.; Lalinde E.; Maitlis P. M.; Styring P. *Liq. Cryst.* **1988**, *3*, 385.

(12) Saccone M. “Sintesi di 3,5-bis [piridil]-1,2,4-ossadiazoli” BSc thesis, Università degli studi di Palermo, Palermo, **2007** (In italian).